VIRAL TRANSMISSION, NEUROPATHOGENESIS AND THERAPEUTIC ANTIBODY STUDIES IN A MURINE MODEL OF ENTEROVIRUS 71 ENCEPHALOMYELITIS.

TAN SOON HAO

THESIS SUBMITTED IN FULFILMENT OF THE REQUIREMENTS FOR THE DEGREE OF DOCTOR OF PHILOSOPHY

FACULTY OF MEDICINE
UNIVERSITY OF MALAYA
KUALA LUMPUR

2017

ABSTRACT

Enterovirus A71 (EV-A71), a single, positive-stranded RNA virus, belongs to the *Picornaviridae* family within the *Enterovirus* genus. Rarely, EV-A71 could lead to severe neurological complications such as aseptic meningitis, encephalitis and poliomyelitis-like acute flaccid paralysis. Patients with fatal brainstem encephalitis usually die within a few hours after hospital admission due to sudden cardiopulmonary arrest. The objectives of this project were to investigate various aspects of viral transmission, neuropathogenesis and effectiveness of therapeutic antibodies in a murine model of EV-A71 encephalomyelitis.

EV-A71 retrograde axonal transport up peripheral spinal nerves has been previously reported. However, whether EV-A71 could use retrograde axonal transport up cranial nerves to enter the brainstem remains unknown. To investigate this, mouse-adapted-virus-strain (MAVS) was injected into unilateral jaw/facial muscles of groups of mice. Infected mice were sacrificed at several time points for pathological (H&E, immunohistochemistry and *in situ* hybridisation) and viral titration analysis. Viral antigens/RNA were visualised within the cranial nerves and brainstem (motor-related region), ipsilateral to the injection site. Brainstem viral titres were also significantly higher than spinal cord titres at early time point.

The distribution of neuronal infection in human or mouse brain was distinct and rather stereotyped. This could be due to the variable susceptibility of different neurons to EV-A71 infection, or related to virus entry routes into the CNS. To study this, 2 groups of mice were intra-cerebrally (thalamus/hypothalamus or pons/medulla) inoculated with MAVS. Infected mice were sacrificed at various time points for pathological and viral titration analysis. In addition, a primary motor neuron cell was also prepared from E14 mouse spinal cord to study the permissiveness of mouse motor

neuron to MAVS infection. Based on the results, MAVS was not found to be replicating extensively in the brain or primary motor neuron cells.

Skeletal muscle injury has been shown to facilitate poliovirus retrograde axonal transport and subsequently enhances viral invasion into the CNS. To study the possibility of involvement of this important paralytic risk factor in EV-A71 infection, groups of mice with muscle-traumatised or non-traumatised hindlimb were intraperitoneally-infected with MAVS. Both groups of mice did not show significant differences in viral antigens/RNA and viral titres in hindlimb muscles and spinal cords.

To date, neither licenced vaccines nor therapeutic drugs were available to prevent or treat EV-A71 patients with CNS manifestations. A mouse IgM MAb was previously developed and showed cross-neutralisation of EV-A71 strains with genotypes B3-B5, and C1-C5. With an optimum dose of MAb given after MAVS CNS infection, a reduction of disease severity (reduced viral antigens/RNA and viral titres in the CNS) and mortality were observed in treated mice.

In conclusion, MAVS could utilise cranial nerves to achieve brainstem infection via retrograde axonal transport. The stereotype distribution of neuronal infection was more likely due to viral entry routes but not due to differences in neuron susceptibility. Skeletal muscle injury did not enhance the retrograde axonal transport of MAVS. Mouse monoclonal antibody was useful in preventing and ameliorating CNS infection.

ABSTRAK

Enterovirus A71 (EV-A71), adalah virus RNA berbenang tunggal yang tergolong dalam keluarga *Pikornaviridae* dalam genus *enterovirus*. Kadang-kala, EV-A71 boleh mengakibatkan komplikasi neurologikal yang serius seperti meningitis aseptik, ensefalitis dan kekakuan dan kelumpuhan flasid. Biasanya, pesakit dengan ensefalitis mati akibat kegagalan jantung atau system pernafasan secara tiba-tiba, selepas beberapa jam diwadkan. Tujuan utama pengajian ini adalah untuk mengaji tentang penyebaran, neuropatogenesis dan kesan antibodi terapeutik dalam model tetikus jangkitan Enterovirus 71. EV-A71 yang disesuaikan dalam tetikus (MAVS) dan tikus ICR yang berumur 2 minggu digunakan dalam sepanjang kajian ini.

Sebelum ini, ramai telah melaporkan bahawa, EV-A71 boleh memasuki saraf pusat melalui hujung saraf otot, akan tetapi, pengajian atas saraf kranial masih tidak diketahui. Oleh itu, MAVS telah disuntik ke dalam otot muka/rahang kanan tikus. Tikus kemudian dikorbankan pada titk masa tertentu untuk patologi (H&E, immunohistokimia dan hibridisasi in situ) dan virus kuantifikasi analisasi. Antigen/RNA virus telah diperhatikan dalam saraf kranial dan batang otak (kawasan neuron motorik), pada sisi suntikan yang sama. Virus dalam batang otak juga jauh lebih tinggi daripada saraf tulang belakang pada masa awal.

Lokasi virus dalam otak manusia atau tetikus adalah unik dan stereotipe. Ini mungkin disebabkan oleh kecenderungan infeksi yang berbeza oleh EV-A71 dalam sel neuron yang berbeza, atau berkait dengan laluan kemasukan virus ke dalam saraf pusat. Dengan ini, MAVS disuntikan ke thalamus/hipotalamus atau pons/medulla dalam 2 kumpulan tikus yang berbeza. Tikus yang terlibat dikorbankan pada titik masa tertentu untuk patologi dan kuantifikasi virus analisasi. Di samping itu, sel neuron motorik dalam tulang belakang juaga diasingkan dari E14 tikus untuk mengaji permisif sel

neuron motorik kepada jangkitan MAVS. Berdasarkan kajian ini, MAVS tidak dapat berkembang biak secara cekap dalam sel-sel otak atau neuron motorik tulang belakang.

Dalam jangkitan poliovirus, kecederaan otot telah dibuktikan akan meningkatkan jangkitan saraf pusat melalui penyebaran hujung saraf otot. Untuk mengaji faktor risiko lumpuh yang penting ini dalam jangkitan EV-A71, 2 kumpulan tikus dengan trauma otot kaki belakang atau tidak, dijangkiti dengan MAVS secara intraperitoneum. Kedua-dua kumpulan tikus tersebut tidak menunjukkan sebarang perbezaan yang signifikasi dalam antigen/RNA virus dan titer virus dalam otot kaki belakang dan tulang belakang.

Setakat ini, tiada vaksin ataupun ubat terapeutik yang berlesen untuk mencegah atau merawat pesakit EV-A71 dengan jangkitan saraf pusat. Satu antibody IgM tetikus (MAb) yang disediakan sebelum ini menunjukkan peneutralan kepada genotipe B3-B5, dan C1-C5 EV-A71. MAb dalam kuantiti yang optimum diberikan selepas jangkitan saraf pusat oleh MAVS, boleh melegakan penyakit teruk (dengan mengurangkan antigen/RNA virus dan titer virus dalam saraf pusat) dan menurunkan kadar kematian dalam tikus yang dirawati.

Kesimpulannya, MAVS boleh menggunakan saraf kranial untuk jangkitan batang otak melalui penyebaran hujung saraf otot. Lokasi virus yang unik dalam jangkitan saraf pusat adalah lebih mungkin disebabkan oleh laluan kemasukan virus dan bukannya disebabkan oleh kecenderungan infeksi yang berbeza dalam sel neuron yang berbeza. Kecederaan otot tidak meningkatkan jangkitan saraf pusat oleh MAVS. Antibodi monoklonal tetikus adalah berguna dalam mencegah dan melegakan jangkitan saraf pusat.

ACKNOWLEDGEMENT

First and foremost, my sincere thanks and appreciation to the University of Malaya for the scholarship support. Special thanks to my most respected supervisors; Professor Dr. Wong Kum Thong and Dr. Ong Kien Chai; for their constant guidance, understanding, and support. I must also thank Dr. Satoshi Koike, Dr. Ohka seii, Dr. Ken Fujii for the teaching and guidance in primary motor neuron cells culture experiments. I am especially thankful to my fellow labmates and friends for the help and inspirations they extended. Last but not least, I would like to extend my heartfelt gratitude to my amazing family members for their never-ending love, vital encouragement, and much-needed motivation.

TABLE OF CONTENT

LIST OF FIGURES

LIST OF TABLES

LIST OF SYMBOLS AND ABBREVIATIONS

µ	micro
AFP	acute flaccid paralysis
BBB	blood-brain-barrier
BSA	bovine serum albumin
$CCID_{50}$	50% cell culture infective dose
CD	Cluster of Differentiation
CNS	central nervous system
CO_2	carbon dioxide
COX-2	cyclooxygenase-2
CPE	cytopathic effect
DAB	3,3'-Diaminobenzidine
DMEM	Dulbecco's Modified Eagle Medium
dpi	days post-infection
EV-A71	Enterovirus 71
FBS	foetal bovine serum
GM	growth medium
H&E	haematoxylin and eosin
HFMD	hand-foot-mouth disease
hpi	hours post-infection

hr	hour
hSCARB2	human Scavenger Receptor Class B, Member 2
IC	intra-cranial/intra-cerebral
IFN	interferon
IgM	immunoglobulin M
IHC	immunohistochemistry
IL	interleukin
IM	intra-muscular
IP	intra-peritoneal
IRF	interferon regulatory factor
IS	intra-spinal
ISH	*In situ* hybridisation
IT	intra-tracheally
IV	intra-venous
IVIG	intravenous immunoglobulin
L	Litre
M	molar
m	milli
MAb	monoclonal antibody
MAVS	mouse-adapted virus strain

MDA5	melanoma-differentiation-associated
MHC	major histocompatibility complex
MIF	macrophage migration inhibitory factor
Min	minute
MM	maintenance medium
MOI	multiplicity of infection
mSCARB2	mouse Scavenger Receptor Class B, Member 2
NBT/BCIP	nitrobluetetrazolium/5-bromo-4-chloro-3-indolyl phosphate
NF-κB	nuclear factor kappa-light-chain-enhancer of activated B cells
NK cell	natural killer cell
PBS	phosphate buffer saline
PEG	polyethylene glycol
PGE2	Prostaglandin E2
PPR	pattern-recognition receptors
PSGL-1	P-selectin glycoprotein ligand-1
RD	human rhabdomyosarcoma cell
RLR	retinoic acid-inducible gene I like receptors
RT	room temperature
SC	subcutaneous
SCARB2	Scavenger Receptor Class B, Member 2

sec	second
TBS	Tris-buffer saline
TD	T cell dependent
Tg	transgenic
TI	T cell independent
TLR	toll-like receptors
TNF	tumour necrosis factors
USA	The United States of America
VCAM-1	vascular cell adhesion molecule 1
VERO	African green monkey kidney cell
VLP	virus-like particles
VSMC	vascular smooth muscle cells
WGA	wheat germ agglutinin
wt/vol	weight/volume

LIST OF APPENDICES

1.0 Introduction

Human Enterovirus A71 (EV-A71) belongs to the *Picornaviridae* family and genus of *Enterovirus* (Fields, Knipe, & Howley, 2013). EV-A71 is one of the major causative agents for hand-foot-mouth disease (HFMD), affecting mainly children below 5 years old. In some cases, it may progress to central nervous system (CNS) causing aseptic meningitis, encephalomyelitis and acute flaccid paralysis (AFP). Severe encephalomyelitis can be fatal, especially in younger patients (Ong & Wong, 2015; Solomon et al., 2010).

EV-A71 was first isolated in 1969, from a CNS-infected patient in California, USA, and reported by Schmidt, Lennette, and Ho (1974). Since then, there have been many more reports of EV-A71 outbreaks periodically in many parts of the world – USA, Europe, Asia, Australia, and Africa (World Health Organization, 2011). Recently, large outbreaks of HFMD mainly due to EV-A71 infection, appeared across the Asia Pacific regions, causing fatal neurologic complications. During the outbreak in mainland China in 2009, 1,155,525 cases with 13,810 severe cases and 353 deaths were reported (World Health Organization, 2011). Typically, after a few days of nonspecific fever, cough, with or without skin lesions, children with severe EV-A71 encephalomyelitis usually die from sudden cardiorespiratory collapse and pulmonary oedema within hours of hospital admission (Ong & Wong, 2015; K. T. Wong et al., 2008). Based on autopsy studies, fatal EV-A71 cases showed severe inflammation within the spinal cord, brainstem, hypothalamus, and cerebellar dentate nucleus (Lu et al., 2009; Wei, Li, & Chen, 2010; K. T. Wong et al., 2008; Yang et al., 2009). This distinct and stereotyped distribution of inflammation suggested the possibility that EV-A71 could utilise retrograde axonal transport via peripheral nerves to reach the CNS.

Several animal experiments support the hypothesis of retrograde axonal transport from peripheral nerves (Ong et al., 2008; Y. F. Wang & Yu, 2014). We hypothesised that EV-A71 can utilise cranial nerves to directly infect the brainstem, resulting in a sudden cardiopulmonary collapse in fatal encephalomyelitis. Very little is known about transmission and spread of EV-A71 within the CNS after viral entry via peripheral nerves. After entry into the CNS, following neuronal infection, viral cytolysis occurs but immune mediated or bystander effects might also play an important role in tissue injury. In support of viral cytolysis, EV-A71 antigens/RNA were visualised within the neuronal bodies and processes in human autopsy reports and animal models (Ong & Wong, 2015).

Among the various possible viral entry receptors for EV-A71, Scavenger Receptor Class B, Member 2 (SCARB2) appears to be the most promising so far. The essential role of SCARB2 in the development of EV-A71 neurological disease *in vivo* was shown in a recent transgenic (Tg) mouse model (Yamayoshi, Fujii, & Koike, 2014). The association of SCARB2 receptors and viral tissue tropism was also suggested in human and other mouse studies but the results have yet to be confirmed (Fujii et al., 2013; Y. He et al., 2014; Jiao, Guo, Huang, Chang, & Qiu, 2014; Yu et al., 2014).

"Provocation poliomyelitis" defined as muscle weakness (or paralysis) caused by poliovirus infection in motor neurons within spinal cord has been known for a long time. It is believed to be due to injured muscle tissues from the trauma of injection that aids the poliovirus infection of the spinal cord (Gromeier & Wimmer, 1998; John & Vashishtha, 2013). Since EV-A71 belongs to the same *Enterovirus* genus as poliovirus, and could cause similar AFP, it is possible that EV-A71 infection may be associated with the same "provocation poliomyelitis" phenomenon (Gorson & Ropper, 2001). EV-A71 provocation AFP was studied by comparing the viral localisation and quantitation

in the CNS in a muscle-traumatised and non-traumatised mouse model of EV-A71 encephalomyelitis.

Although several vaccines are actively being studied and clinical trials are progressing well, there are still no vaccines and therapeutic drugs licenced for EV-A71 infection (Ng, He, & Kwang, 2015). Intravenous immunoglobulin (IVIG) at high neutralising titres, have been recommended as possible therapeutic treatments against severe EV-A71 infection in Taiwan and China (R. Cao, Han, Qin, & Qin, 2011; C. C. Huang, 2001). However, the effectiveness of IVIG varies according to different manufacturers and times of collection causing batch to batch variations in the pooled sera (Ng et al., 2015). Several monoclonal antibodies (MAbs) as an alternative options to IVIG had been proven to have good prophylactic effect in animal models. Nevertheless, to date, most MAbs have been tested on animal models of EV-A71 infection, that display both myositis and CNS infection. Since, myositis and/or CNS infection could lead to limb paralysis or death, improvements in survival or amelioration/prevention of paralysis, without histopathological analysis is not sufficient to show if MAb is effective after CNS infection has occurred. This is particularly important since in human infections, CNS involvement is a major cause of death.

The objectives of this study are as follows:

1. To determine the role of cranial nerves in direct brainstem infection.
2. To investigate neuronal susceptibility to EV-A71 transmission within the brain, and its association with SCARB2 receptors.
3. To investigate the phenomenon of "provocation poliomyelitis" in EV-A71 infection.
4. To investigate the effectiveness of a MAb after established CNS infection.

2.0 Literature review

2.1 Enterovirus 71

2.1.1 Classification

Enterovirus 71 (EV-A71) belongs to the *Enterovirus* genus of the *Picornaviridae* family. The name "Picornavirus" is derived from the prefix pica (meaning very small) + RNA + virus. Picornaviruses are non-enveloped viruses, each with a single positive strand of RNA (Fields et al., 2013). The genus *Enterovirus* consists of 12 species: *Enterovirus A-H, Enterovirus J and Rhinovirus A-C*, based on molecular and biological properties of the viruses. Serotypes EV-A71 and coxsackieviruses A2-A8, A10, A12, A14, A16 and enteroviruses A76, A89-92, A114, A119-121 and the simian enteroviruses SV19, SV43, SV46 and baboon enterovirus A13 are all belong to the species *Enterovirus A* (Adams, King, & Carstens, 2013). EV-A71 can be further classified into three genogroups (A, B and C) based on the complete VP1 sequence. Genogroup A consists of a single member, strain BrCr-CA-70. Genogroups B and C, each can be divided into five distinct subgenogroups (B1 to B5, and C1 to C5) (Brown, Oberste, Alexander, Kennett, & Pallansch, 1999).

Like other enteroviruses, EV-A71 has a diameter of approximately 30 nm, a non-enveloped, pentameric icosahedral capsid, which comprises 60 identical protomers. Each protomer consists of 4 structural viral proteins (VP1 to VP4) (Figure 2.1). The VP1, VP2 and VP3 proteins are located on the external surface of the capsid whereas VP4 is located on the inside (Fields et al., 2013; Plevka, Perera, Cardosa, Kuhn, & Rossmann, 2012). Within the viral capsid is the RNA genome, which is about 7.4 kb. The viral protein (VPg) is covalently anchored at the 5' terminal and acts as a protein primer to initiate RNA synthesis during the viral replication (Figure 2.1). The coding region is flanked by 5' and 3' untranslated regions (UTR) at both ends, respectively,

followed by a variable length of poly-A tract located at the terminal of the 3' UTR (Bedard & Semler, 2004). The protein coding region encodes a 2194 amino acid polyprotein that can be divided into three primary precursor molecules: P1 region encodes for structural proteins VP4, VP2, VP3, and VP1; P2 and P3 for the non-structural proteins 2A to 2C and 3A to 3D, respectively (P. C. McMinn, 2002). Non-structural proteins are essential for genome replication and protein processing (Fields et al., 2013).

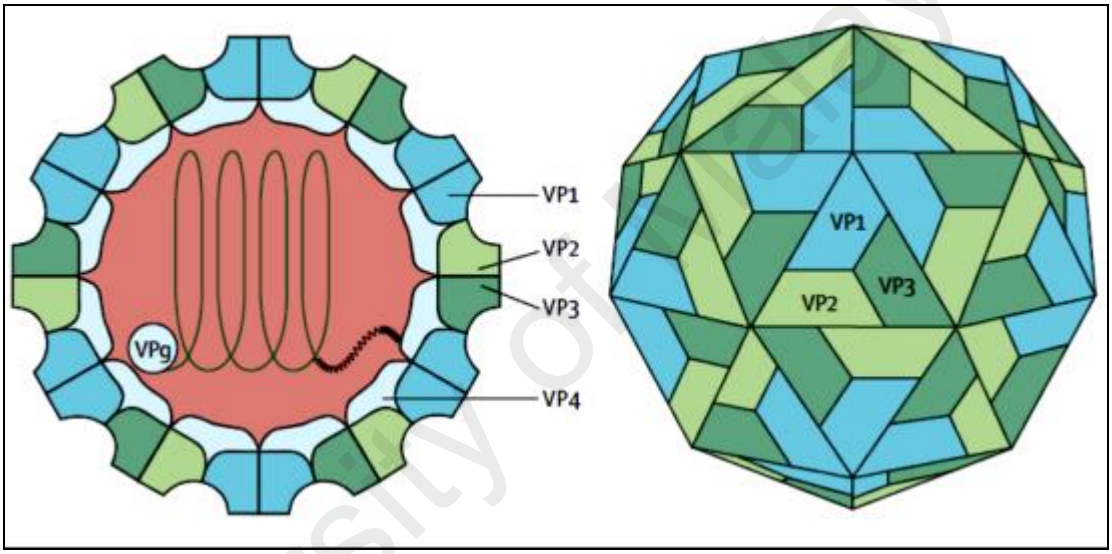

Figure 2.1: Structure of EV71 virion. The icosahedral capsid is formed by 60 protomers, each comprising 4 structural proteins VP1, VP2, VP3 and VP4. VP1-VP3 is located on the surface of the capsid while VP4 is located on its internal side. A 7.5 kb RNA genome forms the core of the capsid and anchors itself to the capsid via VP4. It has a viral protein (VPg) at its 5' end instead of a methylated nucleotide cap structure. (Adapted from Solomon et al., 2010)

2.1.2 Physical and chemical properties

EV-A71 as a non-enveloped virus, is relatively stable to acid (up to pH 3.0) and common laboratory disinfectants such as ether, chloroform, detergent, 70% ethanol, isopropanol, dilute Lysol and quaternary ammonium compounds. However, EV-A71 is oxidant sensitive and is rapidly inactivated by 1% of potassium permanganate, 1% of hydrogen peroxidase, 0.3% of formaldehyde, 0.1N of hydrogen chloride and chlorine. Similar to other infectious agents, EV-A71 can also be inactivated by ultra-violet light, particularly on surfaces but its antigenicity is retained (Fields et al., 2013). EV-A71 is also relatively sensitive to temperature and can be instantly inactivated by boiling water at 65°C for 2.5 minutes (min) and 56°C for 30 min. The high temperature alters the virions and causes RNA release which is irreversible. Drying can also rapidly inactivate the virus but slightly less efficiently in the presence of organic material (Fields et al., 2013).

2.1.3 EV-A71 infection and clinical manifestations

Enterovirus 71 infection is usually asymptomatic especially in adult patients. The most common clinical manifestation of EV-A71 infection is HFMD, seen mainly in children. HFMD patients have fever, sore throat, rash (flat or raised spots) or small blisters on the palms of hands, soles of feet, and/or buttocks, and mouth ulcers in the oral cavity or sides of the tongue (Figure 2.2) (Solomon et al., 2010).

However, the infection can be serious and fatal in young children notably those who are less than five years old because of CNS complications. The trend of EV-A71 infection or clinical manifestations appear to vary at different locations and times. For example, in 1970s, clinical manifestations of an EV-A71 outbreak in Europe were mainly encephalitis and polio-like paralysis with few cases of HFMD. Whereas, an EV-A71 outbreak in Japan at about the same period of time, mainly manifested as self-

limiting HFMD with only a minority of cases with CNS involvement (Ho, 2000; S. S. Wong, Yip, Lau, & Yuen, 2010). In 1998, an EV-A71 outbreak in Taiwan appeared to have caused the largest number of severe cases (405 cases) and deaths (78 cases) at that time (T. Y. Lin, Chang, Hsia, et al., 2002; S. M. Wang et al., 1999). However, only 7% of patients were reported to have CNS complications in Australia at the same period (P. McMinn, Stratov, Nagarajan, & Davis, 2001).

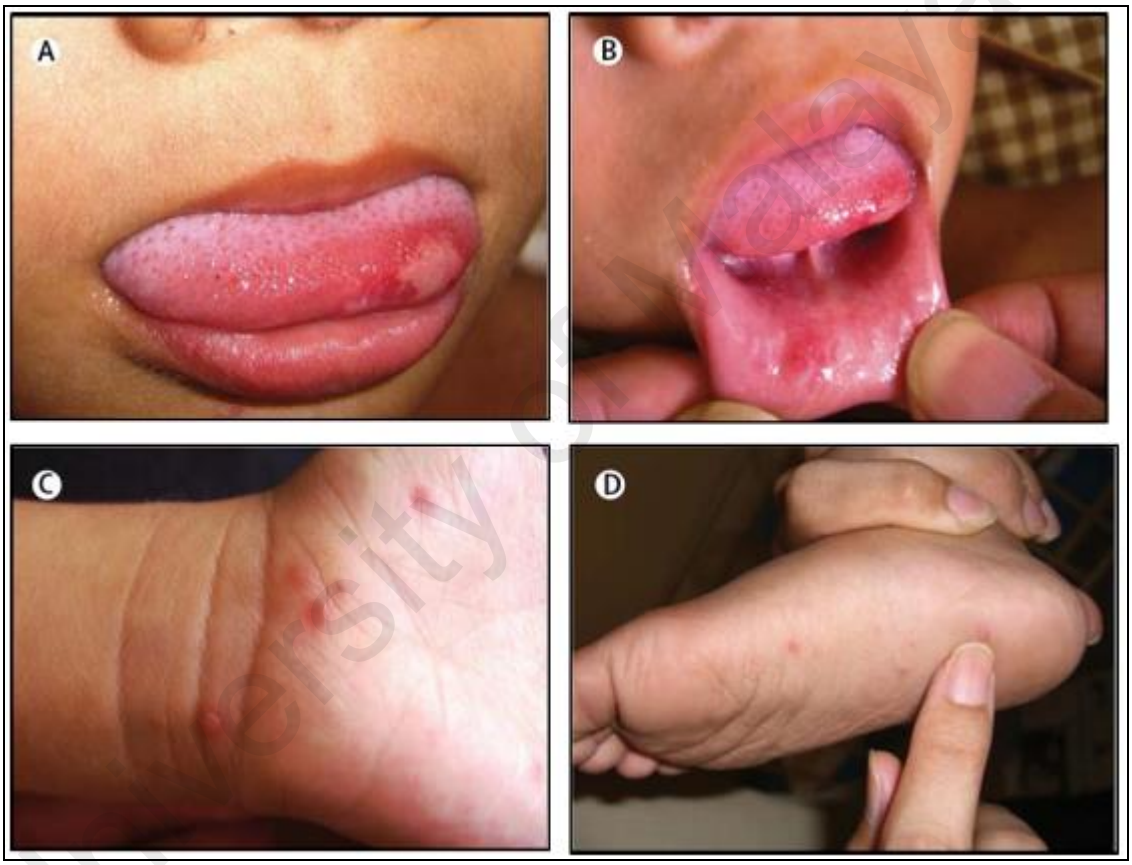

Figure 2.2: Mucocutaneous lesions in hand, foot, and mouth disease. Ulcers on tongue (A) and inside the lip (B); Maculopapular and vesicular lesions on the wrists (C) and the soles (D) of children infected with EV71. (Adapted from Ooi et al., 2010)

Among the neurological diseases are aseptic meningitis (mononuclear infiltration in the meninges), poliomyelitis-like paralysis (or AFP, causing limb weakness), brainstem encephalitis (or rhombencephalitis, brainstem inflammation) and encephalomyelitis (inflammation of the brain and spinal cord) (Weng, Chen, Huang, & Shih, 2010). Patients with brainstem encephalitis or encephalomyelitis have the worst

prognoses and are usually associated with pulmonary oedema and myocardial dysfunction (Lum, Wong, Lam, Chua, & Goh, 1998; Weng et al., 2010). C. C. Huang et al. (1999) had analysed 44 cases of EV-A71 CNS involvement during the 1998 Taiwan outbreak and divided the brainstem encephalitis / encephalomyelitis into 3 stages based on degree of CNS infection. The first stage is defined by muscle tremors and ataxia from which 5% of the children develop permanent neurological sequelae. The second stage is muscle tremors and cranial nerve involvement which is associated with permanent neurological sequelae in 20% of the children. The last stage is defined by rapid cardiopulmonary failure and fatality in 80% of the children. Survivors are often left with serious sequelae (C. C. Huang et al., 1999).

The locations of lesions identified by MRI examination were mainly on the dorsal pons, medulla oblongata (Figure 2.3) and spinal cord (F. Chen, Li, Liu, Wen, & Xiang, 2013; Zeng, Wen, Gan, & Huang, 2012). With increasing disease severity, the lesions also extend to the upper or lower areas or involve other regions such as the midbrain, hypothalamus, and cerebellum. Involvement of the dorsal pons affect the cranial nerve VI and VII nuclei. When the midbrain is involved, the red nucleus, substantia nigra and cranial nerve III and IV nuclei were affected as well. Involvement of the dorsal medulla could affect the dorsal nucleus of the vagus nerve, fasciculus longitudinalis medialis, and reticulate body and lead to respiratory and circulatory dysfunction (Zeng et al., 2012). Patients with flaccid paralysis could show a diffuse lesion from lower medulla throughout the spinal cord, particularly in ventral root and anterior horn (Figure 2.4) (F. Chen et al., 2013; P. McMinn et al., 2001; Zeng et al., 2012). These reports support the hypothesis that EV-A71 damages the medulla leading to very high levels of norepinephrine and epinephrine that may cause cardiac damage and arrhythmia, and pulmonary oedema via raised pulmonary vascular pressures (neurogenic pulmonary oedema).

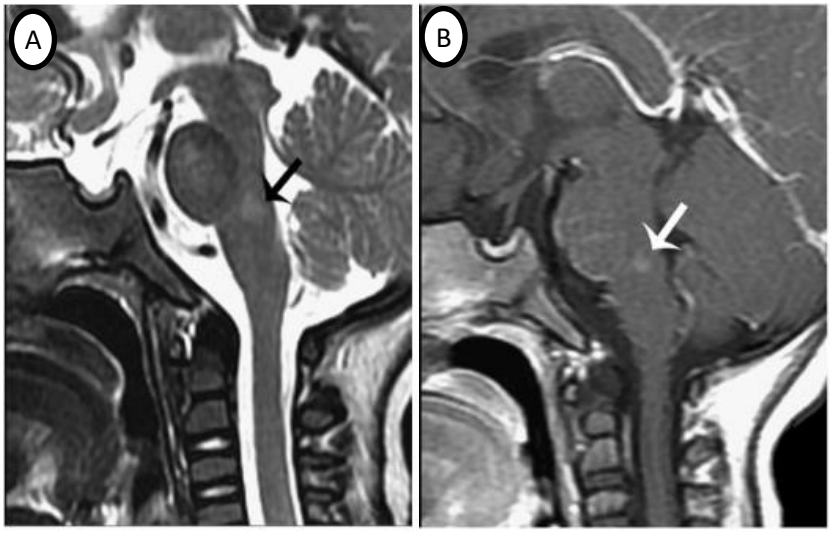

Figure 2.3: MRI characteristics of EV-A71 encephalomyelitis. Sagittal T2 weighted image showed slightly patchy signal (black arrow) at the junction of the pons and medulla oblongata (A) and an enhanced sagittal T1 weighted image showed mild enhancement (white arrow) in a 3 years old boy with HFMD at day 8 (adapted from Zeng et al., 2012).

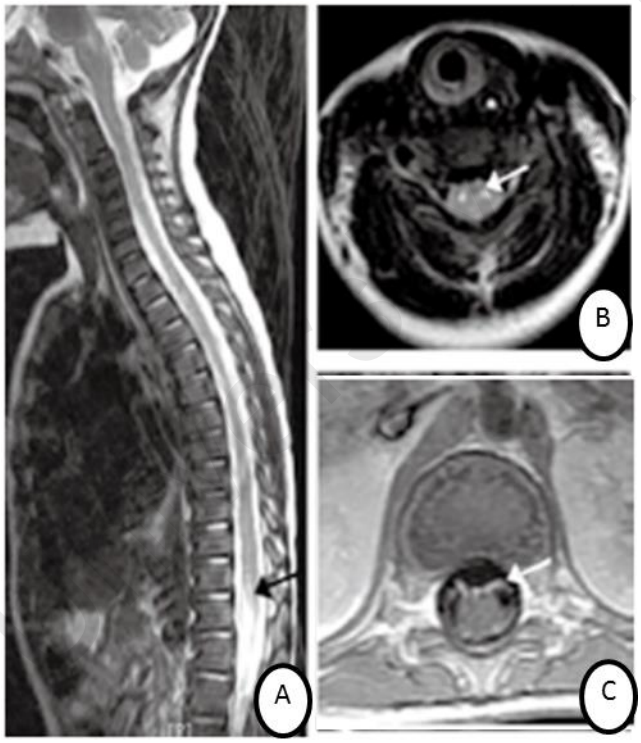

Figure 2.4: MRI characteristics of EV-A71 related AFP. Long strip high signal on T2 weight image in cervical spinal cord (A) and low signal on T1 weight image in anterior horn (B). With Contrast gadolinium-DTPA, there were obvious enhancement in ventral root (C) (adapted from F. Chen et al., 2013).

2.1.4 Pathogenesis

EV-A71 pathogenesis is still not fully understood and is being actively studied at the moment. It is widely accepted that EV-A71 is transmitted via faecal-oral route (Solomon et al., 2010). However, it may also spread through contact with virus-contaminated oral secretions, vesicular fluids, surfaces and respiratory droplets (Ong & Wong, 2015). Similar to what is believed to be happening in poliovirus infection, EV-A71 may start its initial replication in lymphoid tissues of the oropharyngeal cavity (tonsils) and the (Peyer's patches) small bowels. Previous reports had shown that viral titres from throat swabs were significantly higher than viral titres from rectal swabs or faeces (M. H. Ooi et al., 2009; M. H. Ooi, Wong, et al., 2007). Furthermore, viral antigens and RNA were detected in squamous epithelium lining of tonsillar crypts via immunohistochemistry (IHC) and *in situ* hybridisation (ISH) staining, respectively, suggesting that the palatine tonsil and other parts of the oral mucosa could be the primary replication sites for EV-A71 (Y. He et al., 2014). On the other hand, so far gastrointestinal tract has not been found to be infected in any of the infected human cases, but various animal models suggested that the viruses may be able to replicate in gastrointestinal epithelium (Y. C. Chen et al., 2004; Phyu, Ong, & Wong, 2016). In *in vitro* studies, EV-A71 had been shown to infect, replicate and induce apoptosis in endothelial cells (C. C. Liang et al., 2004). Following primary replication, viruses could enter the tonsil and/or oropharyngeal mucosa to further spread into regional lymph nodes and leading to mild viraemia. However, lymph node infection/replication has not been demonstrated so far.

Based on poliovirus CNS infection as a model, EV-A71 could theoretically invade the CNS via two routes, either by a haematogenous route and a retrograde peripheral nerve axonal transport route. EV-A71 could penetrate the blood-brain-barrier (BBB) following viraemia (C. S. Chen et al., 2007) with or without infection of

leucocytes (as with measles and mumps virus). The infected leucocytes may then migrate across the BBB due to upregulation of cellular adhesion molecules (Jackson, 2013; Tyler, 2009). Alternatively, alteration of the BBB's permeability as a result of pro-inflammatory cytokines such as tumour necrosis factor, interleukin 1β (IL-1β) and IL-6, caused by infection in other organs could permit the virus entry or virus may be taken up by receptors. Pinocytotic vesicles on endothelial cells that contain virus may be actively transported into the CNS as in Semliki Forest virus infection (Jackson, 2013; Tyler, 2009). EV A71 may also enter the CNS by retrograde axonal transport via the peripheral motor nerves (C. S. Chen et al., 2007; Ong et al., 2008). Various *in vivo* models and autopsy reports had suggested the possibility of retrograde axonal transport based on tissue tropism and CNS distribution of inflammation and virus (C. S. Chen et al., 2007; Lu et al., 2009; Ong et al., 2008; Y. F. Wang et al., 2004; Y. F. Wang & Yu, 2014; Wei et al., 2010; K. T. Wong et al., 2008; Yang et al., 2009). Furthermore, Ohka, Yang, Terada, Iwasaki, and Nomoto (1998) had shown retrograde transport of intact poliovirus through the axon via the fast transport system in a transgenic mouse model.

2.1.5 "Provocation Poliomyelitis"

"Provocation poliomyelitis" is defined as a phenomenon in which skeletal muscle injury predisposes the patient who has concurrent poliovirus infection to neurological complications such as muscle weakness (or paralysis). The history of "provocation poliomyelitis" can be traced to the 1940s in the USA when vaccines were not yet available. Initially, "provocation poliomyelitis" among unvaccinated children in endemic countries was believed to be due to poor hygiene or immigrant populations. After poliovirus was found to involve spinal cords, the causes of "provocation poliomyelitis was expanded to include the effects of diet, fatigue and hygiene (Mawdsley, 2014). In 1940s, based on 2000 case studies, the Harvard Infantile Paralysis

Commission suggested that tonsillectomies could lead to respiratory paralysis due to bulbar polio (Mawdsley, 2014). On the other hand, German doctors suggested that paediatric injections could provoke poliomyelitis. Although these observations were supported by doctors in France and Italy, it did not gain much attention until the end of World War 2. Several studies from United Kingdom, Australia and USA, reported that diphtheria, tetanus, and pertussis vaccines could provoke poliomyelitis suggesting to some that injured tissues at the injection site could somehow aggravate poliovirus infection. Others believed that the injections delivered poliovirus on the surface of skin into deeper tissues.

In 1955, Salk's polio vaccine, made by inactivating poliovirus with formaldehyde, had been approved by authorities in the USA. Five pharmaceutical companies, Eli Lilly, Parke-Davis, Wyeth, Pitman-Moore, and Cutter were licensed for vaccine production. Two weeks after the release of the vaccine, Cutter's vaccine was immediately recalled, but 380,000 doses had already been administered. Two production pools made by Cutter Laboratories (accounting for 120,000 doses) contained live poliovirus. Among the children who had received the vaccine from these pools, abortive polio (characterised by headache, stiff neck, fever, and muscle weakness) developed in 40,000 children; 51 were permanently paralysed; and 5 died. Cutter's vaccine also started a polio epidemic in which 113 people in the affected children's families or communities were paralysed, and 5 died. Subsequent studies found that cell debris contained in Cutter's vaccine had prevented adequate exposure of virus particles to formaldehyde. Later, safer inactivated polio vaccines successfully decreased the incidence of poliomyelitis (Nathanson & Langmuir, 1995; Offit, 2005).

"Provocation poliomyelitis" in 1980s again became an important issue when WHO introduced vaccines into third world countries where poliovirus epidemics were occurring and children were reported to develop paralysis after vaccination. Studies

proposed that injections within 30 days of onset were a risk factor for paralysis. Although some refused the findings, injections were done more carefully in epidemic regions (Mawdsley, 2014; Strebel, Ion-Nedelcu, Baughman, Sutter, & Cochi, 1995).

The most likely mechanism for "poliovirus provocation" was first published in 1998 by State University of New York. Injured tissues from the physical act of injection induces retrograde axonal transport of poliovirus and thereby facilitates viral invasion of the central nervous system and the progression of spinal cord damage. It was also proposed that other enteroviruses may cause "provocation poliomyelitis" (Gromeier & Wimmer, 1998). As far as we are aware, there have been no report of EV-A71 causing a "provocation poliomyelitis"-like phenomenon.

2.1.6 Autopsy findings in EV-A71 CNS infection

Upon gross assessment of the brain, flattened cerebral gyri, shallowed intervening sulci and cerebral oedema may be observed (Yang et al., 2009). Under light microscopy, inflammation was found in different regions of CNS including all levels of the spinal cord, brainstem and cerebrum (especially hypothalamus and cerebellar dentate nucleus) (Ong & Wong, 2015). Typical viral encephalitic features such as widespread perivascular cuffing, mild mononuclear meningitis, multifocal necrosis, microglial nodules and neuronophagia were observed. However, no viral inclusions were found. These neuropathological changes were mostly found in the medulla, pons, midbrain posterior to the corticospinal tracts (crus cerebri), hypothalamus, subthalamic nucleus and grey matter of anterior and posterior horns of spinal cord. Inflammation in the cerebral cortex was less intense and mostly in the motor cortex (Ong & Wong, 2015; Yang et al., 2009).

EV-A71 antigens and RNA can be found in inflamed regions, although the viral antigens/RNA may be very focal even in severely inflamed areas. EV-A71

antigens/RNA had been shown in the cytoplasm of neuronal cell bodies, processes and inflammatory cells (Ong & Wong, 2015). The inflammatory cells were predominantly CD68+ macrophages/microglias, followed by CD15+ neutrophils, CD4+ lymphocytes, CD8+ lymphocytes and a small percentage of CD20+ B cells. CD68+ macrophages were mostly found in the brainstem, meninges, perivascular areas and in microglia nodules. Whereas, CD15+ neutrophils, lymphocytes and B cells were mainly found as perivascular cuffing and in meninges (Ong & Wong, 2015; Yang et al., 2009).

Some cases showed pulmonary oedema with or without inflammation. However, EV-A71 was never isolated from any lung samples nor antigens/RNA localised within the lung. Whereas, viruses had been isolated from myocardium although the antigens/RNA staining were negative so far. Other organs positive for viral isolation were tonsils, intestine and pancreas (Ong & Wong, 2015).

In conclusion, autopsy studies of EV-A71 patients suggest that EV-A71 could reach the CNS via peripheral motor nerves via retrograde axonal transport, and both severe brainstem encephalomyelitis and neurogenic pulmonary oedema were the major cause of death.

2.1.7 Neuropathogenesis

Neuropathogenesis of EV-A71 infection is actively being studied at the moment. At least two possible mechanisms may be involved in direct neuronal damage by apoptosis/necrosis and immune mediated neuronal damage (Weng et al., 2010). EV-A71 antigens and RNA were often detected in degenerated neurons and in neurons being phagocytosed (neuronophagia) in human autopsy cases and several animal models, suggesting viral cytolysis as a pathogenic mechanism (Ong & Wong, 2015). However, several *in vitro* experiments have suggested that EV-A71 induced apoptosis can occur. Phosphatidylserine had been detected on the outer plasma membranes

indicating an early apoptosis event in EV-A71 infected neuronal cells (S. C. Chang, Lin, Lo, Li, & Shih, 2004). In addition, S. C. Chang et al. (2004) had shown that efflux of cytochrome c from the mitochondria to cytoplasm, and cleaved activated caspase 9 which could lead to apoptosis. In another study, EV-A71 infection triggered Abl and thus activated the cyclin-dependent kinase 5 kinase activity which led to neuronal apoptosis (S. C. Chang et al., 2004). In addition, Li et al. (2002) had shown that EV-A71 3C protease is a key factor in apoptosis. Transient expression of EV-A71 3C protease in SF268 cells (human glioblastoma cell line) caused DNA fragmentation by the caspase 3 pathway. In another study, host cell mRNA polyadenylation could be impaired by cleavage of EV-A71 3C protease protein leading to apoptosis (Weng, Li, Hung, & Shih, 2009).

Another mechanism of tissue injury induced by inflammation in adjacent CNS regions (bystander effect) cannot be excluded. In autopsy studies, the extensive areas of inflammation within the CNS could be due to immune dysregulation by inappropriate activation of pro-inflammatory cytokines, whose actions lead to pathological consequences/ neuronal damage of non-infected cells (Ong & Wong, 2015). Infected inflammatory cells are believed to trigger the pro-inflammatory cytokines production in patients with severe EV-A71 infection. Infected human T cell lines (Jurkat), macrophage cell lines (THP-1) and human peripheral blood mononuclear cells were found to be infected *in vitro* to produce Tumor Necrosis Factor-α (TNF-α) and "macrophage migration inhibitory factor" (MIF) (Gong et al., 2012). Whereas, infected human dendritic cells via the "Dendritic Cell-Specific Intercellular adhesion molecule-3-Grabbing Non-integrin" (DC-SIGN) receptor could trigger the production of IL-6, IL-12 and TNF-α (Y. W. Lin, Wang, Tung, & Chen, 2009). EV-A71 infection could also activate the "nuclear factor kappa-light-chain-enhancer of activated B cells" (NF-κB) pathway which leads to production of Interferon-β (IFN-β) and TNF-α (Chu et al., 1999)

and could increase the expression of "vascular cell adhesion molecule 1" (VCAM-1) which facilitates the binding of neutrophils and leukocytes to "vascular smooth muscle cells" (VSMC) (Tung et al., 2007). Expression of "cyclooxygenase-2" (COX-2), a neurotoxic mediator, increase with EV-A71 infection in SK-N-SH cells. The metabolite of COX-2, "Prostaglandin E2" PGE2, had been shown to accelerate EV-A71 infection in cells (N. Chen & Reis, 2002; Hinson & Tyor, 2001). Lastly, the immune mediated auto-antigen effect cannot be excluded. Fan et al. (2015) suggested that the common epitope between VP1 of EV-A71 and "human mediator complex subunit 25" could lead to autoantigen effect.

2.2 Immune response

Innate immunity, the non-antigen-specific immunity, is the early phase defence against viral infection. It reacts immediately to kill pathogens, by activating the adaptive immunity as well (Elgert, 2009; Levinson & Jawetz, 1992). Immune cells, such as macrophages, and non-immune cells, such as epithelial cells, have "pattern-recognition receptors" (PPRs) located on the surface of cell membranes, within the cytoplasm or in the endosome (Elgert, 2009; Levinson & Jawetz, 1992). PPRs can be triggered by two classes of molecules: "Pathogen-Associated Molecular Pattern" (which included viral DNA/RNA and bacterial lipopolysaccharide), and "Danger Associated Molecular Pattern" (endogenous molecules released from stressed or dying cells such as heat shock protein, high-mobility group box1, cytosolic RNAs, cytosolic DNAs and mitochondria DNAs). All these signals activate innate immunity and pro-inflammatory responses (Pathinayake, Hsu, & Wark, 2015).

There are three major types of PPRs; namely "toll-like receptors" (TLRs), "retinoic acid-inducible gene I like receptors" (RLRs) and "nucleotide oligomerisation domain like receptors" (Pathinayake et al., 2015). Picornaviruses are mainly recognised

by “melanoma-differentiation-associated” (MDA5), RLRs. Binding of viral RNA leads to conformation changes on MDA5, and activation of a series of cascade effects downstream (Gitlin et al., 2006). Briefly, MDA5 activates the mitochondrial antiviral signalling to phosphorylate “interferon regulatory factor 3” (IRF-3) and IRF-7, thereby resulting in the expression of the type I IFN gene (Gitlin et al., 2006; Kato et al., 2006). NF-κB is also activated by mitochondrial antiviral signalling, and in turn activates pro-inflammatory cytokines, adhesion molecules, chemokines, acute phase proteins and inducible enzymes (Takeuchi & Akira, 2008). In addition, TLR3, a member of TLRs, can be activated by RNA of picornaviruses, to activate the NF-κB (Oshiumi et al., 2011). Several studies show that 3C and 2A protease of EV-A71 are the main antagonists of innate immunity by cleaving and binding to different antiviral signalling molecules (such as MDA5, IRF3, IRF7, cellular micro RNAs, mitochondrial antiviral signalling and NF-κB.) (Pathinayake et al., 2015).

Natural killer (NK) cells are also important in innate immunity. Type 1 IFN can increase NK cells cytotoxicity through perforin to cause death of infected cells. Besides, “killer immunoglobulin-like receptors” on NK cells can recognise downregulation of “major histocompatibility complex” (MHC) class I molecules, as transformation or virus infection are known to downregulate its expression. In addition, NK cells can activate both dendritic cells and T cells which are involved in adaptive immunity (Paust, Senman, & von Andrian, 2010; Warren & Smyth, 1999).

Adaptive immunity is involved in a later phase of infection and is important for immunological memory. It is highly antigen-specific and can be divided into cell-mediated and humoral immunity (Elgert, 2009; Pathinayake et al., 2015). Little is known about cell-mediated immunity response to EV-A71 infection, even for other picornaviruses such as poliovirus and coxsackievirus (Dotzauer & Kraemer, 2012; Paust et al., 2010). Dendritic cells and macrophages had been shown to be important antigen

presenting cells via MHC class II molecules in poliovirus and coxsackievirus infection (Dotzauer & Kraemer, 2012). EV-A71 specific CD4+ T cells (T helper cells) were induced in vaccinated children in a few vaccine trial studies (Collins, 1974; L. Liu et al., 2015; Ng et al., 2015; F. C. Zhu et al., 2013). In general, activated T helper 1 cells produce the cytokines IFN-γ and IL-2. IFN- γ secreting T cells had been shown in vaccinated EV-A71 patients, which theoretically can lyse the infected cells via activation of NK cells. Activated T helper 2 cells produce IL-4, IL-5 and IL-10 which are important to regulate antibody and allergic responses (Seder & Hill, 2000). In addition, virus-specific cytotoxic T lymphocytes (CD8+) are believed to be important in preventing viral multiplication. These cells had been shown to help in viral elimination in poliovirus infection via MHC class I pathway (Dotzauer & Kraemer, 2012). However, coxsackieviruses had been reported to strongly inhibit antigen presentation via MHC class I pathway and thus evade CD8+ T cell immunity (Kemball, Alirezaei, & Whitton, 2010).

Humoral immunity is activated when B cell receptors are activated by specific antigens via T cell independent (TI) or dependent (TD) pathways. TI response is faster but is short-lived compared to the TD response. After exposure to viral particles or RNA, the TI response leads to secretion of Immunoglobulin M (IgM) antibodies. TD response is activated when naïve T helper cells or T helper cells recognise the presented viral particle on the MHC class II molecule, resulting in cytokine production which is important in B cell proliferation and antibody production (mainly IgG). IgG antibodies are important for long-term memory (Elgert, 2009). All these neutralising antibodies are important in controlling viraemia and hence could help with the infection (Dotzauer & Kraemer, 2012; Kemball et al., 2010). In addition, certain antibodies could activate the complement system to eliminate infected cells (Elgert, 2009).

Neutralising antibodies could be present in adults, especially in regions with EV-A71 epidemics. Luo et al. (2009) had shown that about 50-60% of pregnant women had serum EV-A71 antibodies which helped in protection against EV-A71 infection immediately after birth. However, the maternal antibodies decline and are almost undetectable in 99% of infants by 6 months (Kim et al., 2015; Luo et al., 2009; E. E. Ooi, Phoon, Ishak, & Chan, 2002). Pre-existing maternal neutralising antibodies could interfere with the production of neutralising antibody secreting cells following active immunisation (Kim et al., 2015). Consequently, EV-A71 vaccines were suggested to target infants > 6 months of age.

2.3 Animal models

The only natural host for EV-A71 infection is human beings. Severe outbreaks in 1990s in the Asia Pacific region, drove researchers to develop several animal models for EV-A71 studies as summarised by Y. F. Wang and Yu (2014) in Table 2.1.

Up to date, none of the models are perfect. Different monkey models (Cynomolgus monkey, adult and neonatal rhesus monkeys) present different tissue tropism, primary viral replication sites and disease manifestations. However, observations in monkey studies had advanced our understanding on viral transmission, clinical manifestations, pathogenesis, viral distribution and immune responses of EV-A71 infection (Y. F. Wang & Yu, 2014). Infected cynomolgus monkeys display both pyramidal tract signs (flaccid paralysis) and extrapyramidal tract signs (including tremor and ataxia) with a broad viral antigen distribution that involves the spinal cord, brainstem, cerebellar cortex, dentate nuclei and cerebrum which was similar to humans (Table 2.1). However, the monkeys do not manifest cutaneous lesions or develop pulmonary oedema (Arita et al., 2007; Arita et al., 2005). Neonatal rhesus monkeys did demonstrate HFMD-like papules and vesicles on the limbs and in the mouths. Although

both medulla oblongata and thalamus contain very high virus titres and display neuropathological lesions, the neonatal rhesus monkeys did not display the typical neurological complications such as flaccid paralysis and ataxia (H. Chen et al., 2012).

So far, mouse models are more frequently used in EV-A71 research. Several infected mouse models demonstrated strong neuronotropism in the CNS which shared many features with the human encephalomyelitis. These models strengthened the hypothesis that virus enters the CNS via peripheral motor nerves (Table 2.1). However, these animal models showed age-dependent susceptibility toward EV-A71 infection and demonstrated strong myotropism. In addition, pulmonary oedema was not demonstrated in any of the models. Virus strains produced by passaging to adapt virus to mouse models have been attempted but full infectivity in adult mice has not been achieved (Table 2.1). In 2013, a SCARB2 Tg mice model became available. These hSCARB2-expressing mice exhibited ataxia, paralysis, and death after infection. The pathological features in these mice were generally similar to those of EV-A71 encephalomyelitis in humans and experimentally infected monkeys. Although the Tg mice showed some level of muscle infection, it should be useful to replace the monkey and other mice models (Y. F. Wang & Yu, 2014). Recently, an orally-infected hamster model for EV-A71 encephalomyelitis which demonstrated squamous lesions in the paws, skin and oral cavity reminiscent of HFMD was described by Phyu et al. (2016). This hamster model which was consistently infected via the natural oral route should be useful to study squamous epitheliotropism, neuropathogenesis, oral/faecal shedding in EV-A71 infection, person-to-person transmission, and to test anti-viral drugs and vaccines.

Table 2.1 Enterovirus 71 animal models for pathogenesis studies (adapted from Y. F. Wang & Yu, 2014)

Animal	Virus strain	Infection route/dose	Clinical manifestations, viral replication and other remarks	Ref
Non-human primate				
Cynomolgus monkey	Clinical isolates and prototype BrCr	IS/10^6 $CCID_{50}$ IV/$10^{5.5}$ to 10^7 $TCID_{50}$	Neurological manifestations including pyramidal and extrapyramidal tract signs, such as flaccid paralysis, tremor and ataxia. The virus replicated in the spinal cord, brainstem, cerebellum and cerebrum. EV-A71 had a wider neurotropism than that of polioviruses.	(Arita et al., 2007; Arita et al., 2005)
Rhesus monkey, adult	Clinical isolate (FY-23, C4 genotype)	IC, IV/$10^{6.5}$ $CCID_{50}$	Monkeys developed CNS infection and neuronal impairment with extra-neuronal pathological changes confined to the lung tissues but not in the pancreas and spleen, where high viral loads were detected. Infiltration of inflammatory cells in the caudate nucleus, pontine nucleus and substantia nigra; neurons retrogression; and pronounced perivascular cuffing	(Zhang et al., 2011)
Rhesus monkey, neonate	Clinical isolate (FY-23, C4 genotype)	IT/$10^{4.5}$ $CCID_{50}$ Oral/$10^{6.5}$ $CCID_{50}$ twice	HFMD-liked papules and vesicles were found on the limbs and in the mouth after intra-tracheal infection. However, neurological complications were not observed. High viral titres were transiently detected in the brown adipose tissue, skeletal muscle and CNS (thalamus, pons and spinal cord).	(H. Chen et al., 2012)
Rodents (immunocompetent)				
ICR, 1 to 14-day-old mouse	Mouse-adapted EV-A71 strain (MP4, C2 genotype)	Oral/5 x 10^6 pfu IM/5 x 10^3 pfu IC/5 x 10^4 pfu	Mice developed rear limb paralysis with massive and widespread necrotising myositis, and neuronal loss and apoptosis in the spinal cord and brainstem before death. The spinal cord, brain and muscle were the major organs for virus replication in the late phase of infection. Retrograde axonal transport in peripheral nerves might represent the major transmission route of EV-A71 in mice.	(Y. F. Wang et al., 2004)
BALB/c, 1 to 7-day-old mouse	Mouse-adapted strain (MP-26 M)	IC/3.4 x 10^4 $TCID_{50}$ IM/3.4 x 10^3 $TCID_{50}$ IP/3.4 x 10^4 $TCID_{50}$	Mice developed limb paralysis followed by death. Skeletal muscle displayed severe necrotising myositis and contained a high viral load. Virus was also isolated from the blood, heart, liver, spleen and brain. The VP1 mutation (G145E) alone was sufficient to increase virulence in mice.	(B. H. Chua, Phuektes, Sanders, Nicholls, & McMinn, 2008)

Table 2.1, continued

Animal	Virus strain	Infection route/dose	Clinical manifestations, viral replication and other remarks	Ref
ICR, 2-week-old mouse	Mouse-adapted strain (MAVs, B3 genotype)	IC, IP, SC, oral/10^5 $CCID_{50}$ IM/3 x 10^5 $CCID_{50}$	Mice developed paralysis followed by death after IC, IP, SC and IM infection but not after oral administration of the virus. The highest viral titres were detected in the skeletal muscle, spleen and spinal cord. The virus might enter the CNS via peripheral motor nerves after skeletal muscle infection.	(Ong et al., 2008)
	Mouse muscle-adapted strain (Fuyang-0805a, C4 genotype)	IP/10^5 $TCID_{50}$	Mice showed strong myotropism manifesting as severe necrotising myositis in both skeletal and cardiac muscles. Virus was detected in the muscle, heart and intestines.	(W. Wang et al., 2011)
Syrian golden hamsters, 2-week-old	Mouse-adapted strain (MAVs, B3 genotype)	Oral/10^4 $CCID_{50}$	Mice demonstrated macroscopic cutaneous lesions around the oral cavity and paws. Viral antigens/inflammation were found in squamous epithelium (lip, oral cavity, paw, skin, and oesophagus), neurons (brainstem, spinal cord, sensory ganglia), acinar cells (salivary gland, lacrimal gland), lymphoid cells, and muscle fibres, liver and gastric epithelium. In addition, virus could be isolated from oral washes and faeces.	(Phyu et al., 2016)
Rodents (immunodeficiency)				
NOD/SCID, 3- to 4-week old mouse	NOD/SCID mouse-adapted strain (EV-A71(NOD/SCID), B1 genotype)	IC/10^6 $CCID_{50}$	Infected mice showed hindlimb paralysis. Viral RNA was first detected in the CNS and serum, followed by high copy numbers in the heart, skeletal muscle and spinal cord.	(Arita, Ami, Wakita, & Shimizu, 2008)
AG129, 10-week-old mouse	A129 and AG129 mouse-adapted strain (B2 genotype)	IP/5.2 x 10^4 $TCID_{50}$	Infected AG129 mice, but not A129 mice, developed limb paralysis, eye irritation, loss of balance and movement control, and exhibited high mortality.	(Caine, Partidos, Santangelo, & Osorio, 2013)

Table 2.1, continued

Animal	Virus strain	Infection route/dose	Clinical manifestations, viral replication and other remarks	Ref
AG129, 2-week-old mouse	Clinical isolate (5865/SIN/00009, B4 genotype)	IP/10^6 pfu Oral/10^7 pfu	Infected mice displayed progressive limb paralysis before death. Virus replication resulted in massive damage in the limb muscles, brainstem and anterior horn of the spinal cord. Low viral particles in the limbs after oral inoculation indicated that the paralysis was a consequence of EV-A71 neuroinvasion rather than myositis.	(Khong et al., 2012)
Gerbils, 21-day-old	Clinical isolate (EV-A71/58301, C4 genotype)	IP/10^5 $TCID_{50}$	Infected animals developed hindlimb paralysis, slowness and ataxia before death. Significantly high viral titres were detected in the spinal cord, brainstem and skeletal muscle.	(Yao et al., 2012)
Transgenic mice				
PSGL-1, 10-day-old	Clinical isolates C4 genotype and Mouse muscle-adapted strain (Fuyang-0805a, C4 genotype)	IP/10^8 $TCID_{50}$	Susceptible to a mouse muscle-adapted EV-A71 strain and not the clinical isolates, exhibiting severe infection that was comparable to those of the wild-type mice upon EV-A71 infection. High viral titres were detected in the muscle, spinal cord and brain after mouse-adapted virus infection. This study concluded that human PSGL-1 alone was not sufficient to facilitate EV-A71 infectivity in mice.	(J. Liu et al., 2012)
SCARB2, 1- to 14-day-old	Clinical isolates, C2, C4, B4 and B5 genotypes and CA16	SC/3 x 10^4 to 10^6 pfu	EV-A71 B genotypes were capable of inducing HFMD-like lesions and neurological disease with limb paralysis in 1-day-old but not Tg mice older than 2 weeks. In contrast, 7- and 14-day-old but not 21-day-old Tg mice were more susceptible to the EV-A71 C genotypes and coxsackievirus A16, exhibiting more severe CNS disease, limb paralysis and death than non-Tg mice.	(Y. W. Lin et al., 2013)
SCARB2, 3-week-old	Clinical isolates (Isehara/Japan/99, C genotype)	SC, IV, IP, oral/10^4 to 10^6 $TCID_{50}$	Mice displayed ataxia, paralysis and death. The CNS, including the spinal cord, brainstem, cerebellum, cerebrum, hypothalamus and thalamus, was the major replication site for the virus, which is similar to the human. Nonetheless, Tg mice were less susceptible to oral infection and pulmonary oedema was not observed. Adult Tg mice did not display the typical cutaneous lesions found in human HFMD.	(Fujii et al., 2013)

IS:intra-spinal; IV:intra-venous; IC:intra-cranial/intra-cerebral; IT:intra-tracheally; IP:intra-peritoneal; IM:intra-muscular; SC: subcutaneous
HFMD: Hand foot mouth disease; PSGL-1: P-selectin glycoprotein ligand-1; SCARB2: scavenger receptor class B member 2

In this laboratory, an EV-A71 encephalomyelitis mouse model that shared many features with human CNS disease was developed, using a "mouse-adapted virus strain" (MAVS). This model, generally demonstrated similar tissue tropism, including neurotropism by most routes of infection (IP, IM, SC and oral). Despite the presence of only sparse inflammation, the distribution of CNS viral RNA and antigens seems to parallel the distribution of inflammation and virus in human EV-A71 encephalomyelitis. Anterior horn of spinal cord, medulla, pons (sparing the pontine nuclei), midbrain, and lateral cerebellar nucleus were often severely infected (Ong et al., 2008). These were also the areas in which inflammation was found to be severe in human cases. In addition, the rarity and absence of virus in the murine motor cortex and cerebellar hemisphere, respectively, also seem to resemble the human infection. Although peripheral nerve viral transmission was first reported using another mouse model (C. S. Chen et al., 2007), based on findings in this model, peripheral spinal motor nerves were postulated to be responsible for viral entry into the CNS, most likely by retrograde axonal transport after skeletal muscle infection.

2.4 Anti-viral therapeutics and vaccines

2.4.1 Inactivated vaccines

Various types of inactivated EV-A71 vaccines have been reported. However, the 3 leading and best developed and/or tested vaccines are all formalin-inactivated EV-A71, subgenotype C4, vaccines (Z. Liang & Wang, 2014). All three vaccines had completed phase III clinical trials and one of them, had just been approved by the China Food and Drug Administration in December 2015 (Mao, Wang, Bian, Xu, & Liang, 2016). From the clinical reports, these vaccines were able to induce high "Geometric Mean Titres", and thus could potentially prevent 80% of EV-A71 associated diseases (F. C. Zhu et al.,

2013; F. Zhu et al., 2014). Unfortunately, these vaccines were all prepared from a single subgenotype C4 strain, and thus showed limited cross-immunity and cross-neutralisation of other genotypes (Z. Liang & Wang, 2014; Ng et al., 2015). This may be challenging if the vaccines are deployed worldwide, as different EV-A71 genotypes circulate in different regions at different times. For example, subgenotype B3 was circulating during the 1997 outbreak in Sarawak, Malaysia (Cardosa et al., 2003), while subgenotypes B4 and C1 dominated in the 2000 outbreak. Subgenotype B5 and C1 was circulating during the 2005 outbreak in Peninsular Malaysia (K. B. Chua et al., 2007). Genomic sequence variations found in different subgenotypes and the antigen destruction/masking by formaldehyde could be some of the reasons behind this limited cross-immunity of the vaccines (Wilton, Dunn, Eastwood, Minor, & Martin, 2014). It is possible that limited cross-immunity could trigger "antibody-dependent enhancement" in which antibodies against the one EV-A71 subgenotype binds to but does not neutralise other subgenotypes, thus enhancing viral entry into the cells (R. Y. Cao et al., 2013; Han et al., 2011; Tirado & Yoon, 2003; S. M. Wang et al., 2010). Furthermore, although these vaccines were intended for use in regions where subgenotype C4 is predominant, there is always the possibility that other subgenotypes may shift to this region and this has to be taken into consideration.

2.4.2 Baculovirus-expressed vaccines

Baculovirus is a lepidopteran-specific (insect-specific) pathogen widely used in protein expression nowadays because of its ability to express native conformation-eukaryotic proteins by post-translational modification, and to produce multi-protein subunit complexes with tertiary structures, which cannot be done in E. coli expression systems (Jarvis, 2009). With the baculovirus system, several groups had successfully produced

EV-A71 virus-like particles (VLPs) which were similar to the native viruses without the viral genome. These VLPs had proven to induce high neutralising titres of up to 1:5042. Particles with complete viral surfaces are able to stimulate both innate and cell-mediated immunity (Chung et al., 2010; Ku et al., 2013; S. Y. Lin et al., 2015). Unfortunately, baculovirus expression systems are too low-yielding and too expensive for mass production of VLPs, despite efforts to increase the yield using different cells.

Others had tried to express the VP1 protein on the surface of the baculovirus envelope, also known as baculovirus surface display vaccines, to improve yield of VLPs. Although the sera derived from this system have neutralising titres lower than the conventional baculovirus system, it is still higher compared to titres with formalin inactivated vaccines. Currently, research groups are focusing on co-display all three VP1-3 on the baculovirus to induce more neutralising epitopes (Meng, Kolpe, Kiener, Chow, & Kwang, 2011; Premanand et al., 2012).

2.4.3 Intravenous immunoglobulin (IVIG) treatment

IVIG, a highly purified blood product containing IgG antibodies, have been actively used in immunocompromised or autoimmune disease patients to provide passive immunisation against infectious diseases such as tetanus, botulism, hepatitis B, rabies, and varicella. In severe cases of EV-A71 infection, it has been successfully used to change both pro- and anti-inflammatory cytokine levels and thus save the patient's life. Moreover, neutralising antibodies against EV-A71 found therein may play a therapeutic as well as prophylactic role. However, IVIG products are subjected to batch-to-batch variations, as a result of blood pooling from a large group of healthy individuals contributing to different compositions and thus different degrees of effectiveness and consistency. Besides, use of blood-derived products could lead to spread of blood-borne

pathogens (R. Cao et al., 2010; Hemming, 2001; Jolles, Sewell, & Misbah, 2005; S. M. Wang et al., 2006).

2.4.4 Monoclonal antibody (MAb)

Specific neutralising antibodies are important in antiviral immunity for preventing and modulating viral infections such as infections by respiratory syncytial virus, human immunodeficiency virus, cytomegalovirus, hepatitis C virus and rabies (Hemming, 2001). Many researchers have reported that anti-EV-A71 MAbs targeted against VP1, VP2 and VP3 are effective against EV-A71 infection (G. H. Chang et al., 2010; Deng et al., 2015; D. L. He et al., 2012; Kiener, Jia, Meng, Chow, & Kwang, 2014; Lee et al., 2013; Lim et al., 2012; C. C. Liu et al., 2011; Xu et al., 2014). However, to date, only 2 antibodies, showed cross-immunity against all EV-A71 subgenotypes, and both of them are IgM antibodies (Ng et al., 2015). As there are no licensed vaccines available at the moment, passive immunisation of antibodies may offer an effective prophylactic/therapeutic measure against encephalomyelitis, to reduce morbidity and mortality. Although a few studies described the efficacy of antibodies in early infection (Bek et al., 2011; G. H. Chang et al., 2010; H. W. Chang et al., 2013; Foo, Alonso, Chow, & Poh, 2007; Y. X. Li et al., 2014; Z. Li et al., 2014; Liou et al., 2010; Tian et al., 2012; Xu et al., 2014), the effectiveness of antibodies after disease onset or more importantly after CNS involvement has not been adequately investigated (Ng et al., 2015). Hence, the effectiveness of MAb was tested in CNS infected mice as part of our investigations.

3.0 Materials and methods

The majority of the work was done at the University of Malaya, Malaysia while all the primary motor neuron studies (section 4.3.3, page 81; section 4.4, page 83) were performed at the Tokyo Metropolitan Institute of Medical Science, Japan.

3.1 Cell lines

African green monkey kidney (VERO) cells were grown in Dulbecco's Modified Eagle Medium (DMEM; Sigma, USA) growth medium (GM), supplemented with 5% foetal bovine serum (FBS), 0.02 M HEPES (pH 7.4), 0.0825% sodium bicarbonate, 1 mM sodium pyruvate and 50 µg/mL gentamycin. Infected VERO cells were maintained in DMEM maintenance medium (MM) supplemented with 2% FBS, 0.02 M HEPES, 0.19% sodium bicarbonate and 1 mM sodium pyruvate and 50 µg/mL gentamycin.

In the Tokyo laboratory, human rhabdomyosarcoma (RD) cells transfected with hSCARB2 receptor gene were grown in RPMI-1640 GM, supplemented with 10% FBS or 6% FBS for MM. These cells were used for virus titration analysis in section 4.4.1.1 (page 83), according to approved protocols submitted to the Animal Use and Care Committee, Tokyo Metropolitan Institute of Medical Science.

3.2 Virus preparation and concentration

All the viruses used in this project (Table 3.1) were propagated in VERO cells or RD cells at a multiplicity of infection (MOI) of 0.1 until 90% of cells showed cytopathic effect (CPE). The infected cells were subjected to 3 freeze-thawing cycles before centrifugation at 4000 rpm, 4°C for 15 min to remove cell debris. The supernatant was then further concentrated by polyethylene glycol (PEG) precipitation as described previously (Yamamoto, Alberts, Benzinger, Lawhorne, & Treiber, 1970). Briefly, PEG 6000 (Fluka, USA) and sodium chloride were added to the virus suspension to a final concentration of 8% (wt/vol) and 0.3 M, respectively. The mixture was stirred overnight at 4°C and centrifuged at 4000 x g, 4°C for 1 hour (hr). The PEG 6000-supernatant was discarded, and virus-containing pellet was re-suspended in a small volume of phosphate buffer saline (PBS, pH 7.4) and filtered through a 0.2 µM pore size filter. Small aliquots were stored at -80^{o}C. Virus stock titre was determined by standard microtitration assay in VERO cells (section 3.6.1.2, page 37).

Table 3.1: Virus strains used and their characteristics

Virus (Subgenogroup)	Virus designation	Genebank No	Country	Year isolated	Clinical syndrome	Used in section	Page
EV-A71 (C1)	9522	AY258300	Malaysia	2003	HFMD*	4.6.2	100
EV-A71 (C2)	8M/6/99	AY126012	Australia	1999	Myelitis	4.6.2	100
EV-A71 (C3)	001-KOR-00	AY125966	Korea	2000	HFMD*	4.6.2	100
EV-A71 (C4)	VN5559	AM490152	Vietnam	2005	HFMD*	4.6.2	100
EV-A71 (C5)	VN5784	AM490158	Vietnam	2005	HFMD*	4.6.2	100
EV-A71 (B3)	13903#	AY207648	Malaysia	1997	Encephalomyelits	4.6.2	100
EV-A71 (B3)	MAVS#	-	-	-	-	4.2, 4.3.1, 4.3.2, 4.5 and 4.6	51, 68, 74, 87, 94
EV-A71 (B4)	A10/4	AF376067	Malaysia	2000	HFMD*	4.6.2	100
EV-A71 (B5)	18431	NA$	Malaysia	2006	Encephalomyelitis	4.6.2	100
CV-A16	North	NA$	Malaysia	2006?	HFMD*	4.6.2	100
EV-A71 (B3)**	MAVS#	-	-	-	-	4.3.3	81
EV-A71 (B3)**	SK-EV006/Malaysia/97	AB051331	Malaysia	1997	Encephalomyelits	4.4	83

*HFMD = Hand, foot and mouth disease
#MAVS is a mouse adapted virus from the EV71 parental, clinically-isolated 13903 strain
$NA = not available
**These viruses were propagated in RD cells, while the rest of the viruses were propagated in VERO cells.

3.2.1 Preparation of fluorescence-labelled EV-A71

EV-A71 (SK-EV006/Malaysia/97 virus) was fluorescence-labelled according to the manufacturer's protocol (Molecular Probes, USA). Briefly, purified EV-A71 in 0.1 M sodium bicarbonate solution was prepared by dialysis. The total protein concentration of the virus was measured using Pierce BCA Protein Assay Kit (Thermo Fisher, USA) according to manufacturer's protocol. Then 50 µL of 1.0 M bicarbonate (pH 8.3) was added to 0.5 mL of 2 mg/mL virus followed by a vial of reactive dye. After stirring at room temperature (RT) for an hour in the dark, excess dye was removed by a NAP5 resin column. The fraction containing the labelled virus was determined by absorbance measurements at 280 nm and 555 nm. The degree of labelling was calculated using the manufacturer's formula. Virus titre was determined by a standard microtitration assay using RD hSCARB2 cells (section 3.6.1.2, page 37).

3.2.2 Preparation of light-sensitive MAVS

MAVS was propagated in VERO cells at an MOI of 0.1 for an hour at 36°C. Then, MM supplemented with 10 µg/ml of neutral red was added and incubated in the dark until 90% of cells showed CPE (about ~ 6 days). Viruses were harvested as usual (section 3.2, page 30) via freeze-thaw cycles but the whole process was performed in the dark.

3.3 Preparation of hyperimmune sera against MAVS

All animal experiments were approved and performed in Malaysia, according to the University of Malaya's Animal Welfare and Use Committee guidelines (2014-02-14/PATHO/R/WKT). Hyperimmune sera with neutralising antibodies against MAVS were prepared by inoculating 16 µg of formaldehyde-inactivated MAVS virus,

containing 0.5 mg/mL aluminium hydroxide as adjuvant, into a group of 6-8 week-old ICR mice (n= 40), followed by 2 boosters given 2 weeks apart via the intra-peritoneal (IP) route. Mock-immunised mice received the same concentration of formaldehyde-fixed VERO cell lysates. All mice were sacrificed 6-week post-immunisation or 3 days after the second booster. Blood was harvested by cardiac puncture at the time of euthanasia, and sera separated, pooled and heat-inactivated at 56°C for 30 min. Sera were tested for neutralising antibodies against EV-A71 by the microneutralisation test using VERO cells (section 3.5, page 34) as described previously (Ong, Devi, Cardosa, & Wong, 2010).

3.4 Preparation of specific monoclonal antibody against MAVS

BALB/c mice were immunised with MAVS by IP inoculation of approximately 10^5 $CCID_{50}$ (50% cell culture infective dose) virus emulsified in complete or incomplete Freund adjuvant (Sigma-Aldrich, USA), in a total of 3 inoculations given 3 weeks apart. Three days after the last booster (without adjuvant), the spleen cells were harvested, and fused with SP2/0 mouse myeloma cells at a ratio of 10:1 as described previously (Lim et al., 2012). The fused cells were suspended in hypoxanthine-aminopterin-thymidine medium. After 10 to 14 days, the supernatant from wells with hybridoma cells were screened by a microneutralising assay as described previously (section 3.5, page 34) (Ong et al., 2010). Hybridoma cells secreting neutralising antibodies were subcloned by limiting dilution and cultured as described previously (Lim et al., 2012). A monoclonal antibody (MAb) designated as MAb 3D1 was selected out of 48 clones for further experiments because it demonstrated complete neutralisation against EV-A71 in the neutralising assay.

3.4.1 MAb characterisation

MAb isotype was determined using the commercially-available IsoStrip Mouse Monoclonal Antibody Isotyping Kit (Roche, German), by dipping the strip into the MAb solution. The Pierce™ BCA Protein Assay Kit (USA) was used for measurement of the protein concentration. Briefly, 25 µL of samples were mixed well with 200 µL of working solution in a 96 well plate. After incubation at 37°C for 30 min, the plate was allowed to cool before absorbance reading at 540 nm.

3.5 Microneutralising assay

Two-fold dilutions of heat inactivated sera or MAb (1:2 to 1:1024) in MM were prepared. Diluted sera or MAb was mixed with equal volumes of 100 $CCID_{50}$ EV-A71 (Table 3.1, page 31) at 37°C for 2 hr and then transferred to duplicate wells containing 90%-confluent VERO cells and incubated at 36°C for 7 days. In this way, neutralising titres defined as the highest dilution of serum that completely inhibited CPE for EV-A71 (C1 – C5 and B3 – B5, Table 3.1, page 31) were determined. Negative control wells contained cells incubated with MM only while positive control wells contained cells incubated with a mixture of MM and virus without any antibodies.

3.6 Mouse infection experiments

All animal experiments were approved and performed in Malaysia, according to the University of Malaya's Animal Welfare and Use Committee guidelines (2014-02-14/PATHO/R/WKT). Hence all mice were sacrificed with lethal dose of isoflurane at the end of experiment or at the moribund stage. Table 3.2 summarises all the animal experiments done in this study.

Table 3.2: Summary of mouse infection experiments

Section	Objective	Page
3.6.1	To investigate cranial nerve involvement in direct brainstem infection.	35
3.6.2	To optimise passive immunisation in unilateral jaw/facial muscles infected mice to obligate viraemia.	38
3.6.3	To confirm unilateral retrograde axonal transport in peripheral nerves, and to show that viraemia spreads virus to contralateral side and contributes to bilateral CNS involvement.	40
3.6.4	To investigate the susceptibility of neurons to MAVS infection, and the association of viral antigens and SCARB2 in the brain.	41
3.6.5	To investigate the "provocation poliomyelitis" phenomenon in MAVS infection following trauma to gastrocnemius muscles.	42
3.6.6	To investigate the link between muscle infection and retrograde axonal transport in spinal cord infection.	44
3.6.7	To investigate the potential of neutralising antibodies as a prophylactic and/or therapeutic against EV-A71 encephalomyelitis.	44

3.6.1 MAVS infection via unilateral jaw/facial muscle inoculation

Cranial nerve involvement in retrograde axonal transport of EV-A71 into the brainstem was investigated using groups of 2-week old ICR mice. A dose of 6.3 x 10^5 $CCID_{50}$ MAVS in 10 µL was delivered via an intra-muscular (IM) route by injecting into the unilateral jaw/facial muscles of the mouse using a 31-G needle. Groups of mice were monitored daily for signs of infection and sacrificed at 12 hours post-infection (hpi) (n= 7), 24 hpi (n= 8), 36 hpi (n= 7), 48 hpi (n =8), 60 hpi (n= 7) and 72 hpi (n= 8). Tissues were harvested from 3 animals from 12, 36 and 60 hpi, and 4 animals from 24, 48 and 72 hpi for histopathological analysis, and the remaining 4 animals from each timepoint for virus titration studies. Mock-infected mice (n= 8) were injected with PBS and sacrificed at 72 hpi and tissues harvested for analysis as described.

3.6.1.1 Histopathological analysis

Tissue fixation and processing were carried out as previously described (Tan, Ong, & Wong, 2014). In brief, the whole animal carcass was fixed in 10 % neutral buffered formalin and then transversely cut into seven standard cross-sectional tissue blocks which include all of the main organs. After overnight decalcification in 5% formic acid and routine processing, 4 µm thick sections were prepared from paraffinised tissue blocks and stained with haematoxylin and eosin (H&E) for light microscopy, immunohistochemistry (IHC) to detect viral antigens and *in situ* hybridisation (ISH) to detect viral RNA.

3.6.1.1 (a) IHC to detect viral antigens

IHC was performed as described previously (Tan et al., 2014). Briefly, slides containing tissues were dewaxed and rehydrated with serial xylene and graded alcohols, respectively. After antigen retrieval with citrate buffer (pH 6) at 99^0C for 20 min, tissue slides were allowed to cool for 10 min. This was followed by peroxidase blocking with 3% hydrogen peroxidase in methanol. Background blocking was done with 5% of normal goat serum in Tris-buffer saline (TBS). Primary polyclonal rabbit anti EV-A71 antibody (A gift from Dr Shimizu, National Institute of Infectious Diseases, Japan) diluted in PBS at 1:3000, was applied for 2 hr at RT. After TBS washing twice, goat anti-mouse secondary antibody polymer complexes (EnVision + System - peroxidase; Dako, Denmark) were added in the dark for 30 min, followed by TBS washing twice. The 3,3'-Diaminobenzidine (DAB) substrate was added and incubated for 5 min. After counterstaining with Harris hematoxylin, tissue sections were mounted with DPX mounting medium. Tissues from a previously known EV-A71 infected mouse served as positive controls whereas normal healthy mouse tissues served as negative controls.

3.6.1.1 (b) ISH to detect viral RNA

ISH was performed as described previously (Tan et al., 2014). Tissue sections were dewaxed and rehydrated as for IHC (section 3.6.1.1 (a), page 36). After treatment with hydrochloric acid and proteinase K at 37^0C for 20 min, approximately 1 ng of digoxigenin-labeled DNA probe (obtained from Ong et al. (2008)) in hybridisation buffer was applied on the tissue sections and heated at 110^0C for 12 min followed by the probe hybridisation step at 42^0C for 16 hr. Hybridised probes were visualised with an anti-digoxigenin antibody conjugated to alkaline phosphatase (Roche, Mannheim, Germany) in the dark for 16 hr and followed by nitrobluetetrazolium/5-bromo-4-chloro-3-indolyl phosphate (NBT/BCIP) substrate development. After counterstaining with Mayer haematoxylin, tissue sections were mounted with Faramount mounting medium (Dako, Denmark). Similar positive and negative tissue controls described in section 3.6.1.1 (a) (page 36) were used.

3.6.1.2 Virus titration analysis

Mouse tissues, sera, hindlimb and forelimb muscles, whole brainstems, upper half and lower half of spinal cords were harvested for viral titration. Different dissection sets and careful handling of harvested tissues were observed to prevent cross contamination between tissue types and between animals. The medium DMEM MM was added to each tissue homogenate to a final 10% (wt/vol) concentration. Serial 10-fold dilutions of homogenates in 50 µl were added to quadruplicate wells each containing 90% confluent VERO cells and incubated at 36°C for 1 hr before topping up with 100 µL of MM per well. Further incubation at 36°C for 7 days was followed by viral titre determination using $CCID_{50}$ by CPE observation and calculated using the Karber method as described

previously (Tan et al., 2014). Viral titre from each organ/tissue were pooled and calculated as a mean titre with standard error of the mean.

3.6.2 Optimisation of passive immunisation in mice infected via unilateral jaw/facial muscle

The optimum volume and inoculation times of IP-delivered hyperimmune serum that could prevent viraemia and subsequent infection of non-injected muscle groups after unilateral jaw/facial muscles infection was determined following the schedule in table 3.3. The MAVS challenge was as described in section 3.6.1 (page 35).

Table 3.3: Schedule of various doses and inoculation times of hyperimmune sera given before MAVS challenge, number of mice studied and types of analysis

Volume of hyperimmune serum (µL)	Hours before MAVS challenge	Hours post-infection at sacrifice	Harvested tissues analysed by	Number of mice sacrificed per timepoint
25	2	24, 48, 72, 96	Histopathology*	2
50	2	24, 48, 72, 96	Histopathology*	2
100	2	48, 72	Histopathology*	2
200	2	48, 72	Histopathology*	2
100 and 50	4 and 2	24, 48, 72, 96	Histopathology*	5
100 and 50	4 and 2	24, 48	Virus titration	3
100	4	24, 48, 72	Histopathology*	3
100	4	24, 48, 72	Virus titration	3
100	4	24, 48, 72, 96	RT-PCR	4

*Histopathology = H&E and IHC staining for viral antigens.

3.6.2.1 Histopathological analysis and IHC

Histopathological analysis and IHC of harvested tissues were performed as before (section 3.6.1.1 (page 36) and section 3.6.1.1 (a) (page 36), respectively).

3.6.2.2 Virus titration analysis

Viral titration assay was performed as before (section 3.6.1.2, page 37).

3.6.2.3 Viral RNA extraction, RT-PCR and qPCR

Tissues, sera, hindlimb and forelimb muscles, whole brainstems, upper half and lower half of spinal cords were harvested as in section 3.6.1.2 for total viral RNA extraction using a commercial kit (Hybrid-R, GeneAll, Korea) following the manufacturer's protocol. Extracted RNA diluted to 1 mg for cDNA generation by reverse transcription (Transcriptor First Strand cDNA Synthesis Kit, Roche, German) was added to the Random Hexamer Primer and denatured for 10 min at 65°C with a heated lid, followed by immediate ice treatment. Buffer, RNase inhibitor, dNTPs and transcriptor reverse transcriptase was added and incubated at 25°C for 10 min, followed by 55°C for 30 min for the reverse transcription step, and heat inactivation at 85°C for 5 min. The first strand cDNA product was then used for PCR and qPCR.

The PCR mixture consisted of 1 µL of cDNA template, 1.5 units of recombinant Taq DNA polymerase (Fermentas, USA), 1X Taq Buffer with ammonium sulfate, 0.5 µM of each primer (Appendix C, page 160) and 0.2 mM dNTP mix. The conditions were: 94°C for 3 min, 35 cycles of thermal cycling (15 seconds (sec) at 94°C, 30 sec at 60°C and 30 sec at 72°C) and final extension at 72°C, 5 min. The PCR products were

analysed by electrophoresis in 15% (wt/vol) Tris-borate-EDTA agarose gel containing 0.5 µg/mL ethidium bromide.

3.6.3 Mice infected via unilateral jaw/facial muscle and treated with optimised passive immunisation

Based on results obtained from Section 3.6.2 (page 38), the optimum dose of 100 µL of hyperimmune sera was IP-inoculated at 4 hr before MAVS infection in a group of mice (n= 18) as described in section 3.6.1 (page 35). Animals were sacrificed at 12 hpi (n= 3), 24 hpi (n= 4), 48 hpi (n= 4), 72 hpi (n= 4) and 96 hpi (n= 3) for histopathological analysis, IHC and ISH. An additional 4 animals were sacrificed at each timepoint, and tissues harvested for virus titration. Mock-immunised mice (n= 8) which received formaldehyde-fixed VERO cell lysates at the same time of MAVS infection, were sacrificed at 72 hpi.

3.6.3.1 Histopathological analysis, IHC and ISH

Histopathological analysis, IHC and ISH staining were performed as before (section 3.6.1.1 (page 36), section 3.6.1.1 (a) (page 36) and section 3.6.1.1 (b) (page 37), respectively).

3.6.3.2 Viral titration analysis

Viral titration assay was performed as before (section 3.6.1.2, page 37).

3.6.4 MAVS infection via intra-cerebral (thalamus/hypothalamus and pons/medulla) inoculation

The susceptibility of neurons to MAVS infection by the intra-cerebral (IC) route, and the association of viral antigens and mSCARB2 in the brain was investigated in 2 animal experiments. In the first experiment, 6.3 x 10^5 $CCID_{50}$ of MAVS in 10 µL was IC-inoculated into the thalamus/hypothalamus region of a 2-week old ICR mouse using 31-G needles. Neurons in this region are known to have a high expression of mSCARB2 (Lein et al., 2007). Tissues were harvested as before from 5 inoculated animals, at 24, 48 and 72 hpi timepoints for histopathological analysis, and 4 additional animals per timepoint for virus titration studies.

In the second experiment, the same amount of MAVS was IC-inoculated into the pons/medulla which also expressed a similar level of mSCARB2 as the thalamus/hypothalamus area. Three mice each were sacrificed at 24, 48 and 72 hpi for histopathological analysis, IHC and ISH, and another 4 animals per timepoint for virus titration analysis. Control mice (n= 6 for each experiment) were mock-infected with sterile PBS.

3.6.4.1 Histopathological analysis, IHC and ISH staining

Generally, histopathological analysis, IHC and ISH staining were performed similar to section 3.6.1.1 (page 36), section 3.6.1.1 (a) (page 36) and section 3.6.1.1 (b) (page 37), respectively. However, in the current IHC procedure, a commercially-obtained, mouse monoclonal anti EV-A71 antibody (Millipore, USA) diluted 1:50, was used instead of the proprietary primary polyclonal rabbit anti EV-A71 antibody because the latter ran out. Our preliminary testing showed this new antibody to be similar to the previous one.

3.6.4.2 Viral titration analysis

Viral titration assay was performed as before (section 3.6.1.2, page 37).

3.6.5 Investigation of the "provocation poliomyelitis" phenomenon in MAVS infection

The phenomenon of "provocation poliomyelitis" was classically described in poliovirus infection in which injured tissues from the act of injection (vaccination), aided poliovirus infection and travel into the spinal cord, causing paralysis. In this experiment, the possibility of a similar phenomenon occurring with EV-A71 infection was investigated. Two groups of 2-week old ICR mice were IP-inoculated with ~90 $CCID_{50}$ of MAVS. In the first group of mice (n= 10), bilateral gastrocnemius muscles were traumatised 5 times by repeatedly inserting a 28-G needle into the muscle at 0 hpi, 12 hpi, 24 hpi, 36 hpi, 48 hpi and 60 hpi. A second group of animals (n= 10) served as a non-traumatised control group. At 72 hpi, tissues were harvested as usual from 5 sacrificed animals from each group for histopathological analysis. The other 5 animals in the same group were sacrificed for virus titration.

The entire experiment was repeated with a higher 1.78×10^2 $CCID_{50}$ MAVS dose. Wheat germ agglutinin (WGA) protein, well known as a retrograde tracer (Ohka et al., 2009), was used to monitor the retrograde axonal transport rate in traumatised and non-traumatised mice. As positive controls, 10 µg of WGA protein were IM-inoculated into the bilateral gastrocnemius muscles of traumatised (n= 3) and non-traumatised mice (n= 3). Mice were sacrificed at 12 hpi for total protein extraction and WGA quantification.

3.6.5.1 Histopathological analysis, IHC staining

Generally, histopathological analysis and IHC were performed as before (section 3.6.1.1 (page 36) and section 3.6.1.1 (a) (page 36).

3.6.5.2 Viral titration analysis

Viral titration assay was performed as before (section 3.6.1.2, page 37).

3.6.5.3 Total protein extraction and WGA quantification

Tissues (hindlimb muscles, upper half and lower half of spinal cords) from sacrificed positive control WGA-inoculated mice were used for total protein extraction according to the manufacturer's protocol (T-PER™ Tissue Protein Extraction Reagent, Thermo Fisher, USA). Briefly, the extraction reagent with protease inhibitor (Pierce™ Protease Inhibitor Tablets, EDTA-free, USA) was added to each tissue to a final concentration of 10% (wt/vol). Homogenised tissues were incubated for 30 min at 4°C, then centrifuged at 10000 x g for 5 min to remove debris.

WGA concentration in extracted protein was semi-quantified by dot blot analysis as previously described (Lancaster & Pfeiffer, 2010). Briefly, 5 µL of each sample was dropped onto a nitrocellulose membrane and air dried. Non-specific sites were blocked by 5% skim milk in TBS-Tween20 for 3 hr at RT. Rabbit anti-lectin (*triticum vulgaris*) primary antibody (Sigma, St Louis, USA) at 1:4000 dilution was added and incubated at 4°C overnight, followed by addition of goat anti-rabbit IgG AP-conjugated (Pierce, USA) secondary antibody (1:5000 dilution, RT in dark for 1 hr) and 1-Step™ NBT/BCIP Substrate Solution (Thermo Fisher, USA) in dark for 10 min for visualisation.

3.6.6 Investigation of the link between muscle infection and retrograde axonal transport in spinal cord infection.

The link between muscle infection and retrograde axonal transport was investigated by IM-inoculating 3.16 x 10^3 $CCID_{50}$ light-sensitive MAVS into both gastrocnemius muscles of 2-week old ICR mice (n= 15). Tissues were harvested in the dark from 5 animals for virus titration study at each 24, 48 and 72 hpi timepoints.

3.6.6.1 Viral titration analysis

Generally, viral titration assay was performed as before (section 3.6.1.2, page 37) with slight modifications. Harvested tissue samples were divided equally into light-treated and light-protected samples. Light-treated samples were exposed to direct white light at 4°C for 30 min before titrated as in section 3.6.1.2 (page 37), and the whole titration process was done in the dark.

3.6.7 Prevention and treatment of MAVS infection using neutralising antibodies

Prevention and treatment of MAVS infection in 2-week old ICR mice using neutralising antibodies was investigated in 3 separate experiments. In experiment 1, 200 µL of hyperimmune sera containing polyclonal antibodies which could neutralise EV-A71 was IP-inoculated into each 2-week old ICR mice 4 hr before MAVS infection, and at 12 hr and 24 hr after MAVS infection, respectively. The mice were then challenged with MAVS as described in section 3.6.1 (page 36). Four animals per group were sacrificed at 72 hpi, and tissues harvested for histopathological analysis, and another 4 animals were sacrificed for virus titration study, respectively. A further 4 animals in

each group were monitored to assess survival over a period of 21 days. Mock-treated infected animals (n= 12) received VERO cell lysate-derived serum at 12 hpi.

In experiment 2, the effectiveness of MAb for treatment was investigated. Six groups (each group, n= 4) of 2-week old ICR mice were infected via the IP route with 10 LD_{50} MAVS in 100 µL. Each group was then IP-inoculated for 2 consecutive days at 24 and 48 hpi with 30, 60, 120 µg of MAb or PBS (mock-treated control group), respectively. Similar groups of mice were likewise treated for 2 consecutive days at 72 and 96 hpi using the same MAb doses. Mice were observed daily for up to 21 days post infection (dpi) for signs of infection. The signs of infection were scored as follows: 0= healthy; 1= weight loss; 2= limb weakness; 3= hind limb paralysis; and 4= moribund and/or death.

In experiment 3, MAb effectiveness before and after CNS involvement was evaluated. Two groups of mice (each group, n= 16) were similarly infected as in experiment 2. Group 1 mice were treated with an optimal 120 µg MAb for 3 consecutive days at 24, 48 and 72 hpi. Group 2 received treatment at 72, 96, and 120 hpi. Group 1 was sacrificed for histopathology (n= 4), virus titration (n= 4) and quantitative real-time PCR (n= 4) at 96 hpi, while the same number of animals from Group 2 was sacrificed at 144 hpi. The remaining 4 treated mice from each group were further observed daily for signs of infection for 21 days. Thirty-two additional PBS-treated, infected mice served as mock-treated controls. From this control group, 4 mice each were sacrificed at 24, 72 and 96 hpi and tissues collected for histopathology and virus titration, respectively. Tissues from an additional 4 mice sacrificed at 96 hpi were obtained for quantitative real-time PCR (qPCR). The remaining 4 mock-treated mice were further observed for signs of infection for 21 days. A summary of the schedule for animal sacrifice and tissue sampling is showed in Figure 3.1.

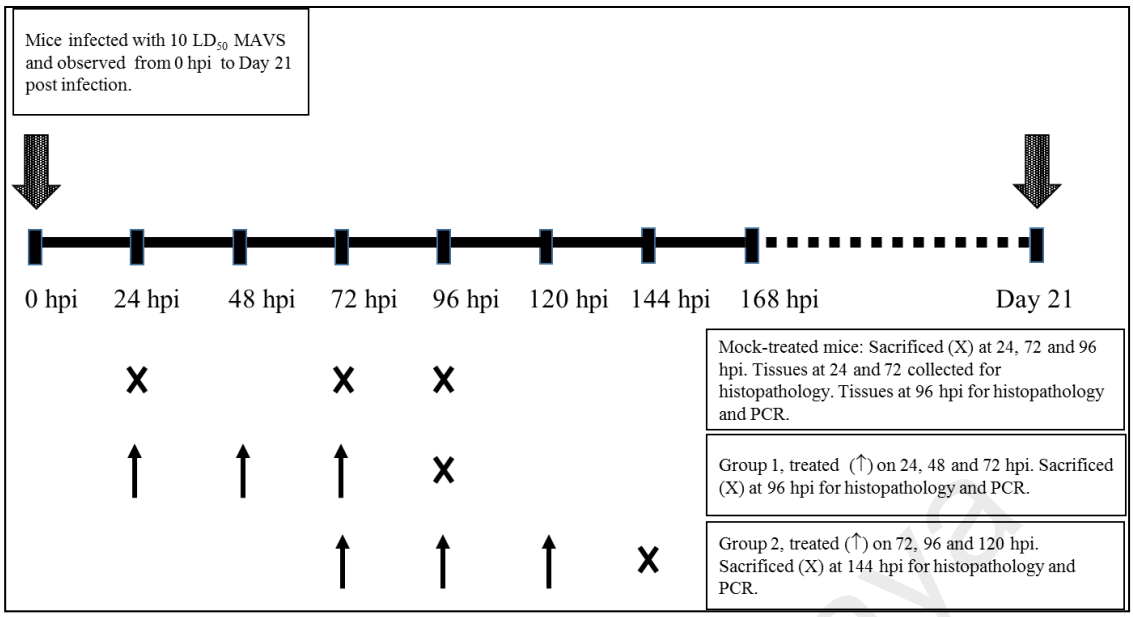

Figure 3.1: Schedule of MAb 3D1 treatment, animal sacrifice and tissue sampling following MAVS infection, in Experiment 3.

3.6.7.1 Histopathological analysis, IHC and ISH staining

Histopathological analysis, IHC and ISH staining were performed as before (section 3.6.1.1 (page 36), section 3.6.1.1 (a) (page 36) and section 3.6.1.1 (b) (page 37), respectively).

3.6.7.2 Viral titration analysis

Viral titration assay was performed as before (section 3.6.1.2, page 37).

3.6.7.3 Viral RNA extraction, RT-PCR, qPCR

Viral RNA extraction and cDNA transcription were performed as before (section 3.6.2.3, page 39). qPCR analysis was performed with the primers (section 3.6.2.3, page 39) according to the manufacturer's protocol using SensiFast Probe Lo-Rox kit (Bioline,

UK). The qPCR mixture consisted of 2 µL of cDNA template, 1X sensifast probe mix, 400 nM of each primer and 100 nm of probe. The conditions were: 95°C for 5 min for polymerase activation and 40 cycles of thermal cycling (10 sec at 95°C and 30 sec at 60°C). Full length of MAVS was reverse transcripted and served as standard control for absolute quantification.

3.7 Primary murine motor neuron culture

Primary motor neuron culture (Ohka et al., 2009) was performed in Tokyo, Japan, following guidelines of Animal Use and Care Committee of the Tokyo Metropolitan Institute of Medical Science. Briefly, spinal cords of E14 mouse embryos were dissected in sterile PBS using a dissecting microscope. The meninges, dorsal root ganglia and dorsal column were removed using a fine-tip forcep. Minced spinal cords tissues were treated with trypsin for 10 min at 37°C with agitation every 5 min followed by DNase I treatment. Tissues were triturated in neurobasal medium supplemented with 10% bovine serum albumin (BSA) in L15 medium and DNase I, to separate the motor neuron cells from the tissue fragments. After the tissue fragments were allowed to settle for 3 min, the supernatant was collected and centrifuged with a cushion of BSA/L15 medium at 1400 rpm for 5 min. Cell pellets were resuspended in a small volume of freshly prepared complete GM and plated at a density of 40 000 cells /mL.

3.7.1 Transfection of primary murine motor neurons

Transfection of primary murine motor neurons was performed according to the manufacturer's protocol (4D-Nucleofector™ System, Lonza, Switzerland). Briefly, primary motor neurons were seeded onto a 24 well plate at 1.5 x 10^5 cells/well. After 4 days of incubation in a humidified 37°C/7% CO_2 incubator, half of media was replaced

with Nb Active 4 media (BrainBits, LLC, UK). The next day, all medium was removed and replaced by AD1 4D-Nucleofector™ Y Kit's solution with 17.5 µg with phSCARB2-FLAG-mCherry vector (courtesy of Dr. Satoshi Koike). A 24-well dipping electrode was placed carefully to prevent air bubble formation underneath. Transfection was done using the ED-158 program in the system and nucleofector solution (Lonza, Swiss) was then replaced by pre-warmed medium immediately.

3.7.2 Double immunofluorescence staining for EV-A71 and hSCARB2

Primary motor neurons were washed twice with growth medium before fixation with 4% paraformaldehyde in PBS supplemented with 20% sucrose. Permeabilisation was done with 0.05% of saponin and 5% of BSA for 2 hr at RT after PBS washing (4 times). Both primary antibodies were added together as in Table 3.4 (no. 1 and 2), followed by secondary antibodies (Table 3.4, no. 3 and 4). Cells were mounted with "Vectashield Antifade Mounting Medium with DAPI" (Vector, USA).

Table 3.4: Summary on primary and secondary antibodies used in double immuno-fluorescence staining

No.	Antigens	Host	Dilution	Duration of Incubation	Incubation Temperature
1.	EV-A71	Mouse Polyclonal (Produced by Dr. Satoshi Koike, Japan)	1:9000	Overnight	4°C
2.	hSCARB2	Goat Polyclonal (R&D System, USA)	1:1250	Overnight	4°C
		Washed four times with PBS			
3.	Mouse IgG	Donkey Anti-Mouse Alexa Fluor® 488 (Invitrogen, USA)	1:1000	90 minutes	Room Temperature
4.	Goat IgG	Donkey Anti-Goat Alexa Fluor® 647 (Invitrogen, USA)	1:1000	90 minutes	Room Temperature

3.8 Statistic Analysis

Statistical analyses were performed using SPSS Statistics 21. All virus titration analysis and viral copy numbers from qPCR results were analysed using the Kruskal-Wallis test to determine statistical significance in viral titres across all tissue types. The Mann-Whitney U test was used to determine if any 2 particular tissue types were different.

The survival and clinical score of treated and mock treated animals (section 3.6.7, page 46) were analysed using the log-rank test. A value of $P < 0.05$ was considered significant.

4.0 Results:

4.1 Fluorescent labelled EV-A71

After EV-A71 was fluorescent-labelled with Alexafluor-555 and purified with a NAP5 resin column, a total of 10 fractions (200 µL/fraction) were collected. The absorbance values for fractions of Alexafluor-555 labelled EV-A71 virus at 280 nm and 555 nm are shown in Figure 4.1. Fraction number 6 with a labelling ratio of 4.05 moles of Alexafluor-555 dye per mole of virus was selected for the experiment (section 4.4, page 83). Alexafluor-555 labelled EV-A71 showed similar infectivity with the clinical isolate EV-A71 (parental virus) based on percentage of CPE from day 1 to day 7 in RD-hSCARB2 cells with titre of 5.6 x 10^6 $CCID_{50}$/ml.

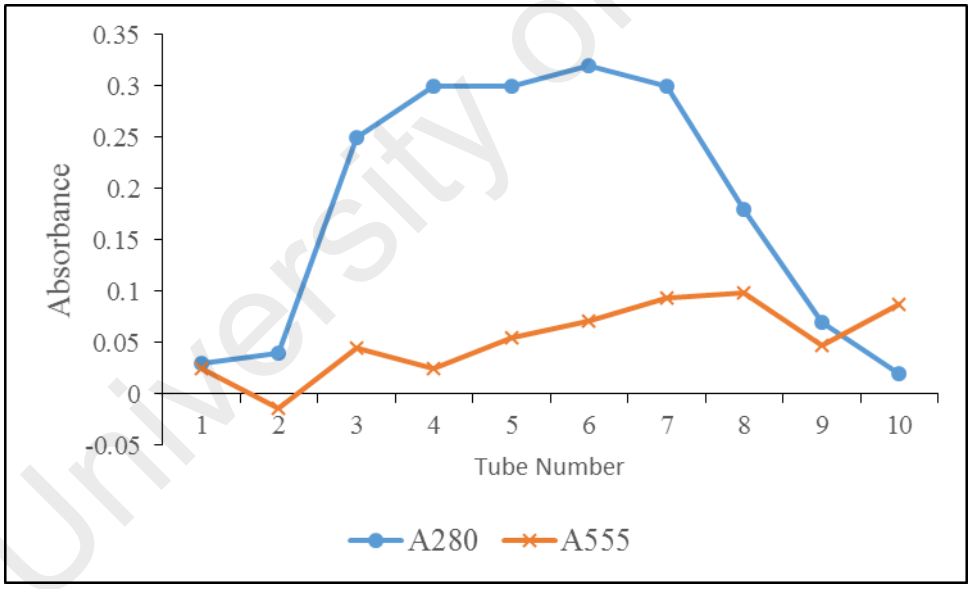

Figure 4.1: NAP5 fractionation of Alexafluor-555 labelled EV-A71. A total of 10 fractions (200 µL/fraction) were collected. Protein and fluorescent dye of each fraction were determined and expressed as absorbance at 280 and 555 nm, respectively.

4.2 Brainstem infection via retrograde axonal transport in cranial nerves

4.2.1 MAVS infection via unilateral jaw/facial muscles

MAVS was inoculated into right jaw/facial muscles of 2-week old ICR mice to evaluate cranial nerve involvement in EV-A71 CNS infection. All infected mice (n= 16) showed signs of infection such as back hunching, fur ruffling and obvious paralysis in both hindlimbs from 60 hpi onwards (Figure 4.2 A, arrows). These signs became more severe at 72 hpi, and all mice were moribund/dead by 96 hpi. Mock-infected mice (n= 8) were all active and healthy throughout the experiment.

4.2.1.1 Pathological studies

Figure 4.3 (mouse A1 – A18) shows the approximate topographic distribution of viral antigens/RNA in CNS tissues in each infected mouse. At 12 hpi (n= 3), the IHC and ISH showed no evidence of viral infection in the CNS. Viral antigens/RNA in the CNS were first detected at 24 hpi (Figure 4.3, mouse A1 – A4), in the motor trigeminal nucleus, reticular formation (medulla) and facial nucleus, ipsilateral to the injection site only. Moreover, some cranial nerves ipsilateral to the injection site were positive for viral antigens/RNA (Figure 4.2 B - F). An ipsilateral anterior horn cell in lumbar spinal cord was found to be infected in one mouse (Figure 4.3, mouse A2). All CNS neurons appeared normal by light microscopy with no obvious inflammation or other abnormalities observed.

Minimal and focal viral antigens/RNA without obvious inflammation were detected in the injected jaw/facial muscles at 12 hpi. Later, at 24 hpi, skeletal muscles around the injected area showed more viral antigens/RNA and demonstrated mild myositis. Focal and scanty viral antigens/RNA were also detected in a few fibres in

contralateral jaw/facial muscles, and other skeletal muscles such as tongue and limbs bilaterally. All other tissues were negative.

Bilateral CNS infection was observed in all mice starting from 36 hpi (Figure 4.3, mouse A5 - A7). The distribution of viral antigens/RNA in brainstem neurons was almost similar to the findings at 24 hpi. However, in general, CNS infection on the ipsilateral side was more severe compared to the contralateral side (Figure 4.3, mouse A5 – A7). Viral antigens/RNA were found mainly in the motor trigeminal nuclei (Figure 4.4 A - D), reticular formation (Figure 4.4 E) and facial nuclei (Figure 4.4 F). A few neurons in thalamus (Figure 4.3, mouse A7; Figure 4.4 Q) and motor cortex (Figure 4.3, mouse A5 and A6; Figure 4.4 G) were infected too. Infected neurons showed neuronal vacuolation and damage (Figure 4.4 A). Bilateral involvement of anterior horn cells in spinal cord was observed in a single mouse (Figure 4.3, mouse A7). MAVS inoculated jaw/facial muscles showed dense viral antigens/RNA, severe inflammation and necrosis. Brown adipose tissues and other systemic skeletal muscles were infected bilaterally but inflammation was minimal.

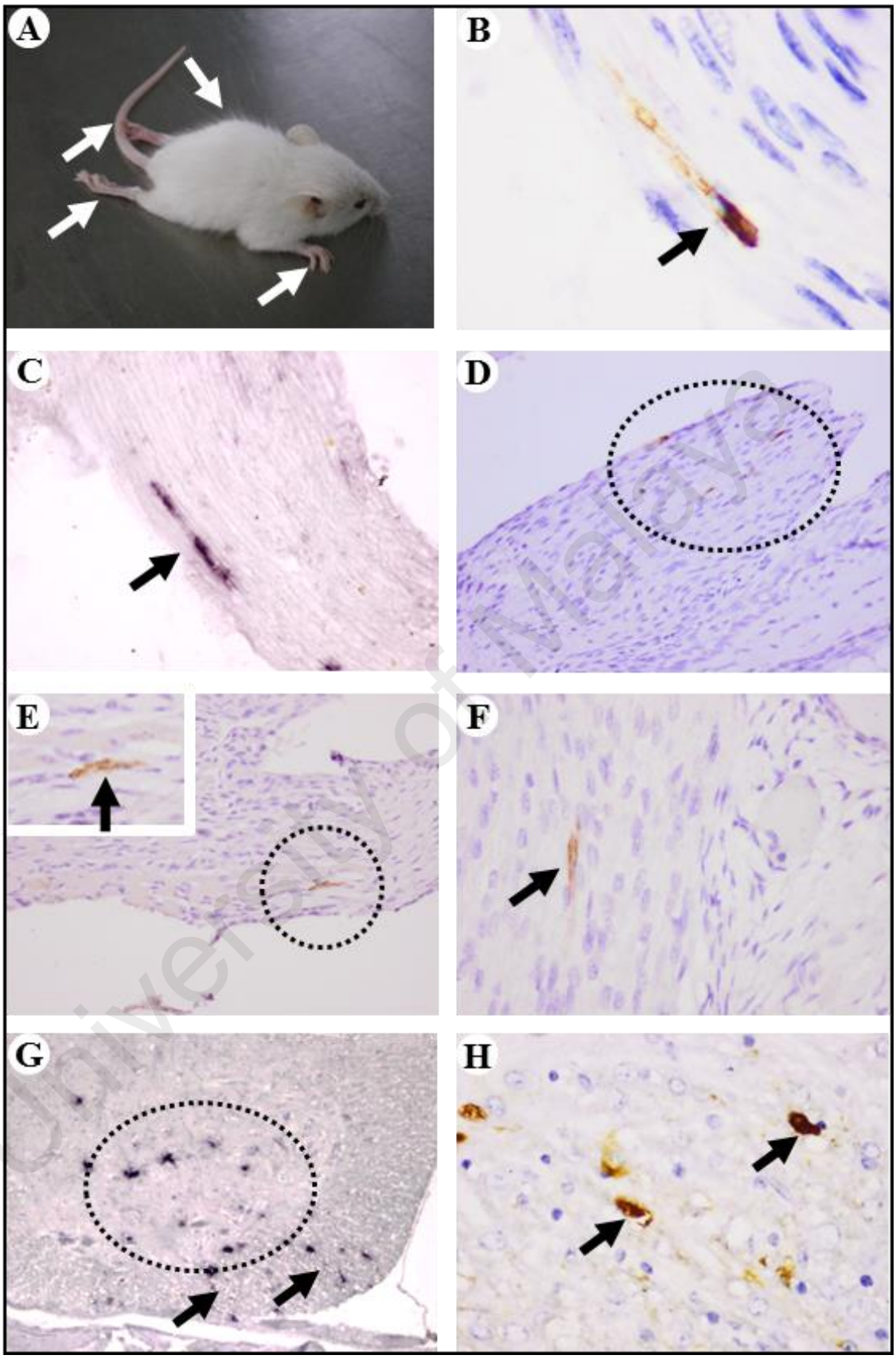

Figure 4.2: Clinical observation, and pathological findings following unilateral jaw/facial muscle infection. Infected mice showed back hunching (arrow), and obvious paralysis in both hindlimbs (arrows) and forelimbs (arrow) at 72 hpi. Viral antigens (B arrow, D circle, E circle and F arrow) and RNA (C arrow) were found in cranial nerves ipsilateral to the injection site. In the spinal cord, viral RNA (G arrows) and antigens (H arrows) were often detected in white matter axons adjacent to anterior horn cells that were positive for viral antigens or RNA (G circle). IHC with DAB chromogen and haematoxylin counterstain (B, D – F and H). ISH with haematoxylin counterstain (C and G). Original magnification: 100x objective (B); 40x objective (C, F, H and inset); 20x objective (D and E); 10x objective (G).

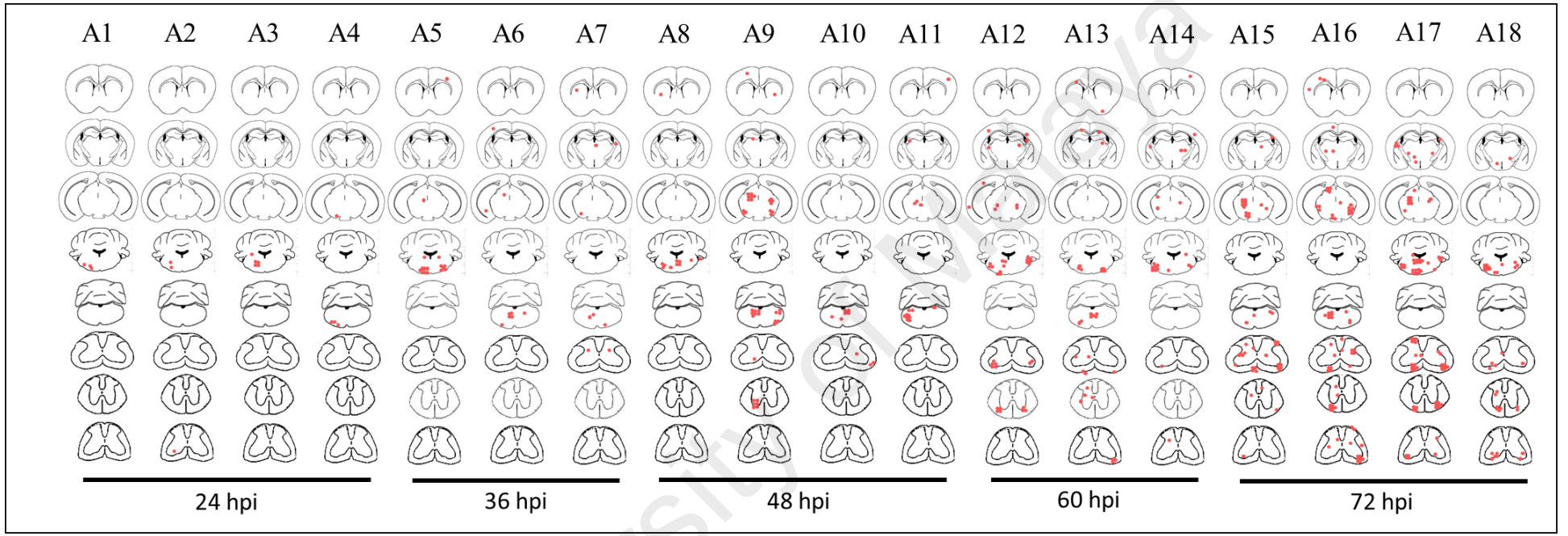

Figure 4.3: Approximation of the distribution of viral antigens/RNA in the CNS following unilateral jaw/facial muscle infection. Mice showed ipsilateral brainstem involvement after 24 hpi, and bilateral involvement after 36 hpi. Each red dot represents the equivalent of a positive neuron/white matter axon. For each mouse, cross sections of cerebral cortex, diencephalon/cortex, midbrain/cortex, caudal pons/medulla/cerebellum, medulla/cerebellum, cervical, thoracic, and lumbar spinal cords are displayed.

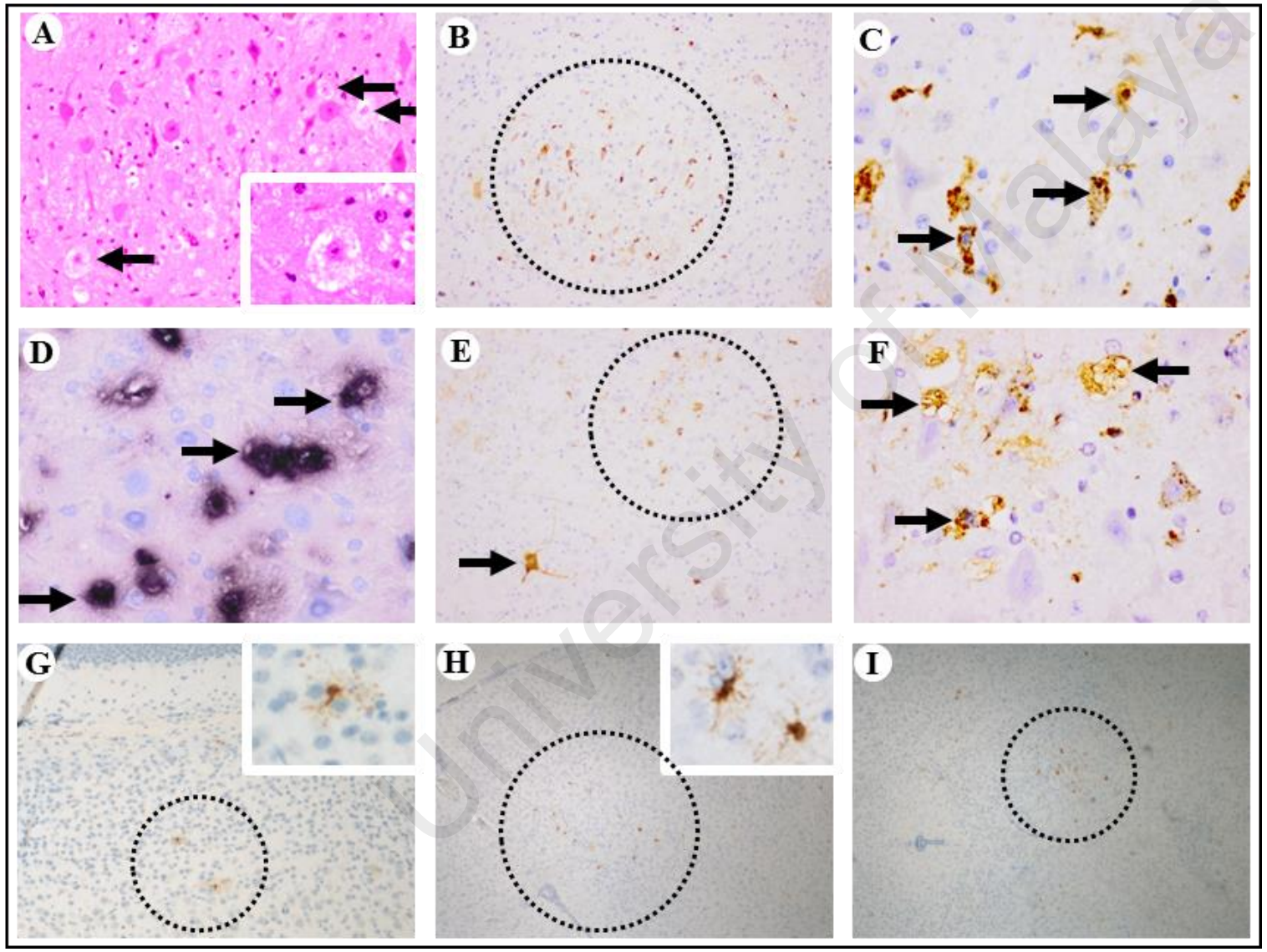

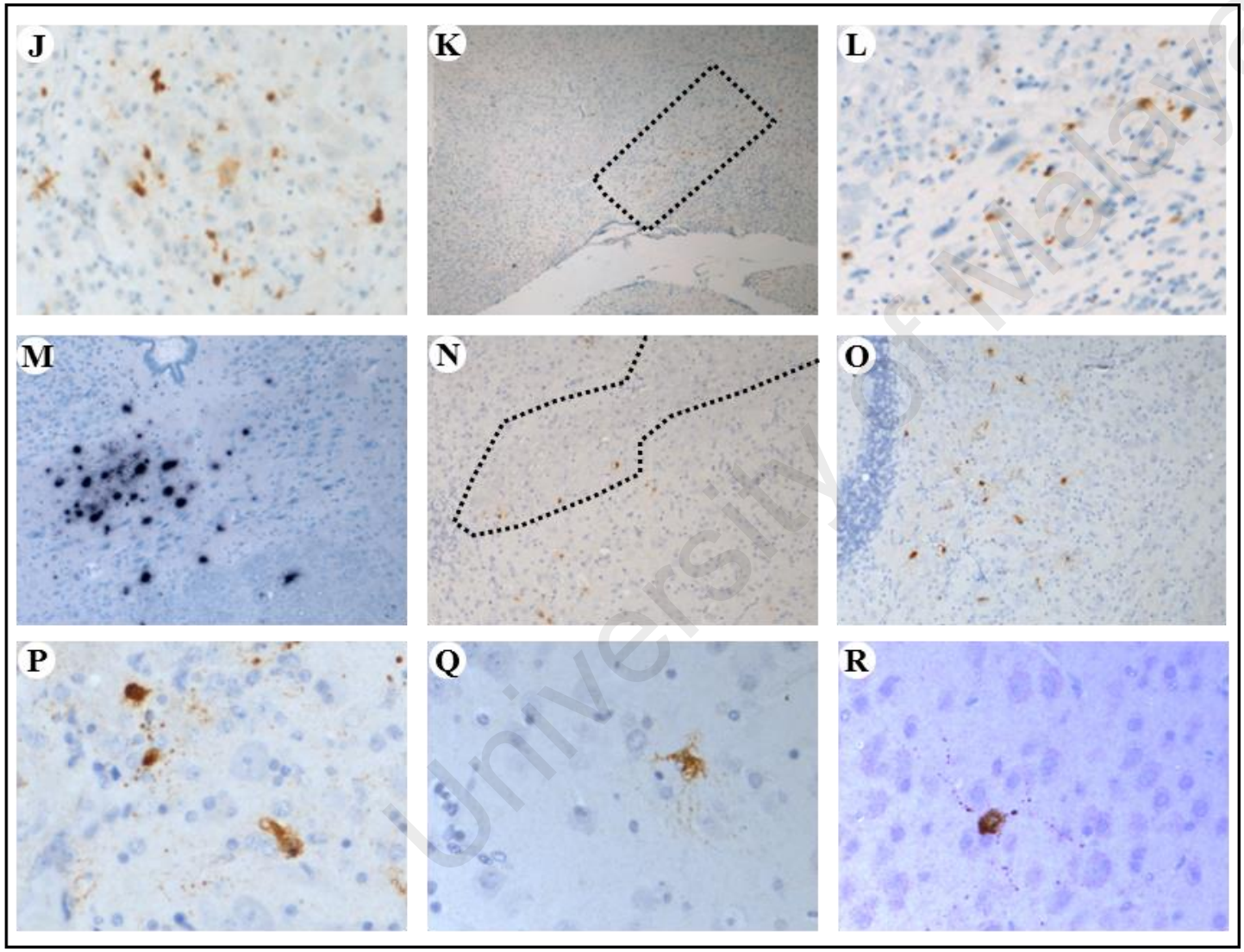

Figure 4.4: Pathological findings following unilateral jaw/facial muscle infection. Infected motor trigeminal nucleus demonstrated neuronal degeneration, necrosis and vacuolation (A arrows, inset), viral antigens (B circle; C arrows), and viral RNA (D arrows). Reticular formation (E circle), gigantocellular reticular nucleus (E arrow), facial nucleus (F arrows), motor cortex (G circle, inset), midbrain (H circle, inset), red nucleus (I circle, J), solitarius nucleus (K square, L), hypoglossal nucleus (M), area within spinal tract of trigeminal nerve (N) and dentate nucleus (O and P) were positive for viral antigens/RNA too. In some mice, thalamus (Q) and sensory cortex (R) were infected too. H&E stain (A). IHC with DAB chromogen and haematoxylin counterstain (B, C, E, F, G – L, N - R). ISH with haematoxylin counterstain (D and M). Original magnification: 40x objective (C, D, F, P - R and inset); 20x objective (A, J and L); 10x objective (B, E, G, M - O); 4x objective (H, I and K).

At 48 hpi (Figure 4.3, mouse A8 – A11), CNS infection in the mice was more advanced. In addition to the other areas involved at 36 hpi, in 2 mice (Figure 4.3, mouse A9 and A11), a few neurons in the midbrain (Figure 4.4 H) and red nucleus (Figure 4.4 I and J) were also infected. In the spinal cord, neuronal infection mainly involved anterior horn cells in two of the mice (Figure 4.3, mouse A9 and A10). Infected neurons showed neuronal vacuolation and damage. Axons in the white matter immediately adjacent to infected anterior horn cells at or near the site where peripheral motor nerves usually exit, were positive for viral antigens/RNA. Muscle fibres at the injection site demonstrated extensive and dense viral antigens/RNA, severe inflammation and necrosis. Other skeletal muscles and brown adipose tissues showed some viral antigens/RNA bilaterally with minimal inflammation.

At 60 hpi (Figure 4.3, mouse A12 – A14) and 72 hpi (Figure 4.3, mouse A15 – A18) there was more extensive, bilateral involvement of the CNS. The gigantocellular reticular nucleus (Figure 4.4 E), solitarius nucleus (Figure 4.4 K and L), hypoglossal nucleus (Figure 4.4 M), spinal tract of trigeminal nerve area (Figure 4.4 N), lateral cerebellar nucleus (dentate nucleus) (Figure 4.4 O and P) and motor and sensory cortex (Figure 4.4 R) were also positive for viral antigens/RNA. In the spinal cord, viral antigens/RNA were found in the anterior, intermediate and posterior horns bilaterally, although anterior horn cells showed a higher degree of infection compared to intermediate and posterior horn cells. Overall, no obvious CNS inflammation was observed.

Brown adipose tissues and systemic skeletal muscles were more severely infected bilaterally at 60 and 72 hpi. Muscle degeneration and necrosis along with severe inflammation were observed. There was no evidence of viral infection in lung, heart nor evidence of pulmonary oedema, pneumonia, myocarditis or other abnormalities, in any of the mice examined.

4.2.1.2 Viral titration analysis

Figure 4.5 shows the mean viral titres in muscle tissues (n= 4, for each time point), left and right forelimb and left and right hindlimb muscles, and sera. Mean sera viral titres remained high throughout the experiment, gradually increasing from 3.6 to 4.5 log $CCID_{50}$. However, the mean viral titres for all muscle groups did not differ significantly ($P< 0.05$) from each other at respective time points (Figure 4.5). Nonetheless, muscle mean viral titres gradually increased from 12 hpi to 72 hpi with titres of around 5.3 log $CCID_{50}$.

The mean viral titres (n= 4, for each time point) of all CNS tissues (whole brainstem, upper and lower spinal cord segments), and sera are shown in Figure 4.6. The CNS viral titres were always lower than sera and muscle titres at respective time points. However, CNS mean viral titres gradually increased over time to peak at 60 hpi to 72 hpi with titres of around 3.5 log $CCID_{50}$. Moreover, brainstem viral titres were significantly higher ($P< 0.05$), compared to upper and lower spinal cords from 12 hpi to 48 hpi (Figure 4.6).

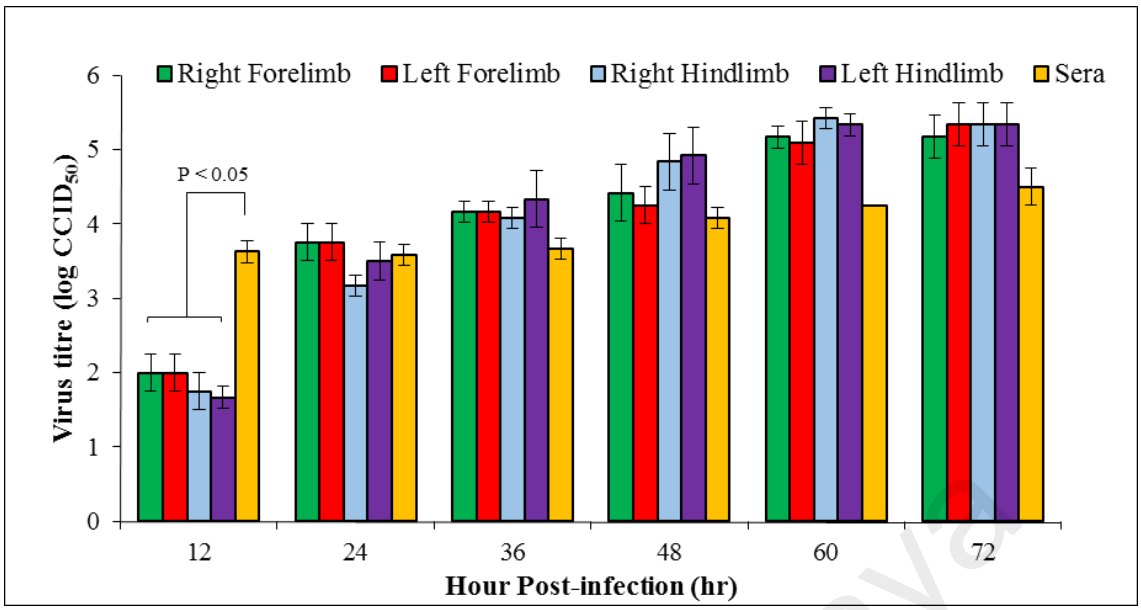

Figure 4.5: Viral titres in muscle tissues and sera following unilateral jaw/facial muscles infection. Sera viral titres were significantly higher (P< 0.05) than all muscles viral titres at 12 hpi. At 24 hpi, muscles viral titres increased drastically and finally was significantly higher (P< 0.05) than sera viral titres at 60 hpi onward. Mean viral titres are expressed as log $CCID_{50}$ ± standard error of mean.

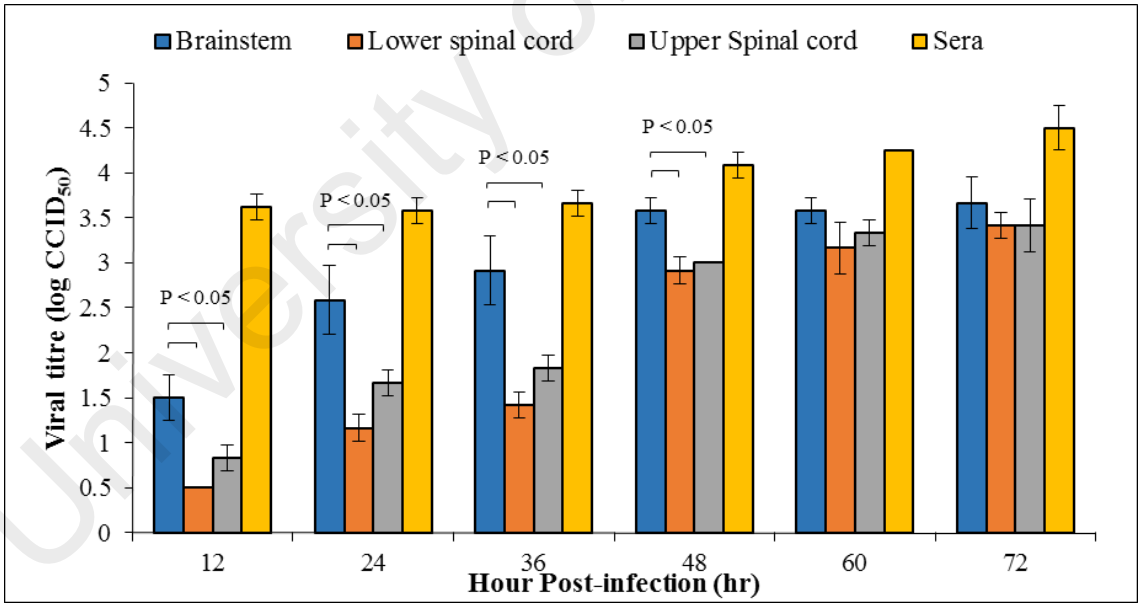

Figure 4.6: Viral titres in CNS tissues and sera following unilateral jaw/facial muscles infection. Sera viral titres were significantly higher (P< 0.05) than CNS viral titres at all time. At 48 hpi and before, brainstem viral titres were significantly higher (P< 0.05) than upper and lower spinal cord viral titres. Mean viral titres are expressed as the log $CCID_{50}$ ± standard error of mean.

4.2.2 Optimisation of passive immunisation in unilaterally-infected mice to abrogate viraemia

Following unilateral jaw/facial muscle inoculation, bilateral CNS involvement starting from 36 hpi (section 4.2.1.1, page 51) was most likely due to viraemia causing widespread virus infection. Hence hyperimmune sera were given at various doses and time points before inoculation in an attempt to abrogate viraemia to confirm unilateral retrograde axonal transport in peripheral nerves, and to show that bilateral CNS involvement follows viraemia that spreads virus to the contralateral side.

Mice (n= 8) receiving 25 µL of hyperimmune sera 2 hr before infection showed delayed onset of CNS infection compared to mock-treated mice. Treated mice sacrificed at 24 hpi (n= 2), showed viral antigens in the injected right jaw/facial muscles, part of shoulder muscles and forelimb muscles bilaterally as shown in Figure 4.7 A and B, respectively, without CNS involvement. In mice sacrificed at 48 hpi (n= 2), viral antigens were also found bilaterally in the brainstem reticular formation and motor trigeminal nucleus (Figure 4.7 C). Spinal cord anterior horn cells were involved at 72 hpi (n= 4).

Mice (n= 8) receiving a higher dose (50 µL) of hyperimmune sera at 2 hr before infection, showed viral antigens in injected right jaw/facial muscles and part of shoulder muscles (Figure 4.7, D and E) at 24 hpi (n= 2). At 48 hpi (n= 2), bilateral brainstem reticular formation and motor trigeminal nucleus (Figure 4.7 F) and forelimb muscles were infected. Anterior horn cells of the spinal cord were involved from 96 hpi (n= 2).

Mice (n= 4) receiving 100 µL of hyperimmune sera at 2 hr before infection, showed similar results to mice receiving 50 µL of hyperimmune sera at early time points, up to 48 hpi. However, there was no evidence of infection in the forelimb muscles and spinal cord (Figure 4.7 G - I). In the fourth trial, mice (n= 4) receiving the

highest dose of 200 µL of hyperimmune sera at 2 hr before infection, only showed minimal infection in the injected right jaw/facial muscles throughout the experiment (Figure 4.7 J - L) without any CNS involvement.

Further variations of passive immunisation in which mice (n= 20) receiving 100 µL of hyperimmune sera at 4 hr before infection and 50 µL of hyperimmune sera at 2 hr before infection showed minimal infection at the injected right jaw/facial muscles throughout the experiment without CNS infection (Figure 4.7 M - O). Finally, mice (n= 9) receiving 100 µL of hyperimmune sera at 4 hr before infection, showed minimal involvement in the injected right jaw/facial muscles only and unilateral brainstem involvement after 48 hpi. Sera, left and right forelimb and hindlimb muscles collected for viral titration (n= 9) were negative. Viral RNA were not detectable in the extracted samples (n= 16) by RT-PCR. Hence this passive treatment modality was used in Section 4.2.3.

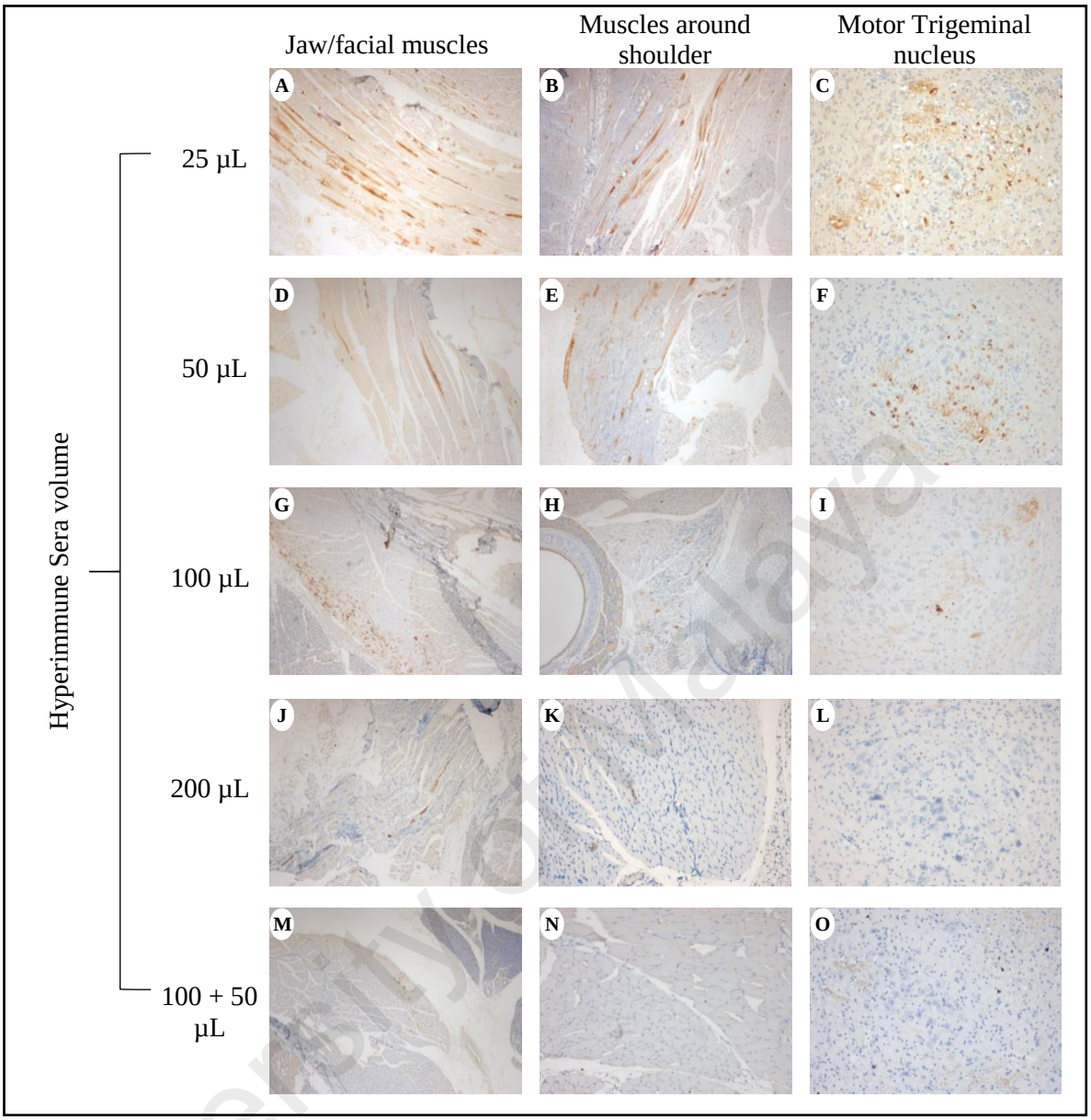

Figure 4.7: Viral antigens in muscles and motor trigeminal nucleus following unilateral jaw/facial muscles infection of pre-immunised mice. Mice pre-immunised with 200 µL and 100 + 50 µL of hyperimmune sera were protected from CNS infection completely. Whereas, lower volume of hyperimmune sera was able to delay the onset of disease. Original magnification: 10x objective (C, F, I, L and O); 4x objective (A, B, D, E, G, H, J, K, M and N).

4.2.3 Mice unilaterally-infected in the jaw/facial muscles and given optimised passive immunisation to abrogate viraemia

None of the mice (n= 18) receiving the highest optimal dose (100 µL) of hyperimmune sera 4 hr before MAVS inoculation into the right jaw/facial muscles showed any signs of disease. Mock-immunised animals (n= 8) showed signs of disease, and death occurred at 96 hpi as described (section 4.2.1, page 51).

4.2.3.1 Pathological studies

Optimally-treated mice to abrogate viraemia which were sacrificed at 12 hpi (Figure 4.8, mouse A1 – A3) and 24 hpi (Figure 4.8, mouse A4 – A7) showed similar results under histopathological examination. Viral antigens/RNA were found only in the ipsilateral jaw/facial muscles where infected muscles showed minimal necrosis and no obvious inflammation.

At 48 hpi (Figure 4.8, mouse A8 – A11), there was minimal viral antigens/RNA and found exclusively in the ipsilateral brainstem such as motor trigeminal nucleus (Figure 4.9 A - E) and reticular formation (Figure 4.9 F) but not in the facial nucleus. Furthermore, the density of viral antigens/RNA was much lower compared to the corresponding areas in non-immunised mice described in section 4.2.1.1 (page 51). There was no evidence of viral antigens/RNA in the spinal cord or other brain regions outside the brainstem. Viral antigens/RNA was detected in the injected muscle only focally and sparsely. All other muscles and non-CNS tissues were not infected. Similar findings were obtained in animals sacrificed at 72 hpi (Figure 4.8, mouse A12 – A15) and 96 hpi (Figure 4.8, mouse A16 – A18). Inflammation around damaged neurons was mild to moderate (Figure 4.9 A - C), and inflammatory cells consisted mainly of neutrophils and macrophages (Figure 4.9 C and F).

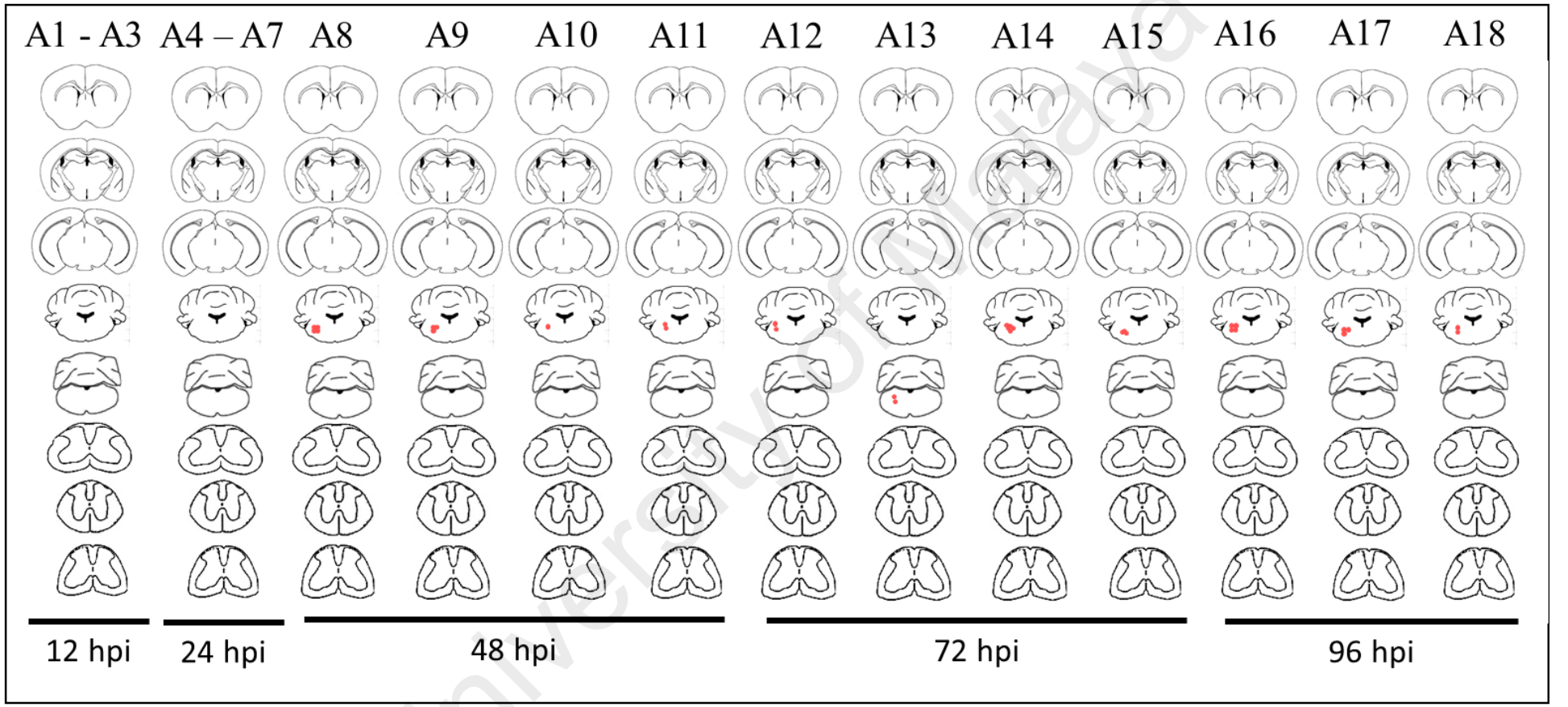

Figure 4.8: Approximation of the distribution of viral antigens/RNA/inflammation in the CNS following unilateral jaw/facial muscles infection in pre-infection immunised mice without presence of viraemia. Viral antigens/RNA/inflammation was only observed in the ipsilateral brainstem at 48 hpi onward. No evidence of infection observed in other CNS regions. Each red dot represents the equivalent of a positive neuron/inflammatory focus. For each mouse, cross sections of cerebral cortex, diencephalon/cortex, midbrain/cortex, caudal pons/medulla/cerebellum, medulla/cerebellum, cervical, thoracic, and lumbar spinal cords are displayed.

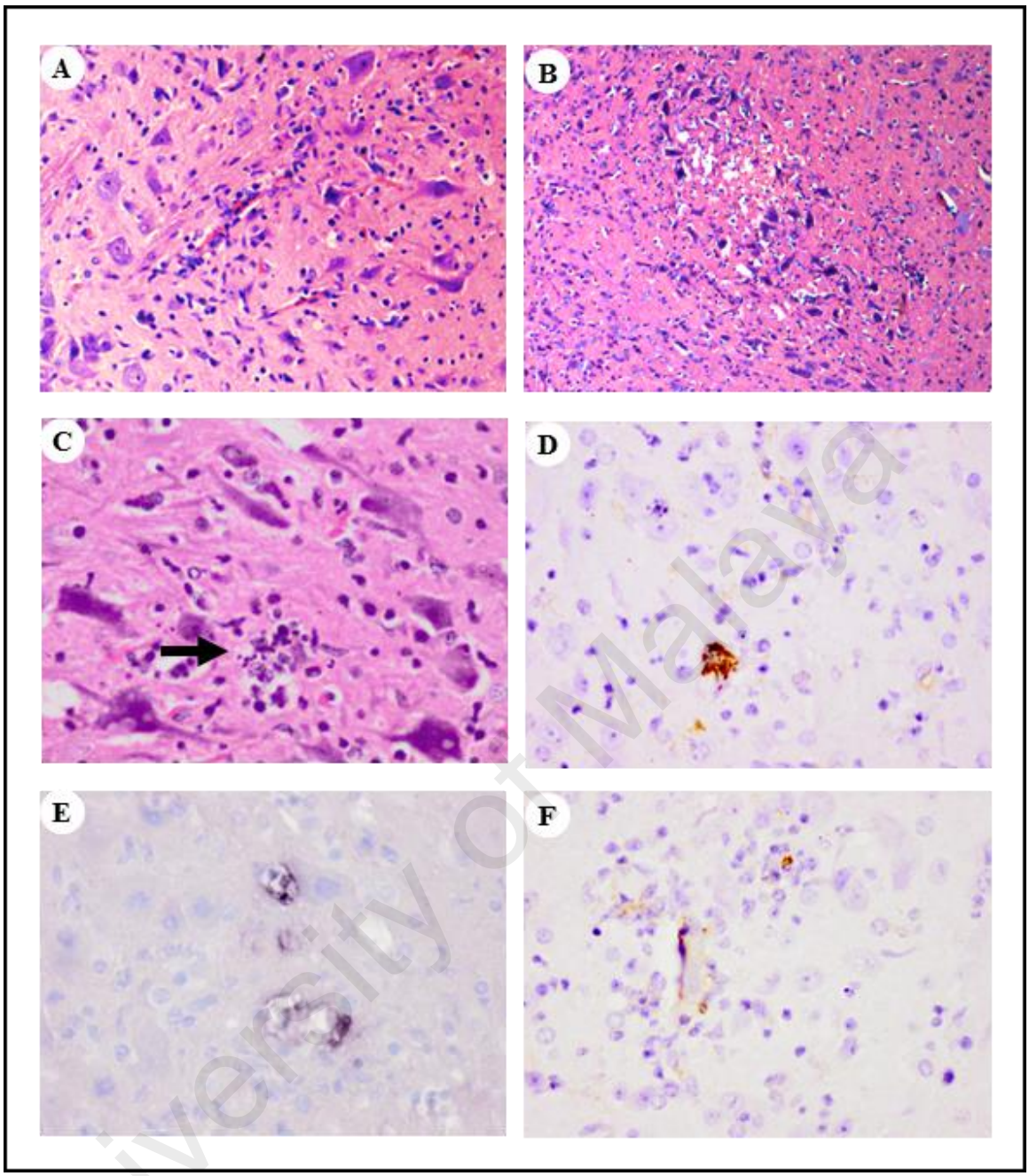

Figure 4.9: Pathological findings in mice following unilateral jaw/facial muscle infection and passively immunised to abrogate viraemia. Neuronal degeneration, vacuolation and inflammation were observed in the motor trigeminal nucleus (A - C). Viral antigens (D) and RNA (E) were positive in the motor trigeminal nucleus. Viral antigens were seen surrounded by inflammatory cells in reticular formation (F). H&E stain (A - C). IHC with DAB chromogen and haematoxylin counterstain (D and F). ISH with haematoxylin counterstain (E). Original magnification: 40x objective (C - F and inset); 10x objective (B); 4x objective (A).

4.2.3.2 Viral titration analysis

In the optimally-treated mice (n= 20), the mean viral titres in the brainstem at 12, 24, 48, 72 and 96 hpi were 0.625, 1.25, 1.5, 0.625 and 0.813 log $CCID_{50}$, respectively (Figure 4.10). Viral titres did not significantly ($P< 0.05$) change over time. The viral titres in the upper and lower spinal cords, serum and pooled muscles were below detection levels (Figure 4.10). Overall, mean viral titres in this group of mice were all significantly lower ($P< 0.05$) than non-immunised mice (section 4.2.1.2, page 59) at all time points and for all tissue types.

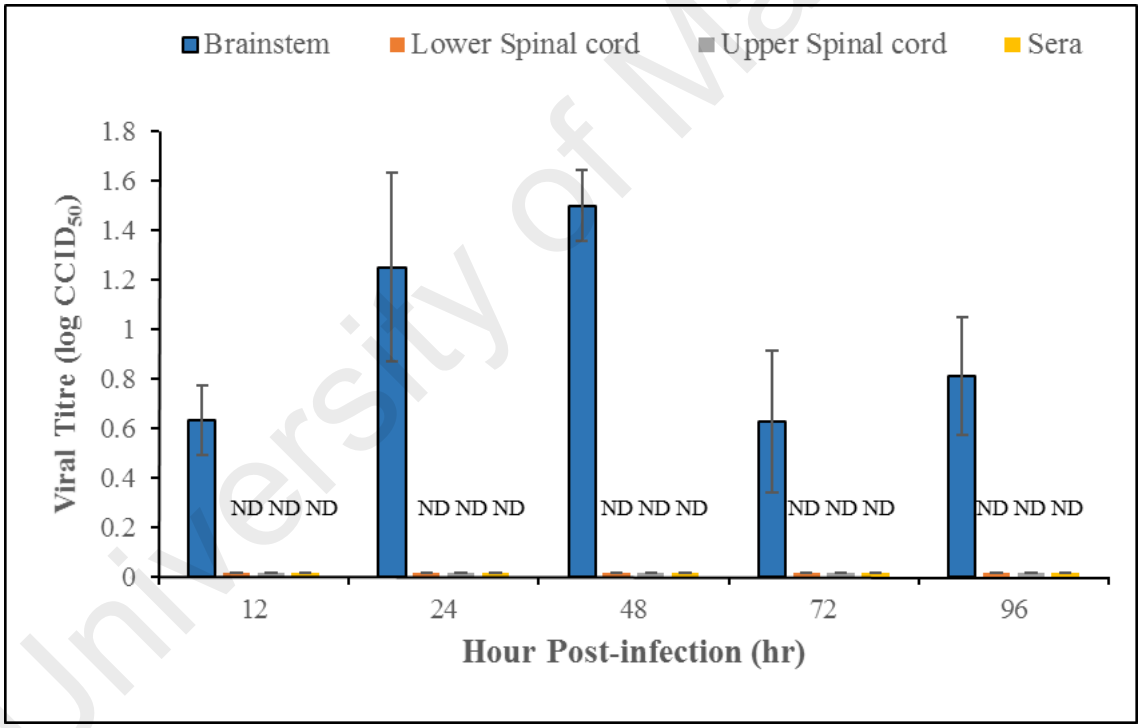

Figure 4.10: Viral titres in CNS tissues and sera following unilateral jaw/facial muscle infection and passively immunised to abrogate viraemia. Viral titres of all tissues except brainstem were below detection limit. Brainstem viral titres were significantly lower than non-immunised mice in section 4.2.1.2 (page 59). Mean viral titres are expressed as the log $CCID_{50}$ ± standard error of mean. *ND= not detected.

4.3 Susceptibility of neurons to direct MAVS infection

4.3.1 MAVS infection of neurons in IC-inoculated (thalamus/hypothalamus) mice

MAVS was unilaterally and IC-inoculated into the thalamus/hypothalamus area to study neuronal and non-neuronal cell susceptibility to direct viral infection. All mice (n= 9) inoculated by this route developed mild paralysis in both hindlimbs at 72 hpi, while mock-infected mice (n= 7) remained healthy.

4.3.1.1 Pathological studies

Figure 4.11 shows the approximate topographic distribution of viral antigens in CNS tissues in each mouse (mouse A1 – A15). Non-specific tissue damage with haemorrhages was observed at the injection site/needle tract (Figure 4.12 C). At 24 hpi (Figure 4.11, mouse A1 – A5), viral antigens/RNA were detected focally around the needle tract in the thalamus region, part of cerebral cortex (retrosplenial cortex and posterior parietal association cortex) (Figure 4.12 A) and around the corpus callosum (Figure 4.12 A, outlined). The antigen-positive cells were mostly non-neuronal cells such as glial cells and astrocytes. In addition, a few neurons in dentate gyrus of the hippocampus (Figure 4.12 B) were positive in 2 of the mice (Figure 4.11, mouse A2 and A4). There was no evidence of viral infection in other CNS regions. Inflammatory cells with viral antigens were seen in the meninges near to the injection site (Figure 4.12 D). Outside the CNS, brown adipose tissues and a few fibres in limb skeletal muscles were positive for viral antigens/RNA. Thus, at 24 hpi, there was already evidence of extra CNS infection.

In mice sacrificed at 48 hpi (Figure 4.11, mouse A6 – A10), viral antigen density around the injected site was relatively lower than at 24 hpi. Well away from the injected site, the brainstem reticular formation and motor trigeminal nucleus were infected

bilaterally (Figure 4.12 E). Several different levels of spinal cords were infected in 3 of the mice, mainly involving anterior horn cells (Figure 4.11, mouse A6, A8 and A10). Brown adipose tissues and skeletal muscles were relatively more severely infected compared to 24 hpi.

In mice sacrificed at 72 hpi (Figure 4.11, mouse A11 – A15), viral antigens/RNA around the injected site were further reduced compared to 48 hpi and 24 hpi (Figure 4.12 F). In other parts of the CNS, away from the injected site, there was even more extensive bilateral brainstem infection involving the midbrain (motor-related regions such as reticular nucleus, ventra tegmental area, periaqueductal gray, red nucleus, substantia nigra (reticular part), anterior tegmental nucleus), motor trigeminal nucleus (Figure 4.12 G and H), dentate nucleus and reticular formation compared to 48 hpi. The viral antigen distribution within the midbrain and brainstem was similar to the IM-infected mice (Section 4.2.1.1, page 51). In the spinal cord, neurons in the anterior, intermediate and posterior horns were involved, although anterior horn cells were more severely infected. Infected CNS neurons showed neuronal damage and vacuolation with mild inflammation. Brown adipose tissues and skeletal muscles were all severely infected.

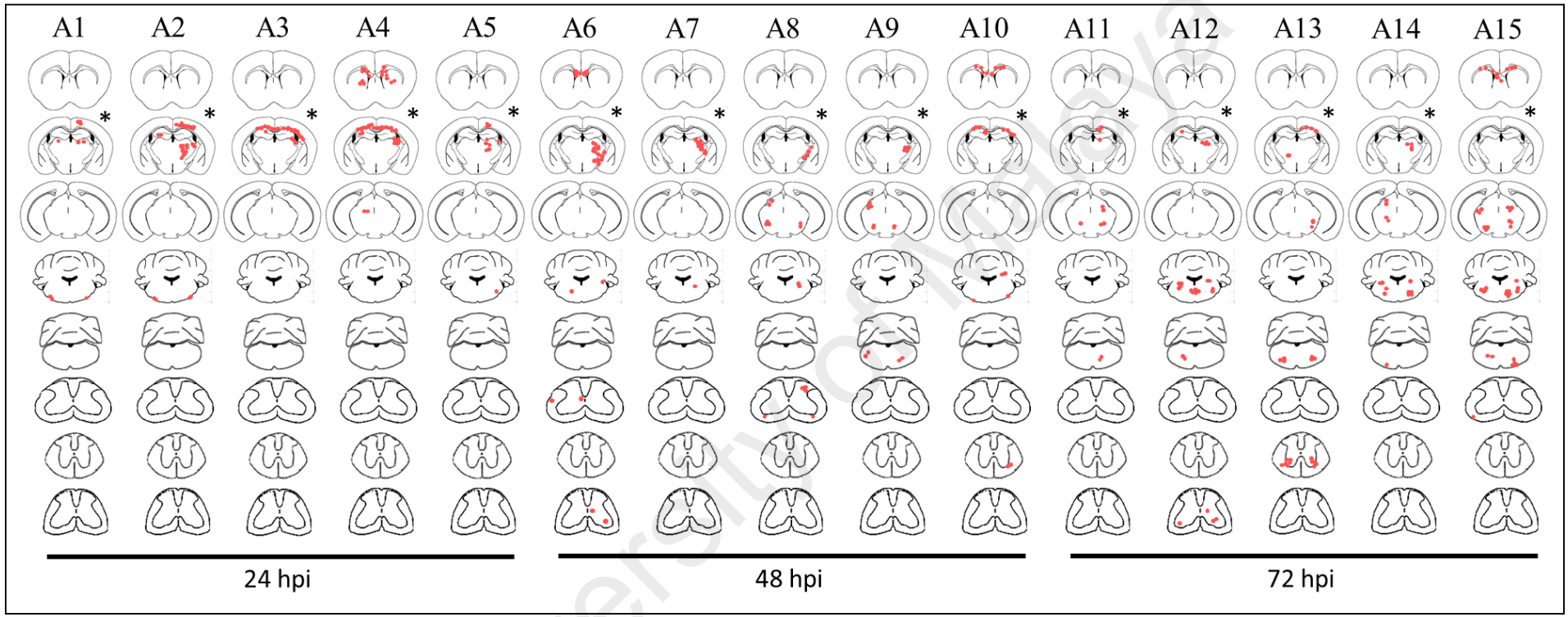

Figure 4.11: Approximation of the distribution of viral antigens in the CNS following IC-inoculation (right thalamus/hypothalamus*). At 24 hpi, viral antigens were found in the injected site/needle tract only. At 48 and 72 hpi, distribution of viral antigens were mostly in the motor-related regions in the brainstem similar to IM (jaw/facial muscles) inoculated mice in Figure 4.3, (page 55). Each red dot represents the equivalent of a positive neuron/white matter axon. For each mouse, cross sections of cerebral cortex, diencephalon/cortex, midbrain/cortex, caudal pons/medulla/cerebellum, medulla/cerebellum, cervical, thoracic, and lumbar spinal cords are displayed.

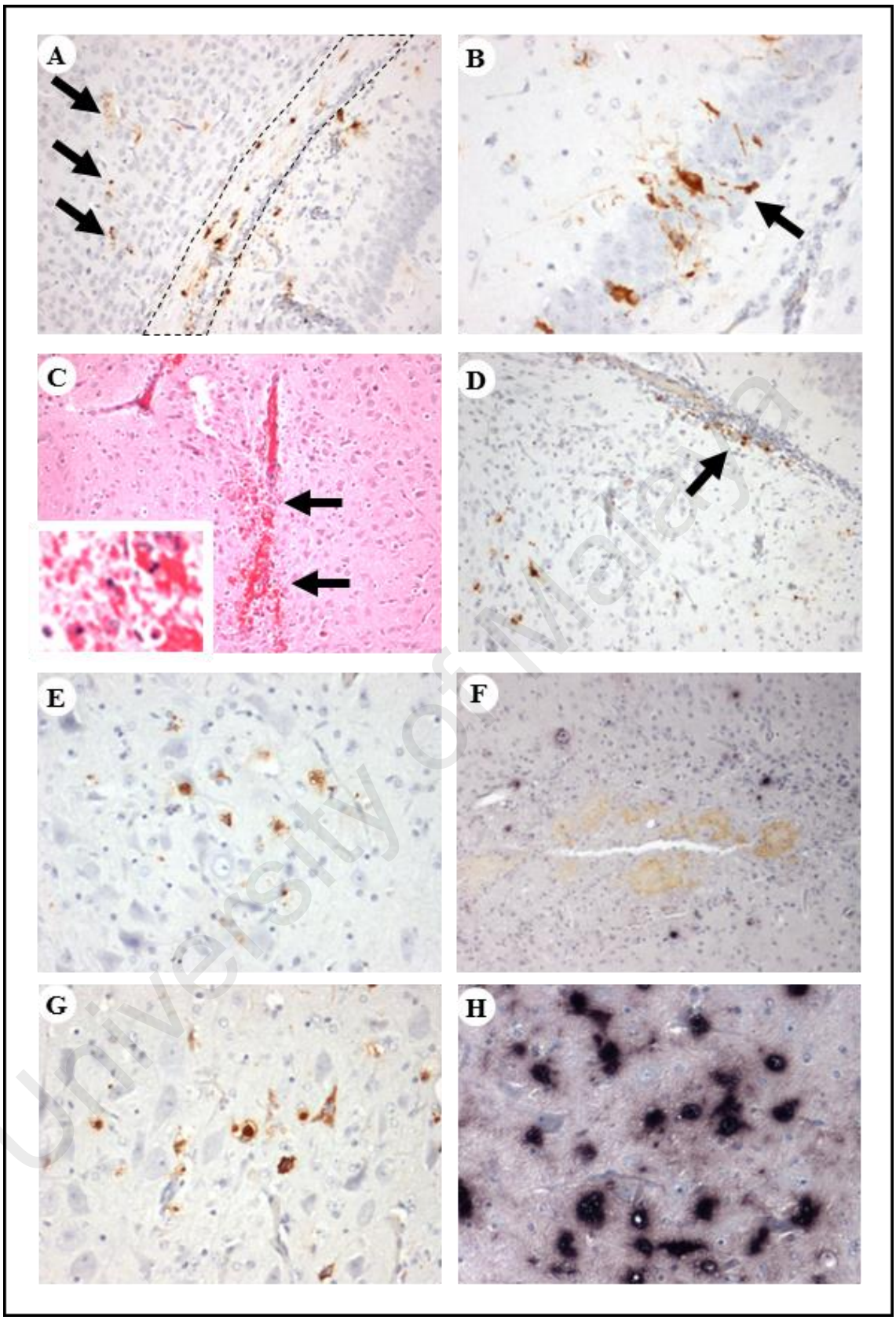

Figure 4.12: Pathological findings following IC-inoculation (thalamus/hypothalamus). Viral antigens were found in the cerebral cortex (A, arrows), corpus callosum (A, outlined), dentate gyrus of hippocampus (B, arrow) at the MAVS injected site. Neuronal tissue damage and haemorrhage (C, arrows); meningitis and viral antigens (D, arrow) were observed at/near the injected site. At 48 hpi, motor trigeminal nucleus were infected (E). At 72 hpi, viral antigens and RNA (F) density was lower at/near the injected site. However, motor trigeminal nucleus was severely infected (G and H). IHC with DAB chromogen and haematoxylin counterstain (A, B, D, E and G). H&E stain (C). ISH with haematoxylin counterstain (F and H). Original magnification: 20x objective (B, C inset, E, G and F); 10x objective (A, C, D and F).

4.3.1.2 Viral titration analysis

Figure 4.13 shows the mean viral titres of sera and all harvested muscle tissues from IC-inoculated (thalamus/hypothalamus) mice (n= 4). The sera mean viral titre was from 2.8 to 3.0 log $CCID_{50}$ throughout the experiment with no significant variations ($P< 0.05$) between time points. The mean viral titres from bilateral forelimb and hindlimb muscles were similar at each specific time points. However, mean muscle viral titres was lowest at 24 hpi ranging from 2.7 to 2.9 log $CCID_{50}$, increasing rapidly and significantly ($P< 0.05$) to 4.3 to 4.4 log $CCID_{50}$ at 48 hpi to peak at 72 hpi with a range of 4.7 to 5.2 log $CCID_{50}$.

The mean viral titres for sera and CNS tissues (whole brainstem, upper and lower spinal cord segments) from the same mouse groups are shown in Figure 4.14. At 24 hpi, the brainstem viral titre (1.08 log $CCID_{50}$) was significantly lower ($P< 0.05$) compared to upper and lower spinal cord viral titres at 2.17 and 1.83 log $CCID_{50}$, respectively. At 48 hpi, brainstem viral titre increased significantly ($P< 0.05$) to 2.25 log $CCID_{50}$ and peaked at 72 hpi with 2.67 log $CCID_{50}$. Upper and lower spinal cord mean viral titres were maintained at 2.42 log $CCID_{50}$ at 72 hpi after a slight increase at 48 hpi.

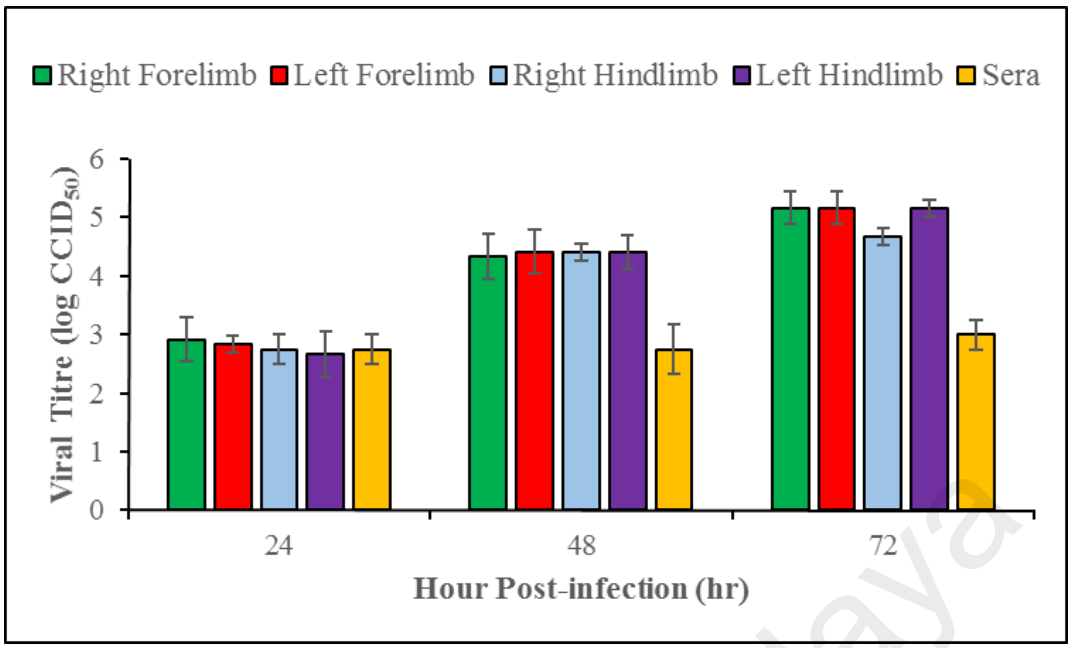

Figure 4.13: Viral titres in muscle tissues and sera following IC-inoculation (thalamus/hypothalamus). Overall, mean viral titres of muscles were insignificant (P< 0.05) different at each specific time point. Muscle tissues mean viral titres were increased over time and peak at 72 hpi. Mean viral titres are expressed as the log $CCID_{50}$ ± standard error of mean.

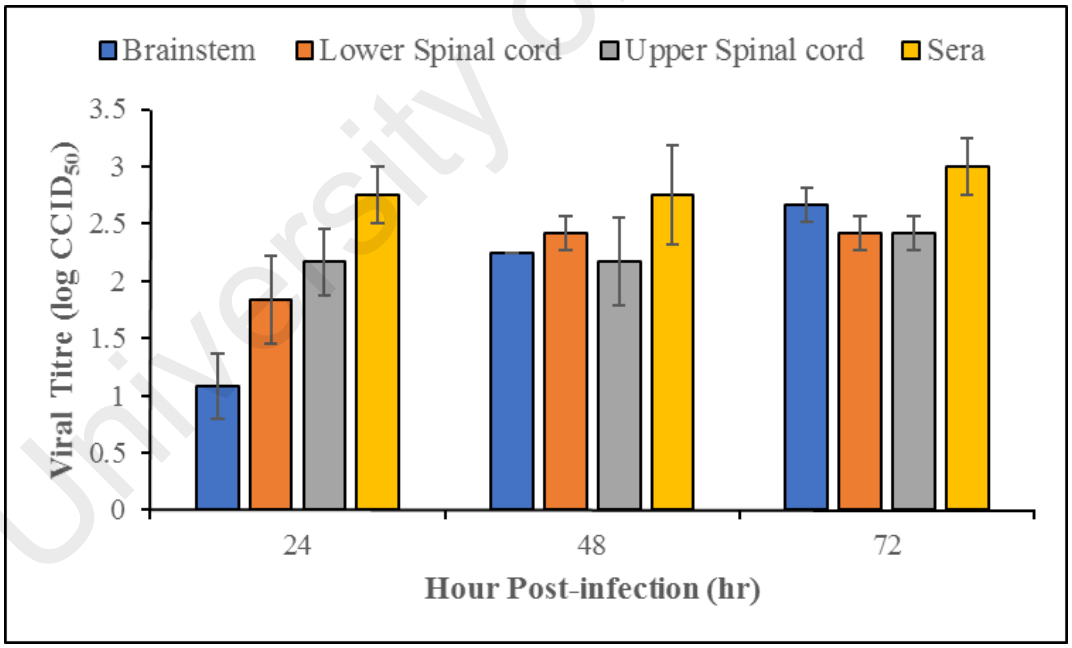

Figure 4.14: Viral titres in CNS tissues and sera following IC-inoculation (thalamus/hypothalamus). Brainstem mean viral titres were lower than upper and lower spinal cord at 24 hpi. In general, CNS and sera mean viral titres were increased gradually but insignificantly (P< 0.05) over time. Mean viral titres are expressed as the log $CCID_{50}$ ± standard error of mean.

4.3.2 MAVS infection of neurons in IC-inoculated (pons/medulla) mice

IC-inoculated (pons/medulla) mice were used to study the neuronal and non-neuronal cell susceptibility to direct viral infection. All MAVS infected mice (n= 7) developed mild paralysis in both hindlimbs at 72 hpi, but mock-infected mice (n= 6) were healthy throughout the experiment.

4.3.2.1 Pathological studies

The approximate topographic distribution of neuronal viral antigens/RNA or damaged neurons in CNS tissues in each mouse is shown in Figure 4.15. In mice (Figure 4.15, mouse A1 – A3) sacrificed at 24 hpi, viral antigens and RNA were only detectable focally around the needle tract in the brainstem (reticular nucleus) and also spinal cord anterior horn cells. Parenchymal damage with haemorrhage in the brainstem, due to the needle tract, was observable under light microscopy (Figure 4.16 A). Viral antigens/RNA were observed around the needle tract, and mainly associated with glial-like or possibly small neuronal cells (Figure 4.16 B). Inflammatory cells with viral antigens/RNA were also found around the meninges near to the injection site. Other regions of the brain were negative for viral antigens/RNA, and appeared normal by light microscopy. A single anterior horn cell in the spinal cord was positive for viral antigens (Figure 4.15, mouse A1 – A3). Brown adipose tissue and a few fibres in both hindlimbs muscles were infected too.

In all mice sacrificed at 48 hpi (Figure 4.15, mouse A4 – A6). Viral antigens around the needle tract were relatively less dense compared to 24 hpi (Figure 4.16 C - F) and mostly found in/around inflammatory cells. However, viral RNA remained dense in that area (Figure 4.16 G and H). The reticular formation and motor trigeminal nuclei also demonstrated positive IHC and ISH staining. Overall, the distribution of viral

antigens/RNA in the brain was mainly motor related neurons (motor trigeminal nucleus and reticular formation) and shared a lot in common with IM-infected mice (Section 4.2.1.1, page 51). Cervical spinal cords were more severely infected in the posterior, intermediate and anterior horn cells compared to 24 hpi. Large skeletal muscle groups such as hindlimb and forelimb muscles were severely infected with advanced necrosis and myositis. A few muscle fibres in small skeletal muscles such as tongue and jaw/facial muscles were positive for viral antigens too.

In mice sacrificed at 72 hpi (Figure 4.15, mouse A7 – A10), CNS infection was more extensive compared to 48 hpi. Again, viral distribution in CNS resembled findings in IM-infected mice (section 4.2.1.1, page 51). Viral antigens were found in the motor trigeminal nuclei (Figure 4.16 J), reticular formation, facial nuclei, thalamus, hypothalamus, red nucleus, dentate nucleus and motor cortex. The relative density of viral antigens/RNA around the needle tract was further reduced (Figure 4.16 I). However, spinal cord infection was mainly in the anterior horn cells (Figure 4.15, mouse A7, A8 and A10). All skeletal muscles were severely infected and had advanced necrosis and myositis.

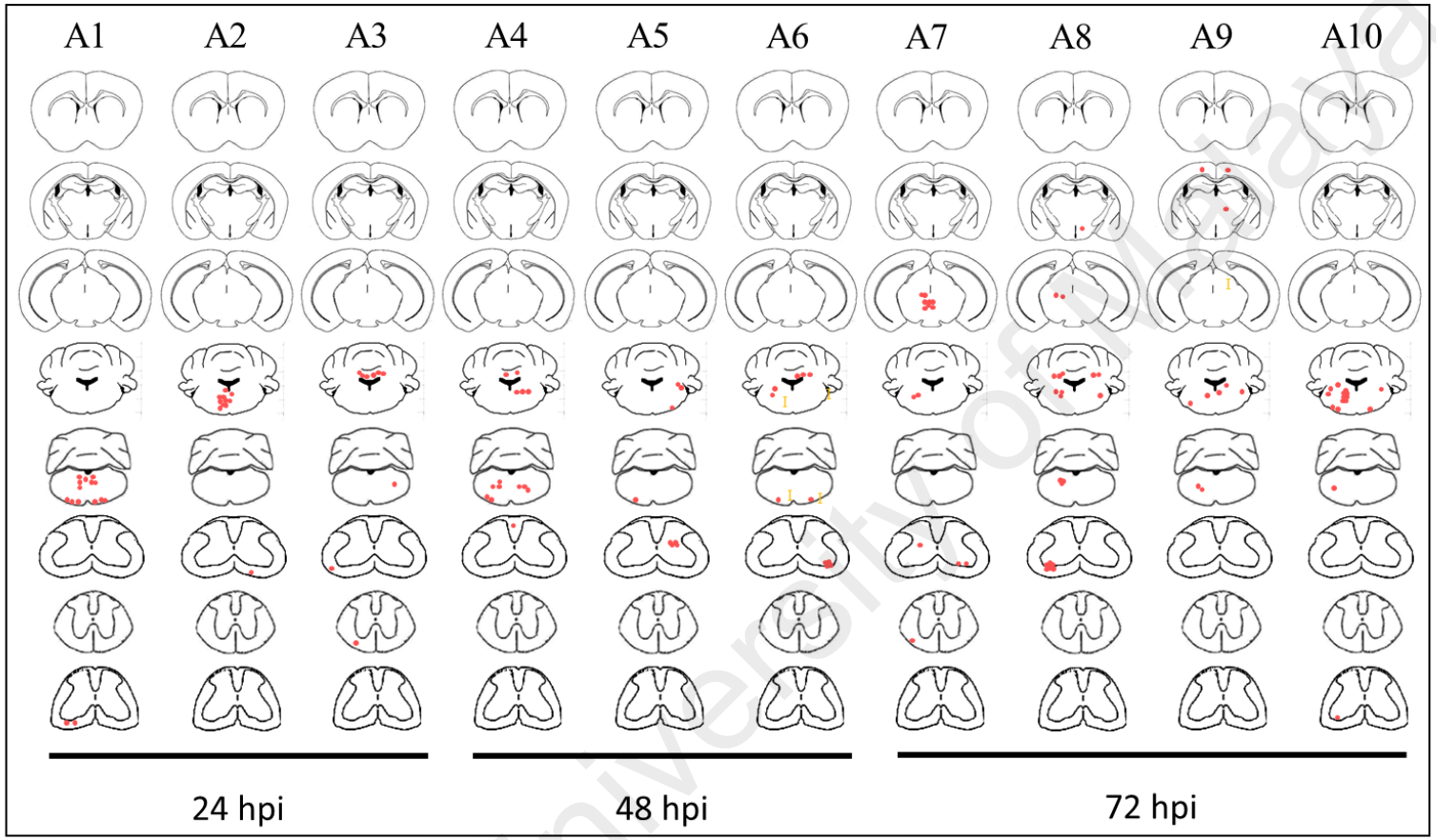

Figure 4.15: Approximation of the distribution of viral antigens/RNA in the CNS following IC-inoculation (pons/medulla). At 24 hpi, viral antigens/RNA was only detectable in the brainstem (pons/medulla) at the injected site. Viral distribution at 48 and 72 hpi was mainly motor related neurons (motor trigeminal nucleus and reticular formation). Each red dot represents the equivalent of a positive neuron/white matter axon. For each mouse, cross sections of cerebral cortex, diencephalon/cortex, midbrain/cortex, caudal pons/medulla/cerebellum, medulla/cerebellum, cervical, thoracic, and lumbar spinal cords are displayed.

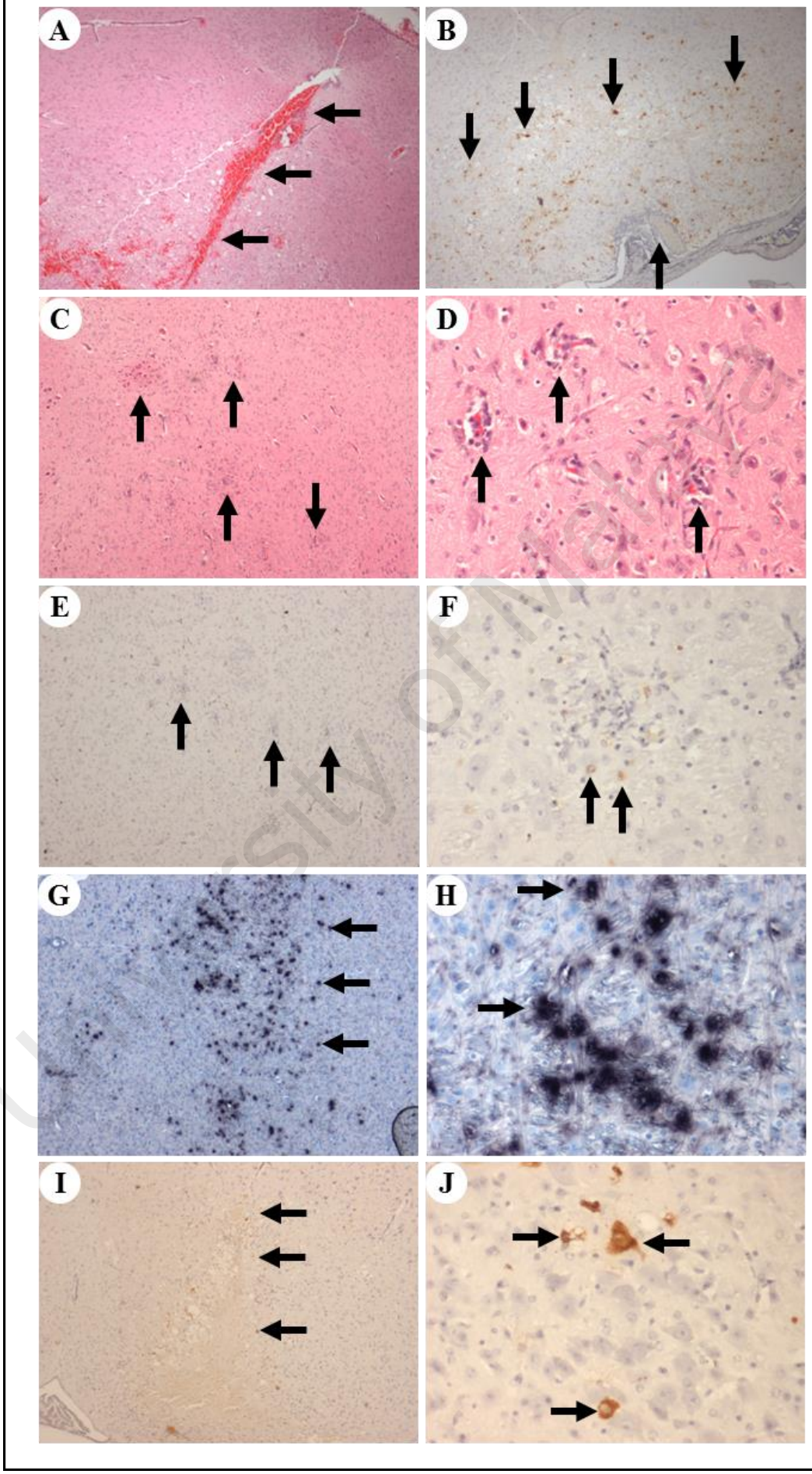

Figure 4.16: Pathological findings following IC-inoculation (pons/medulla). Neuronal tissue damage and haemorrhage (A, arrows). Viral antigens were found in the brainstem at the injection site at 24 hpi (B, arrows). At 48 hpi, mild inflammation was observed at the injection site (C and D, arrows). Viral antigens were reduced (E, arrows) compared to 24 hpi and an increase of inflammatory cells was observed (F, arrows). However, viral RNA was seen all around needle tract (G and H, arrows). At 72 hpi, viral antigens were minimal around the injected site (I, arrows) and few neurons in motor trigeminal nucleus were stained up (J, arrows). IHC with DAB chromogen and haematoxylin counterstain (B, E, F, I and J). H&E stain (A, C and D). ISH with haematoxylin counterstain (G and H). Original magnification: 20x objective (D, F, H and J); 4x objective (A - C, E, G and I).

4.3.2.2 Viral titration analysis

Figure 4.17 shows the mean viral titres of sera and all harvested limb muscle tissues from IC-inoculated (pons/medulla) mice (n= 4). Sera viral titres gradually increased over time ranging from 2.44 to 2.69 log $CCID_{50}$, but showed no significant difference ($P< 0.05$) between time points. Mean viral titres from all muscle groups were similar at each specific time point. However, the mean muscle viral titres at 24 hpi ranging from 2.63 to 2.94 log $CCID_{50}$, increased significantly ($P< 0.05$) to 4.13 to 4.50 log $CCID_{50}$ at 48 and at 72 hpi, respectively.

The mean viral titres of sera and all CNS tissues (whole brainstem, upper and lower spinal cord segments) derived from the same infected mice are shown in figure 4.18. At 24 hpi, brainstem mean viral titre at 3.44 log $CCID_{50}$ was significantly higher ($P< 0.05$) than upper and lower spinal cord viral titres at 2.69 and 2.81 log $CCID_{50}$, respectively. At 48 hpi, brainstem, upper and lower spinal cord viral titres dropped significantly ($P< 0.05$) to 1.56, 1.00 and 1.88 log $CCID_{50}$, respectively. Later, all CNS viral titres rose slightly to 2.19 log $CCID_{50}$ at 72 hpi.

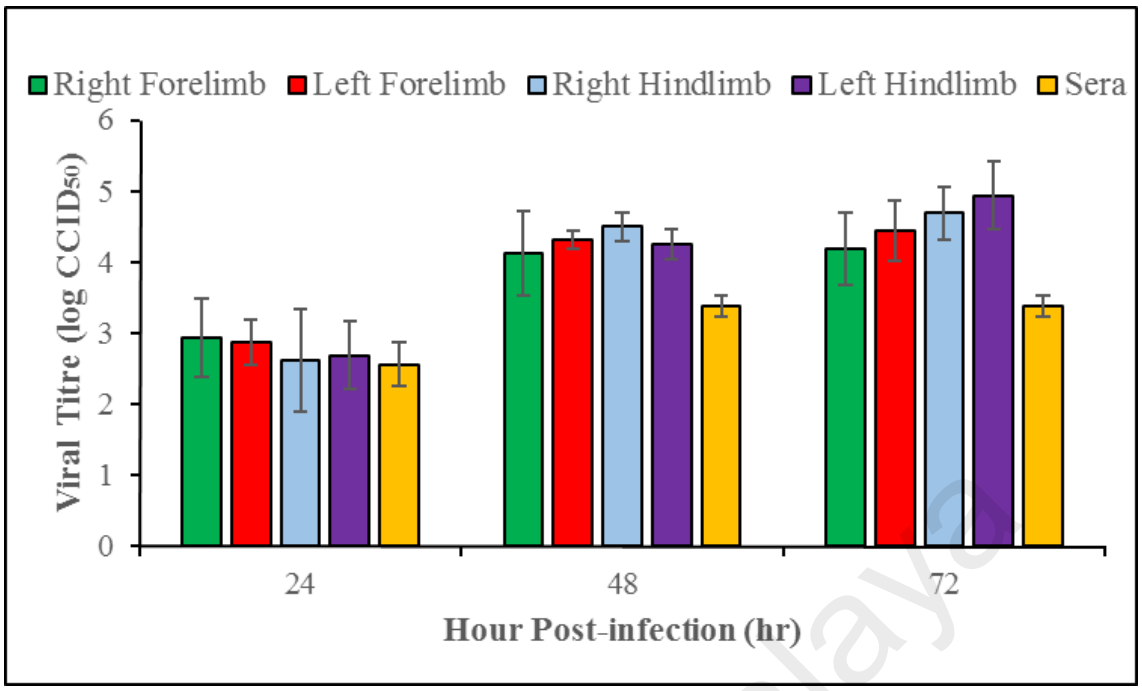

Figure 4.17: Viral titres in muscle tissues and sera following IC-inoculation (pons/medulla). Muscles mean viral titres were insignificant ($P< 0.05$) different at each specific time points. Over time, mean viral titres of all muscle types were increasing and peaked at 72 hpi. Mean viral titres are expressed as the log $CCID_{50}$ ± standard error of mean.

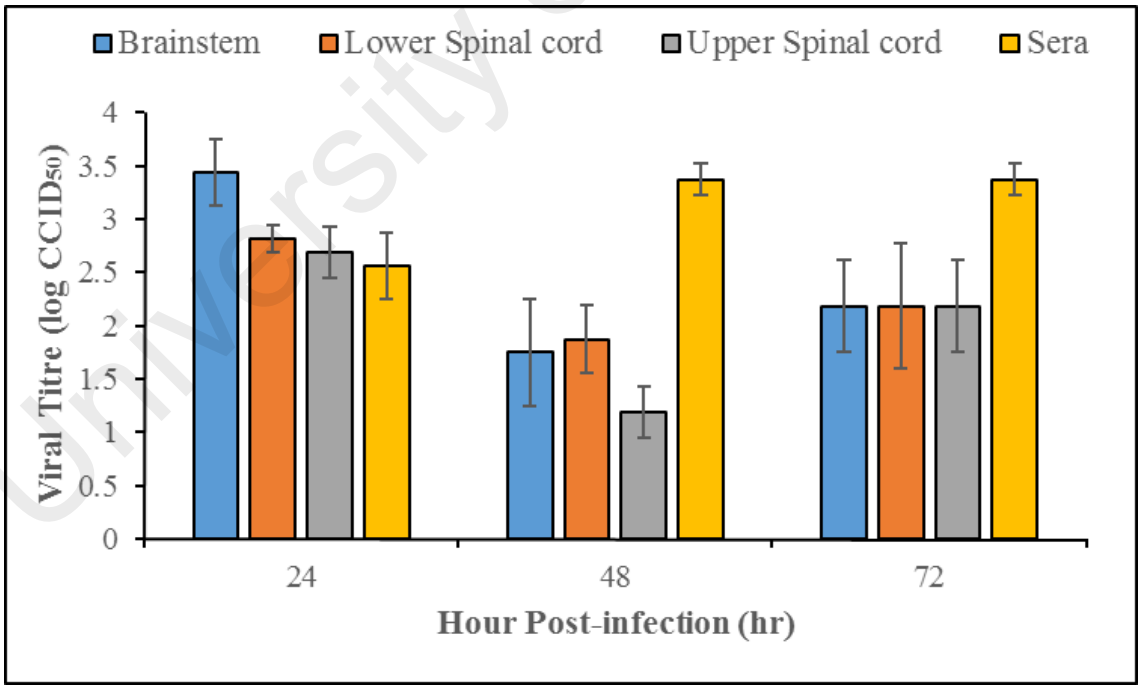

Figure 4.18: Viral titres in CNS tissues and sera following IC-inoculation (pons/medulla). CNS viral titres were high at 24 hpi and dropped significantly ($P< 0.05$) at 48 hpi. Subsequently, CNS titres increased slightly at 72 hpi. Mean viral titres are expressed as the log $CCID_{50}$ ± standard error of mean.

4.3.3 MAVS infection of primary murine motor neurons

Neuronal susceptibility to MAVS infection was further evaluated in a primary cell culture system. Primary motor neurons isolated from 14 day-old ICR mouse embryo were found to be only very rarely infected by MAVS. Less than 10 neurons were infected in a pool of 10^6 of cells incubated with MAVS of 1.13 x 10^5 $CCID_{50}$/ml. Figure 4.19 shows a single motor neuron cell positively stained for viral antigens.

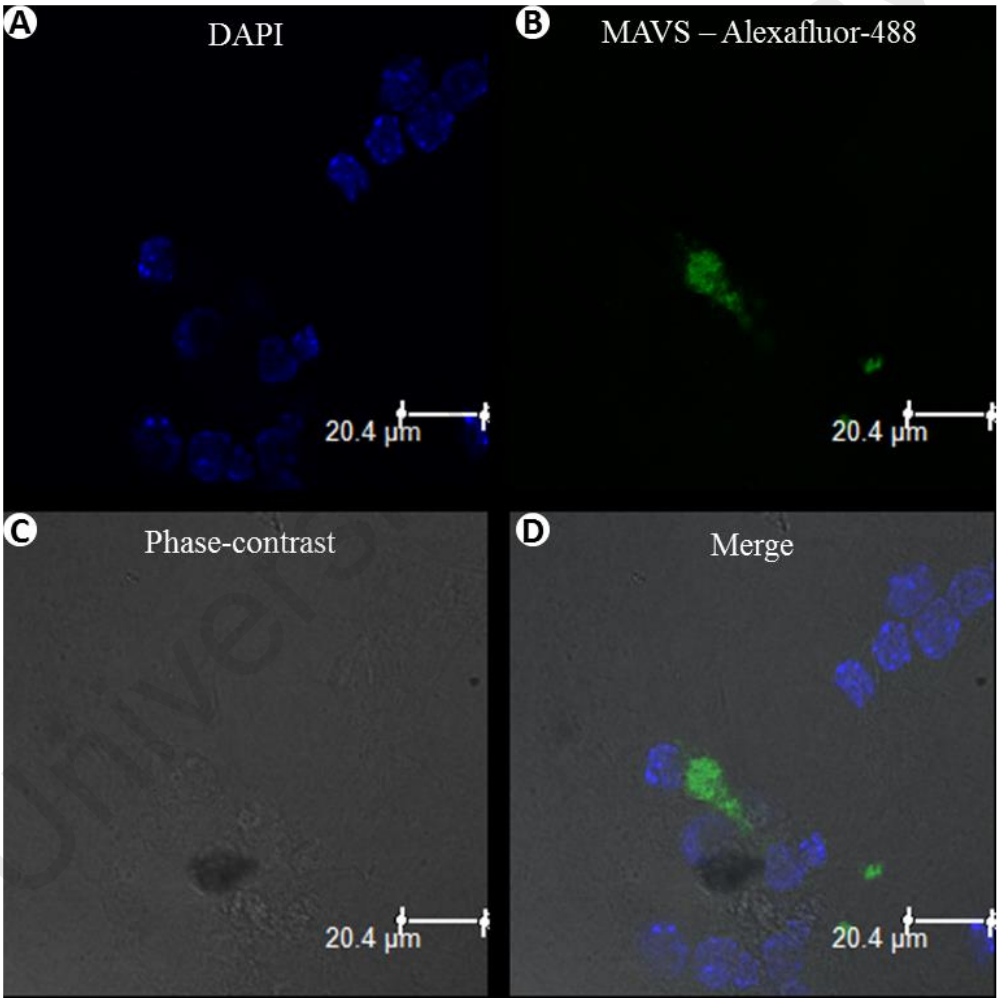

Figure 4.19: EV-A71 infection of primary murine motor neurons. A single primary motor neuron cell showed positive immunofluorescence signal (B) and nucleus counterstaining by DAPI (A). Phase contrast image was observed under white light (C) and images were superimposed in (D).

4.3.3.1 MAVS infection of primary murine motor neurons transfected with hSCARB2

Since primary murine motor neurons were rarely infected by MAVS, the cells were transfected with hSCARB2 along with mCherry fluorescent protein as positive control, to increase EV-A71 infectivity. About 60% of the cell population were found to express hSCARB2 receptors and about 40% (of the hSCARB2 expressing cells) were infected by EV-A71 (Figure 4.20).

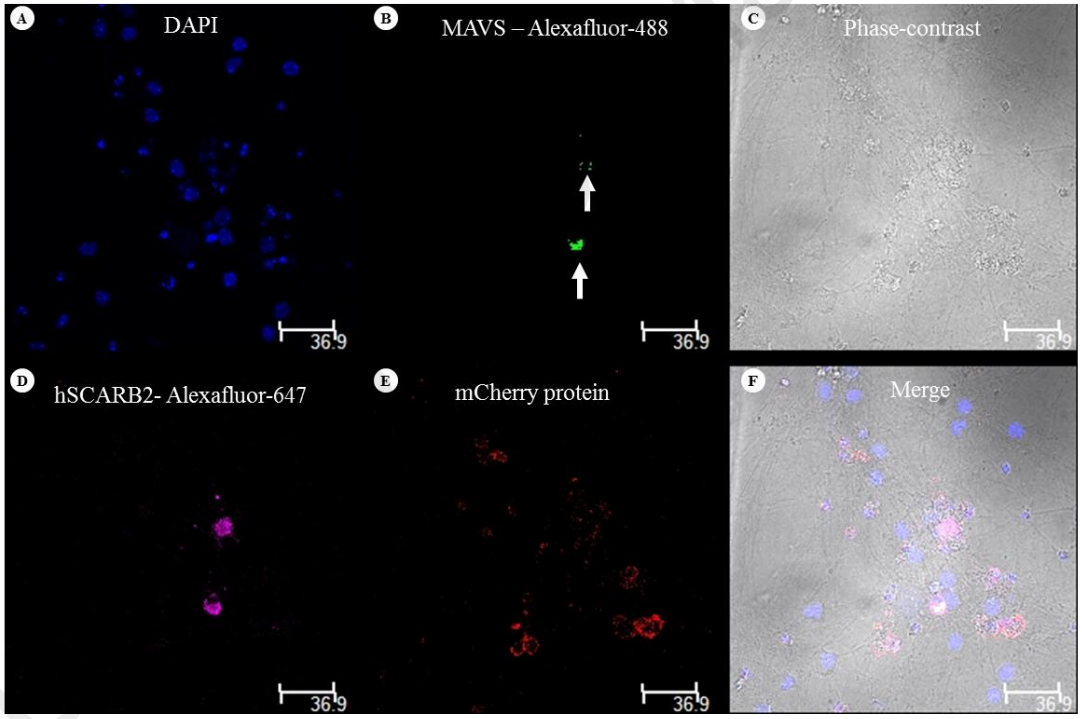

Figure 4.20: EV-A71 infection of primary murine motor neurons transfected with hSCARB2. Primary motor neuron isolated from ICR mice, transfected with hSCARB2-mCherry gene (D and E) was infected by MAVS (B). Nucleus was counterstained with DAPI; MAVS were labelled with Alexafluor-488; hSCARB2 receptor was stained with Alexafloour-647; mCherry-protein served as transfection positive control.

4.4 Retrograde axonal transport in hSCARB2 primary murine motor neurons

4.4.1 Primary motor neuron study

As primary motor neuron cells from ICR mice were less susceptible and the transfection with hSCARB2 was not efficient (Section 4.3.3 (page 81)), primary motor neuron cells cultured from hSCARB2 Tg mouse embryo were seeded into a microfluidic chamber, to direct growth of axons away from respective neuronal bodies into a fluidically isolated environment. Alexa-555-labelled EV-A71 was introduced either into the chamber containing neuronal cell bodies or the chamber with axon terminals. EV-A71 was observed to travel from axon terminals towards the direction of neuronal cell bodies or retrograde transmission, 5 min post-infection (Figure 4.21). Conversely, viral transportation from cell bodies toward the axon terminals or anterograde transmission was never observed. Figure 4.22 shows co-localisation of hSCARB2 receptor and EV-A71 in neuronal cell body when EV-A71 was introduced into the chamber with axon terminals.

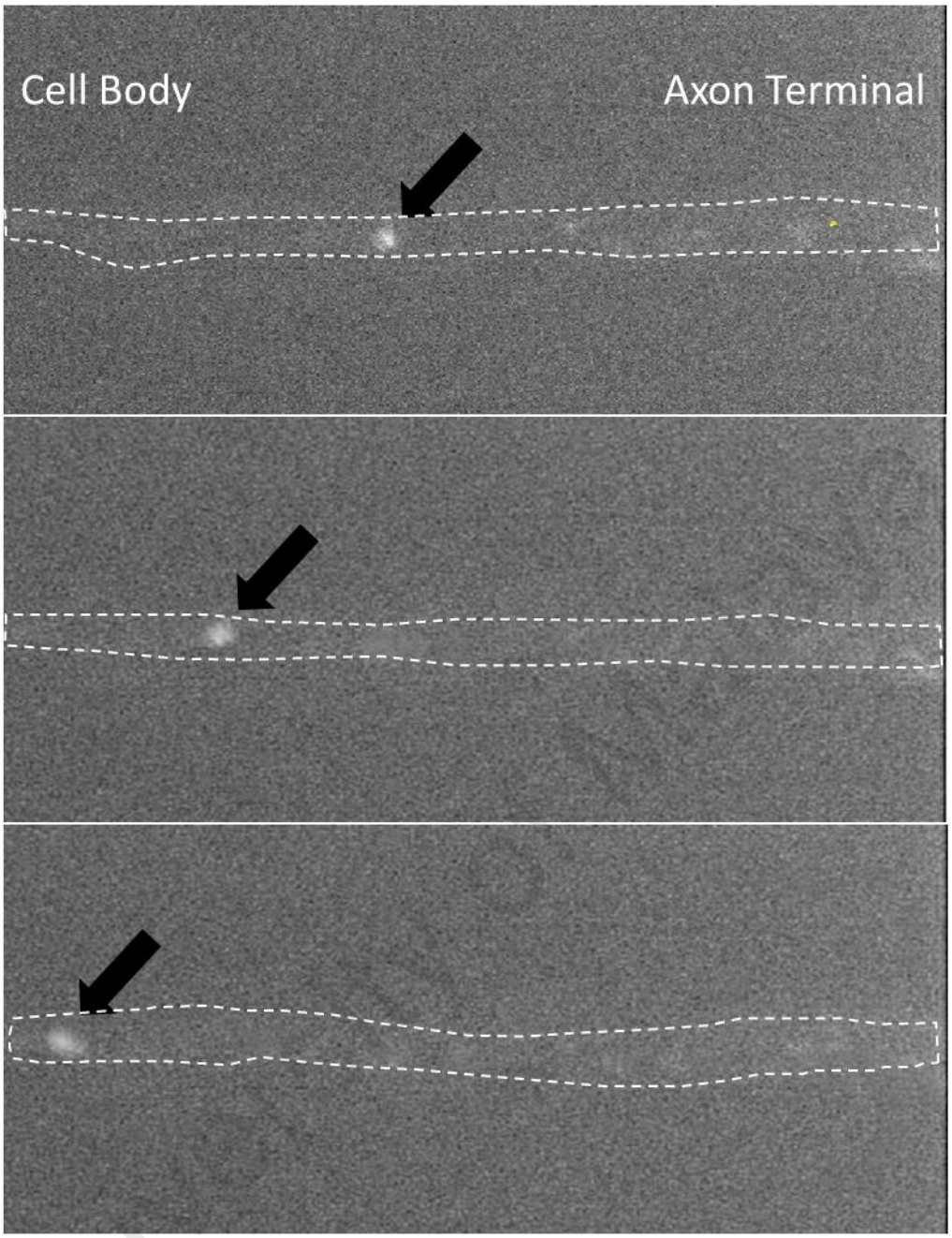

Figure 4.21: Live cell imaging of infected primary motor neurons. Alexa-555 labelled EV-A71 was seen along the axonal tract of primary motor neurons moving towards the cell body (retrograde axonal transport) at 60x objective magnification.

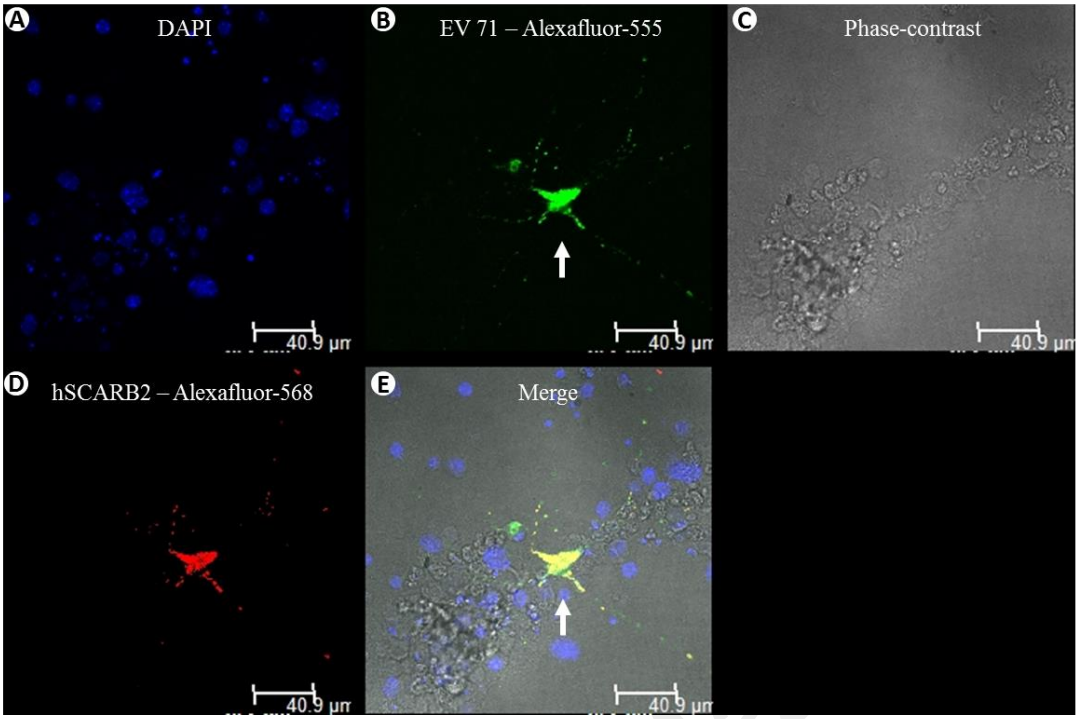

Figure 4.22: Double immunofluorescence staining of EV-A71 and hSCARB2. When EV-A71 was introduced into the chamber with axon terminals, neuronal cell body was infected, at 24 hpi.

4.4.1.1 Viral titration analysis

When virus was added into the chamber containing neuronal cell bodies, viral titres obtained from the axon terminal chamber were below detection limit at all-time points (Figure 4.23). However, when virus was added into the axon terminal chamber (Figure 4.24), a mean viral titre of 0.3 log $CCID_{50}$ was obtained from the neuronal cell body chamber, as early as 16 hpi, increasing to 3.0 log $CCID_{50}$ at 48 hpi. In addition, the mean viral titres in the axon terminal chamber were significantly ($P< 0.05$) higher than the viral titres obtained from the neuronal cell body chamber at 0, 16 and 20 hpi (Figure 4.24). At 48 hpi, the viral titres obtained from cell body chamber were similar to the original inoculated viral titre in the axon terminal chamber.

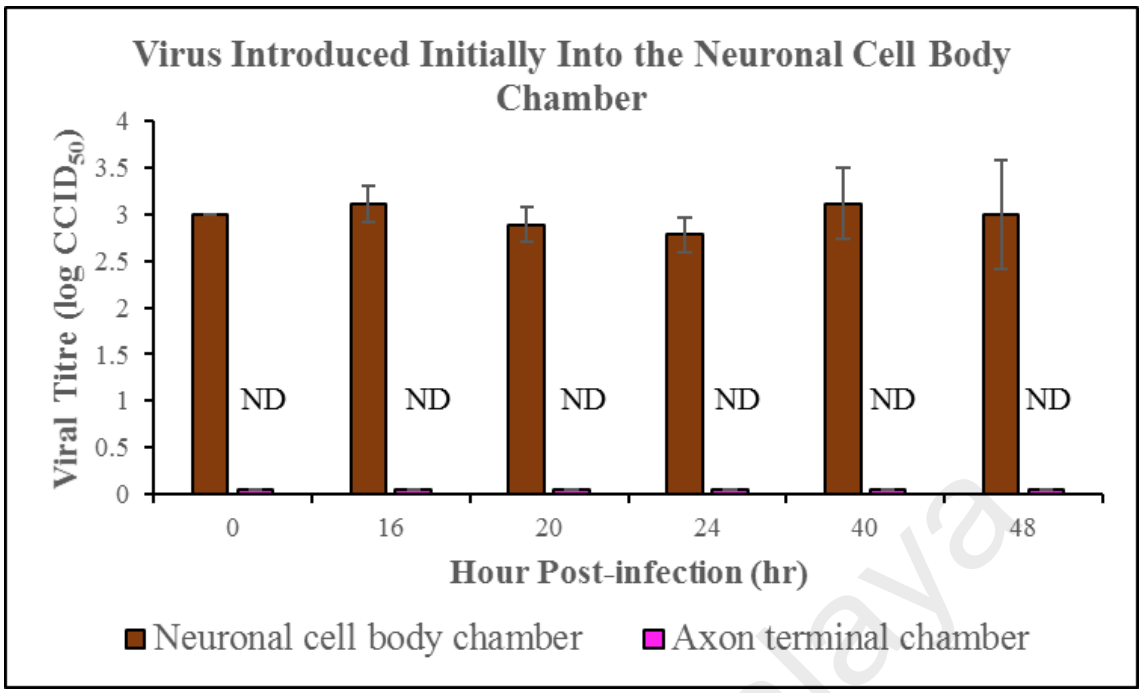

Figure 4.23: Mean viral titres from both neuronal cell body and axon terminal chambers, after introduction of virus into the cell body chamber. Viral titres obtained from the axon terminal chamber were below detection limit at all time points. Mean viral titres were expressed as mean viral titres ± standard error of mean. *ND= not detected.

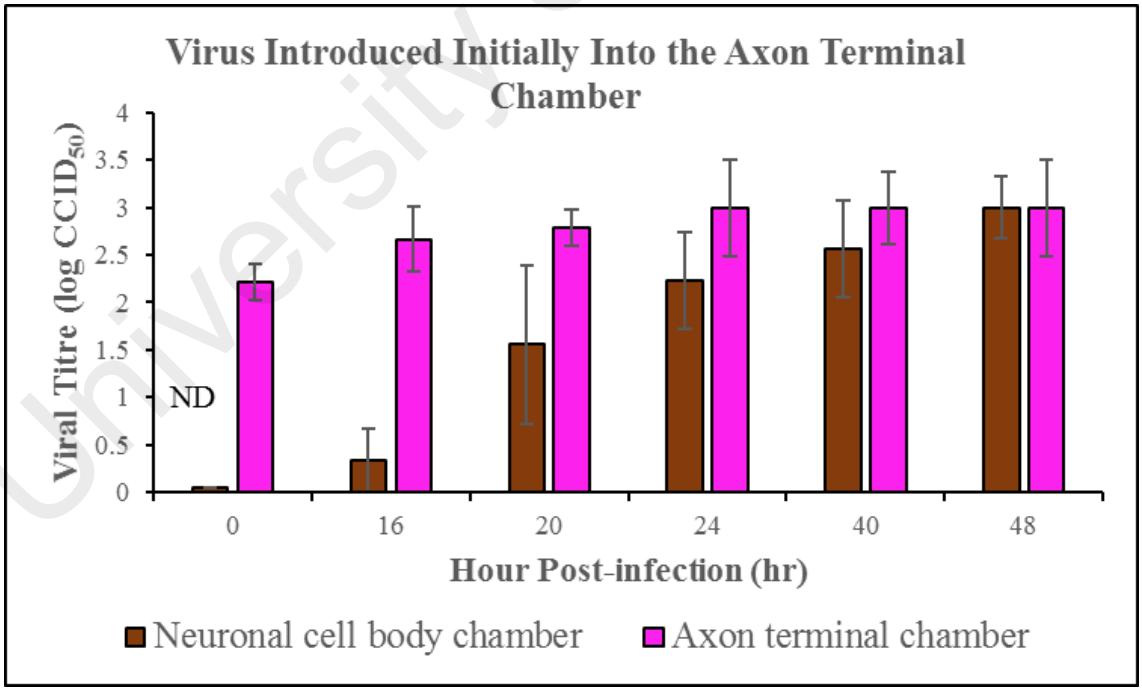

Figure 4.24: Mean viral titres from both neuronal cell body and axon terminal chambers, after introduction of virus into the axon terminal chamber. Viral titres obtained from cell body chamber were gradually increased over time. Mean viral titres were expressed as mean viral titres ± standard error of mean. *ND= not detected.

4.5 EV-A71 "Provocation poliomyelitis"

4.5.1 MAVS infection in mice with experimentally-traumatised gastrocnemius muscles

Since patients with muscle injury following IM-injection of vaccines or therapeutic agents have increased risks of developing "provocation poliomyelitis" due to poliovirus, EV-A71 infection may be associated with similar risks. To investigate this potential phenomenon in EV-A71 infection, half of IP-infected mice were traumatised experimentally in the both gastrocnemius muscles. All mice in the traumatised group (n= 5) and in the non-traumatised group (n= 5) infected with 1.78×10^2 $CCID_{50}$ MAVS showed similar weakness in both hindlimbs at 72 hpi. However, the same mouse groups infected with a lower viral dose of 90 $CCID_{50}$ of MAVS did not show any signs of infection throughout the experiment.

4.5.1.1 Pathological studies

Animals in the 4 mouse groups were sacrificed at 72 hpi for pathological examination. Overall, viral antigen densities were similar in all tissue types in traumatised (n= 5) and non-traumatised (n= 5) mice after infection with either 1.78×10^2 $CCID_{50}$ or 90 $CCID_{50}$, MAVS (Figure 4.25).

All mice (n= 10) infected with 1.78×10^2 $CCID_{50}$ showed early infection in the CNS, specifically in the spinal cords where a few anterior horn cells were positive for viral antigens. In traumatised and non-traumatised mice there was no difference in viral density (Figure 4.25 E - H). Skeletal muscles were severely infected, with high viral antigen densities (Figure 4.25 A - D). There was no evidence of CNS infection in the 2 mouse groups infected with 90 $CCID_{50}$ of MAVS. However, muscles were severely infected and inflamed.

Control mice (n= 6) were injected with WGA at 10 µg per mouse in 10 µL to verify that the experimentally-traumatised muscle could facilitate retrograde axonal transport. Traumatised mice showed a higher concentration of WGA in lower spinal cords segment compared to non-traumatised mice at 12 hpi (Figure 4.26).

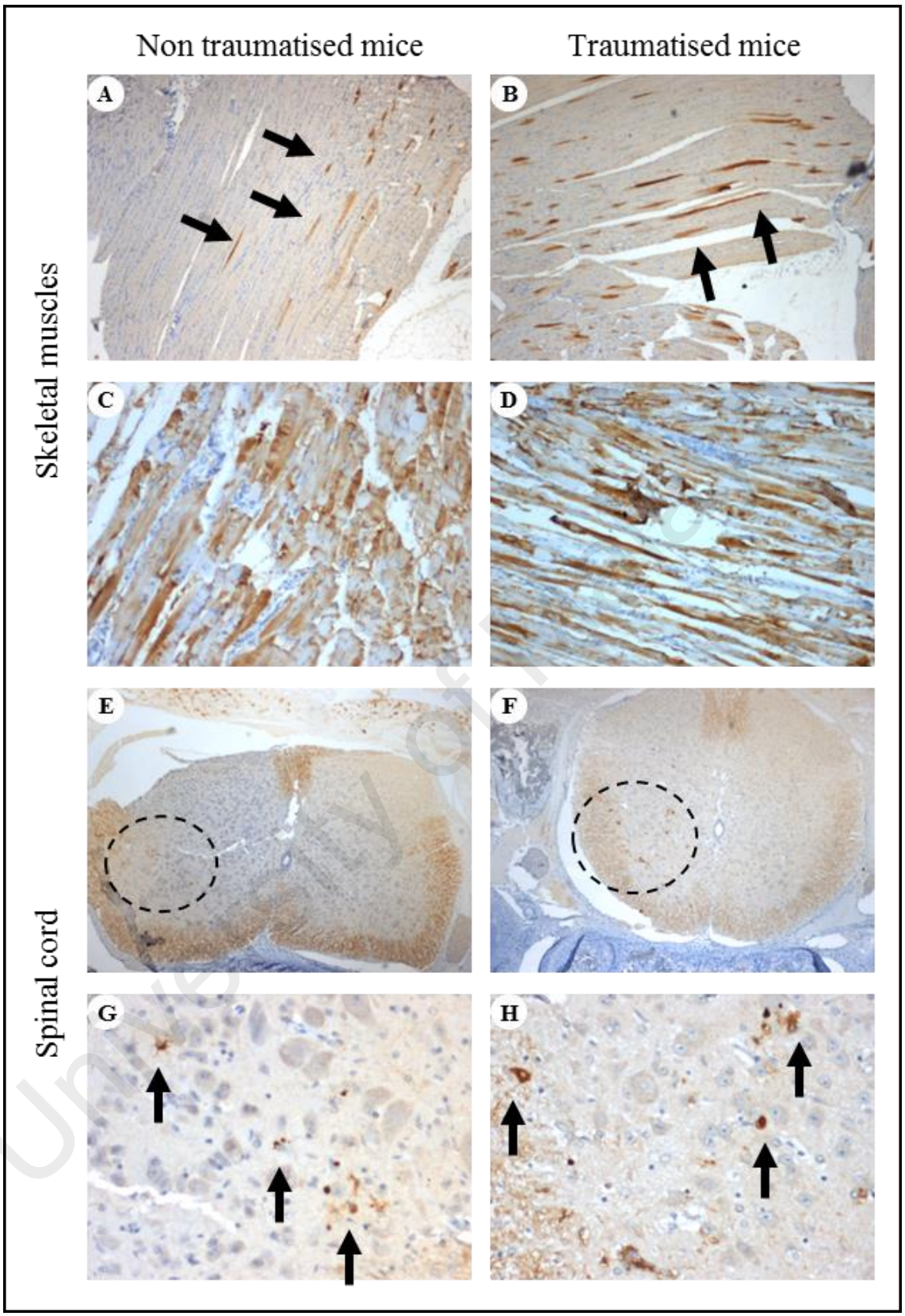

Figure 4.25: Pathological findings following IP-inoculation, in gastrocnemius muscle-traumatised and non-traumatised mice. Viral antigens density was similar in traumatised and non-traumatised mice in comparable tissues. IHC with DAB chromogen and haematoxylin counterstain (A - H). Original magnification: 20x objective (G and H); 10x objective (C and D); 4x objective (A, B, E and F).

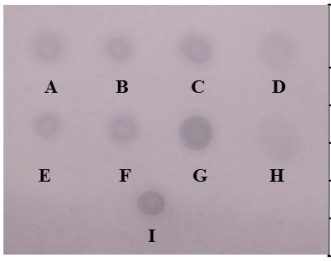

Tissues	Non-traumatised mice	Traumatised mice
Right hindlimb	A	E
Left hindlimb	B	F
Lower Spinal cord	C	G
Upper Spinal cord	D	H
Positive control	I	

Figure 4.26: IHC detection of WGA dot blotted onto nitrocellulose membrane. WGA concentration in the lower spinal cord was higher in the experimentally-traumatised mice (G) compared to non-traumatised mice (C), suggesting WGA was retrograde axonally transported at a faster rate into lower spinal cords in experimentally-traumatised mice. 1 µg of WGA served as positive control (I).

4.5.1.2 Viral titration analysis

In all mice (n= 10) infected with 90 $CCID_{50}$ MAVS, all CNS viral titres were below detection limits at 72 hpi (Figure 4.27B). The mean viral titres for muscle tissues in non-traumatised mice (n= 5) were insignificantly different ($P< 0.05$) from traumatised mice (n= 5), and ranged from 2.4 to 2.5 log $CCID_{50}$. Viral titres in all tissues of mice (n= 10) infected with 1.78×10^2 $CCID_{50}$ MAVS, were insignificantly different ($P< 0.05$) between traumatised (n= 5) and non-traumatised (n= 5) mice (Figure 4.27A). Lower spinal cord segments and muscle tissues showed mean viral titres at 1.1 and 3.5 to 3.9 log $CCID_{50}$, respectively (Figure 4.27A).

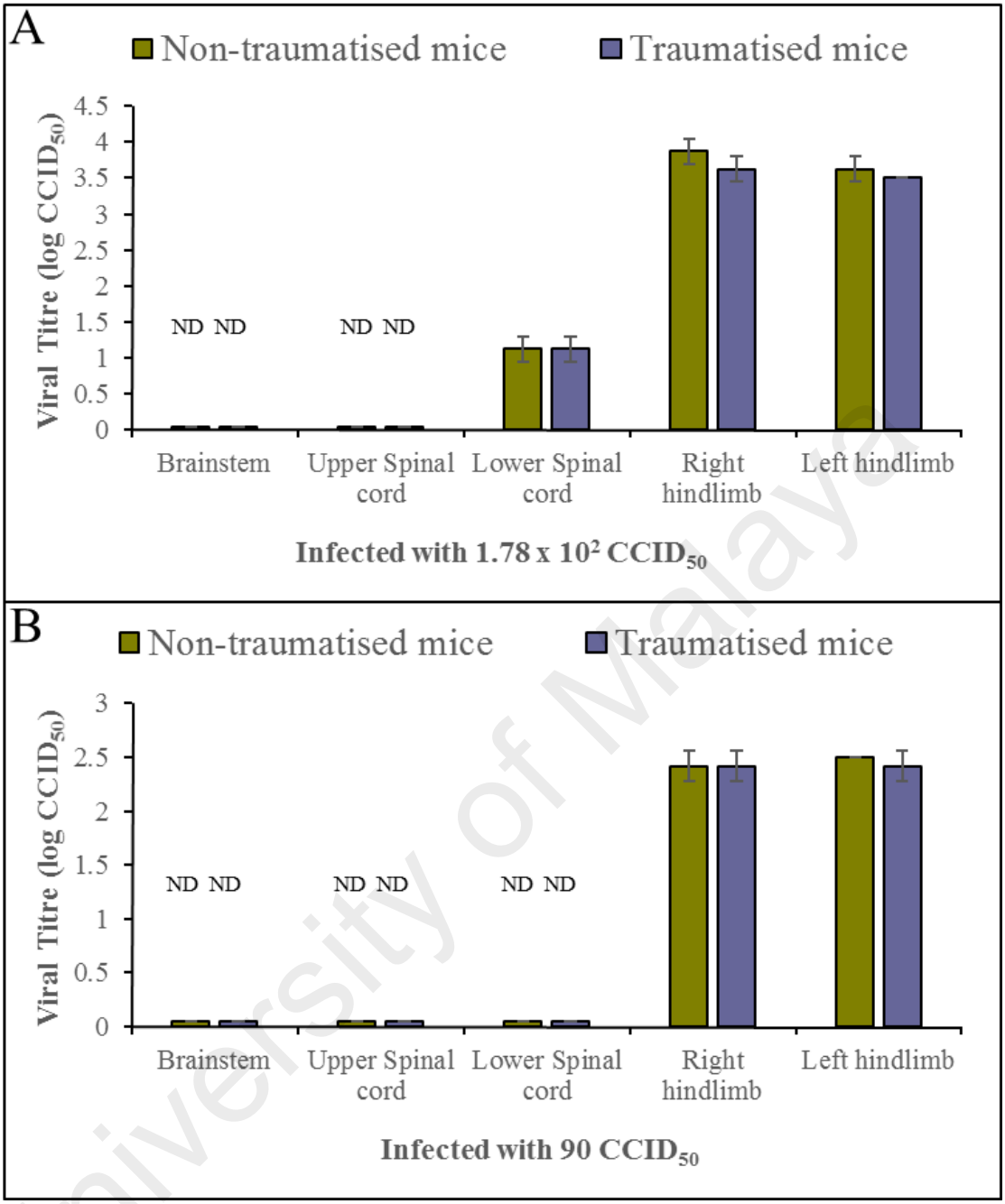

Figure 4.27: Viral titres in CNS and muscle tissues following IP-inoculation at 1.78 x 10^2 $CCID_{50}$ (A) and 90 $CCID_{50}$ (B), in gastrocnemius muscle-traumatised and non-traumatised mice. Mean viral titres were insignificantly ($P < 0.05$) different between traumatised and non-traumatised mice in all type of tissues regardless of MAVS dose. Mean viral titres are expressed as the log $CCID_{50}$ ± standard error of mean. *ND= not detected.

4.5.2 Infection studies with light-sensitive MAVS

4.5.2.1 Viral titration analysis

Light-sensitive MAVS was inoculated into the gastrocnemius muscle of ICR mice to provide further insights into viral replication and transmission into the CNS. Since newly-synthesised virus *in vivo* is not sensitive to light, light treatment could be used to distinguish it from the original inoculum. Figure 4.28 shows mean viral titres of hindlimb muscles, whole brainstem and upper and lower spinal cord segments at 24 hpi, 48 hpi and 72 hpi (Figure 4.28). Overall, all mean viral titres from light-protected samples (mixture of original inoculum and newly synthesised virus) were not significantly ($P< 0.05$) different from corresponding light-treated samples (newly synthesised virus).

At 24 hpi, all CNS viral titres (n= 5) were below detection levels whereas, hindlimb muscle titres were 2.75 log $CCID_{50}$ and 2.42 log $CCID_{50}$ for light-protected and light-treated samples, respectively (Figure 4.28A). At 48 hpi, viral titres from upper and lower spinal cord segments (n= 5 each) were 1.5 log $CCID_{50}$ and 0.5 log $CCID_{50}$ in light-protected samples and in light-treated samples were 1.42 and 0.5 log $CCID_{50}$, respectively. Whereas, muscle titres increased to 4.6 log $CCID_{50}$ and 4.1 log $CCID_{50}$ in light-protected samples and in light-treated samples, respectively (Figure 4.28B). At 72 hpi (n= 5), CNS infection, including brainstem infection, was established but brainstem viral titres were the same at 1.67 log $CCID_{50}$ for both light-protected and light-treated samples. Conversely, muscles titres increased slightly to 4.7 log $CCID_{50}$ and 4.2 log $CCID_{50}$ in light-protected samples and in light-treated samples, respectively, and yet was not significant in between two samples (Figure 4.28C). Hence, viruses isolated from the CNS were mostly “newly-synthesised viruses”.

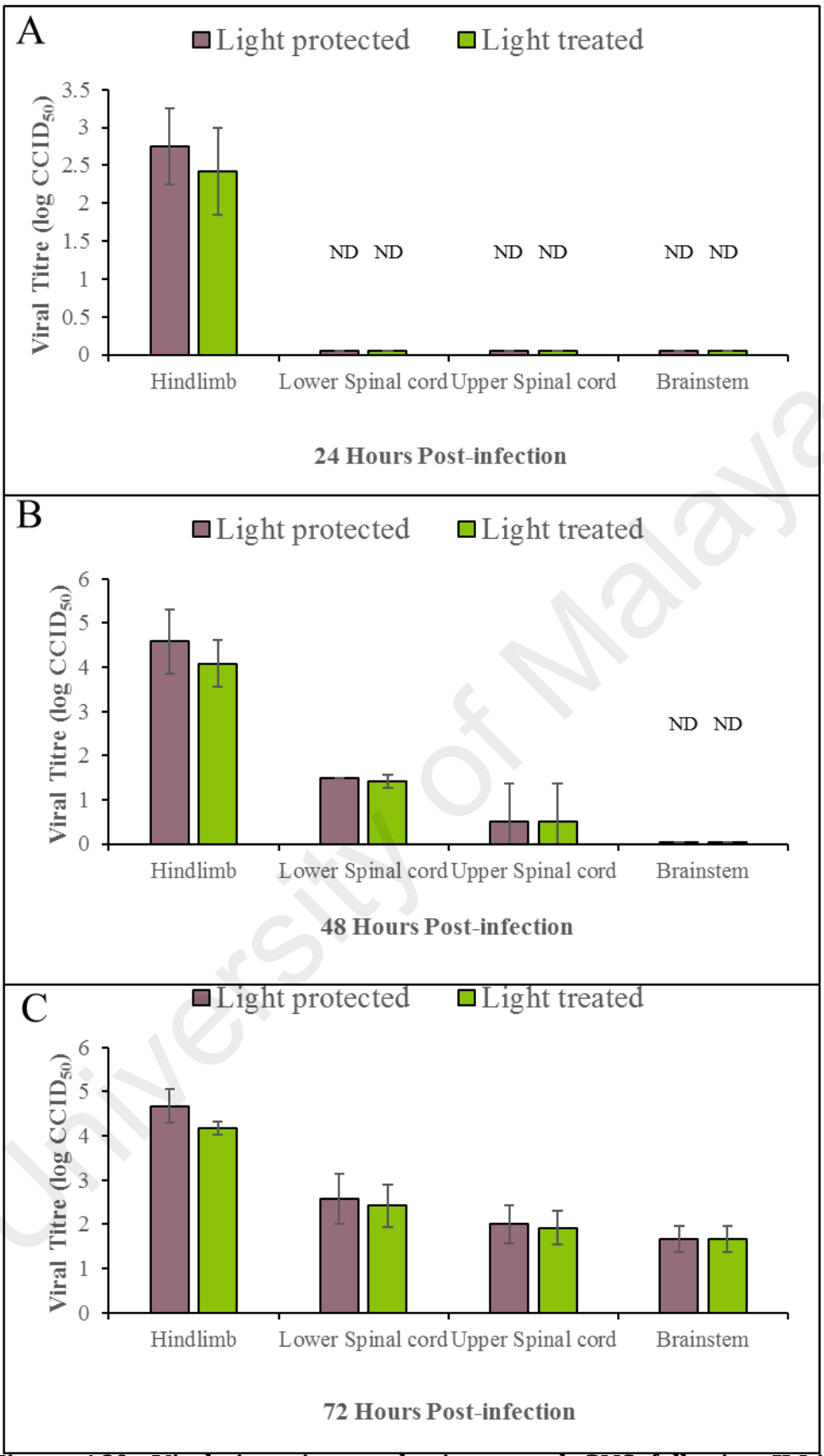

Figure 4.28: Viral titres in muscle tissues and CNS following IM-inoculation, sacrificed at 24 (A), 48 (B) and 72 hpi (C). Mean viral titres were not significant ($P < 0.05$) different between light-protected and light-treated samples in all type of tissues and time. Mean viral titres are expressed as the log $CCID_{50}$ ± standard error of mean. *ND= not detected.

4.6 Prevention and treatment of MAVS infection using neutralising antibodies

4.6.1 Hyperimmune sera treatment of MAVS-infected mice with CNS involvement

4.6.1.1 Survival analysis

Hyperimmune sera which showed a high neutralising titre against EV-A71 at 1/512 dilution in VERO cells, were IP-inoculated into mice infected via the right jaw/facial muscles to evaluate the effectiveness of hyperimmune sera in preventing and treating CNS infection. All treated groups (n= 4 for each group) and mock-treated mice (n= 4) were kept and observed daily for 21 days (Figure 4.29). The mouse group receiving 200 µL of hyperimmune serum at 4 hr pre-infection did not show any signs of infection. In the group receiving hyperimmune sera at 12 hpi, two out of four mice showed ruffled fur and weight loss with no observable paralysis from day 8 onwards but died on day 13 (Figure 4.29). Two out of the four mice in the group receiving hyperimmune sera at 24 hpi, showed ruffled fur and mild paralysis of one hindlimb from 72 hpi onwards and died on day 10 (Figure 4.29). One additional mouse from this group which showed only weight loss from day 6, died on day 11 (Figure 4.29). The mock-treated control mice all showed signs of infection such as back hunching, fur ruffling and obvious paralysis in both hindlimbs from 60 hpi onward, becoming more severe at 72 hpi and progressed to moribund/death stage at 96 hpi (Figure 4.29).

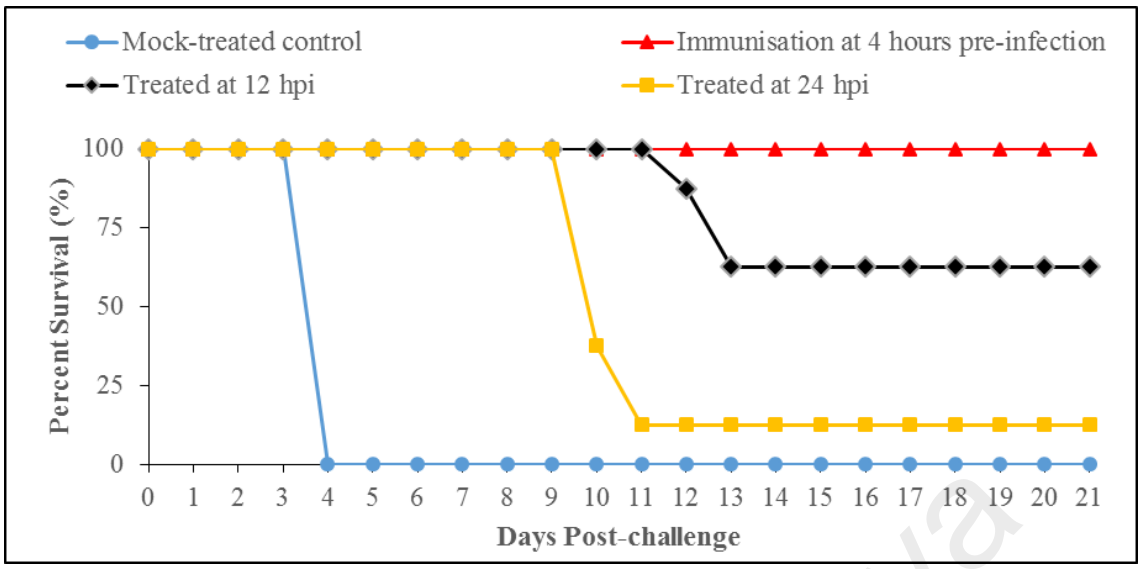

Figure 4.29: Survival graph of infected animals in mock-treated, 12 hpi treated, 24 hpi treated, and pre-infection immunised groups followed for 21 days. Treated mice showed improved survival, whereas all mock-treated animals died. Pre-infection immunised mice all survived.

4.6.1.2 Pathological studies

Figure 4.30 shows the approximate topographic distribution of viral antigens in CNS tissues in each mouse (A1 – A16) sacrificed at 72 hpi. In mice receiving 200 µL of hyperimmune serum at 4 hr pre-infection, viral antigens/RNA were not detectable in the muscles (Figure 4.31 B and F), CNS (Figure 4.30, mouse A1 – A4; Figure 4.31 J and N) or other tissues. However, mice receiving early treatment at 12 hpi (Figure 4.30, mouse A5 – A8) and 24 hpi (Figure 4.30, mouse A9 – A12) showed very focal viral antigens/RNA exclusively in the brainstem, involving bilateral motor trigeminal nuclei (Figure 4.31 K and O), reticular formation and facial nuclei, except for a slightly higher density of viral antigens/RNA in the latter (Figure 4.31 D, H, L and P). Overall, viral antigens/RNA density in the CNS was very much less in the 2 post-infection treated groups compared to the mock-treated controls (Figure 4.30, A13 – A16; 4.31 A, E, I and M). Infected neurons showed vacuolation with minimal or no inflammation.

Skeletal muscles throughout the body were most extensively and severely infected in mock-treated animals followed by mice treated at 24 hpi and 12 hpi, respectively (Figure 4.31 A - H).

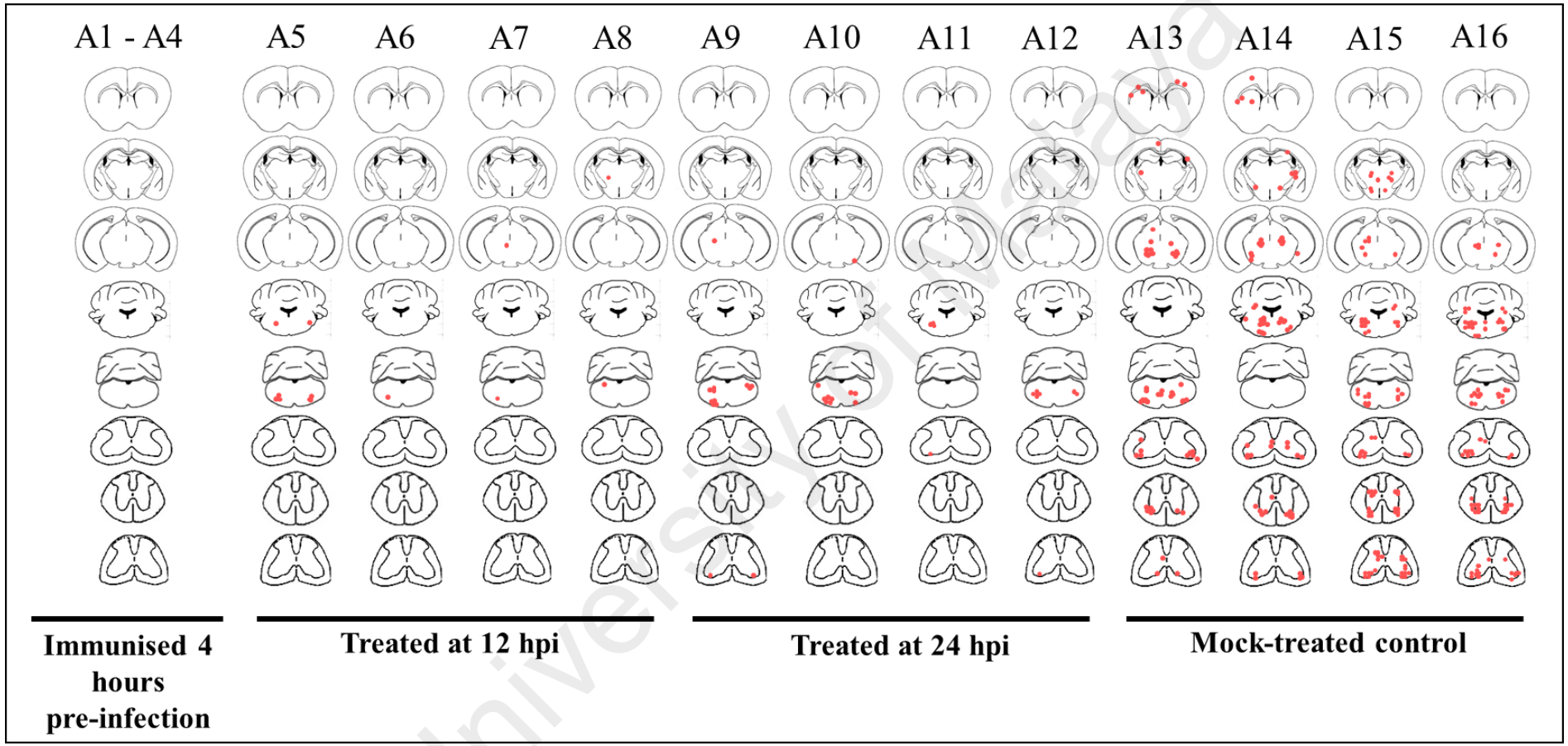

Figure 4.30: Approximation of the distribution of viral antigens/RNA in the CNS following unilateral right jaw/facial muscles inoculation in treated and mock-treated mice. In the groups treated at 12 and 24 hpi, the brainstem was much less involved compared to the mock-treated group. The pre-infection immunised mice were totally protected. Each red dot represents the equivalent of a positive neuron/white matter axon. For each mouse, cross sections of cerebral cortex, diencephalon/cortex, midbrain/cortex, caudal pons/medulla/cerebellum, medulla/cerebellum, cervical, thoracic, and lumbar spinal cords are displayed.

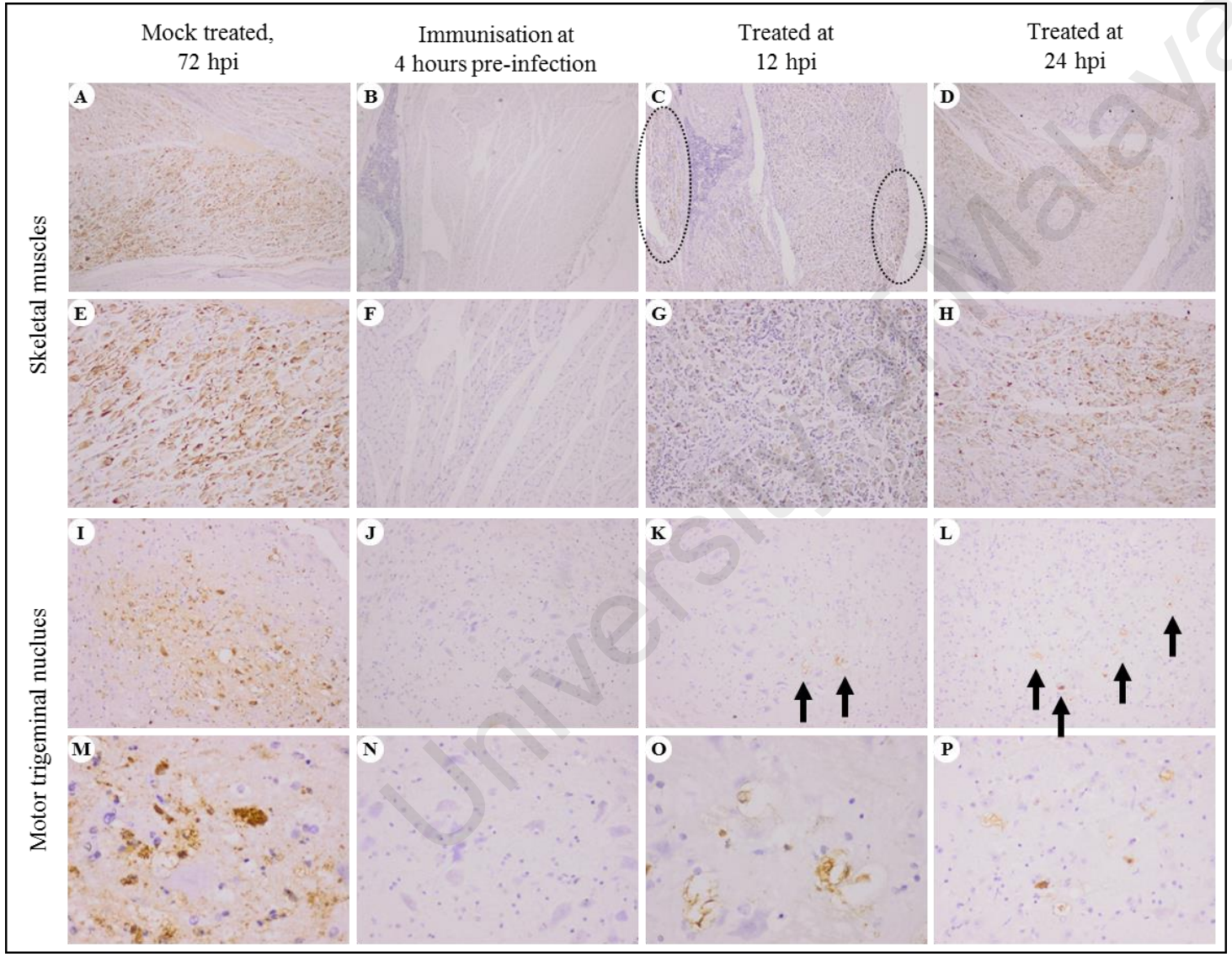

Figure 4.31: Viral antigens in mock-treated, 12 hpi treated, 24 hpi treated, and pre-infection immunised mice. Viral antigens were greatly reduced in both post-treated animals. CNS infection was prevented in pre-infection immunised mice. Viral antigens were very focal (C circles) in infected muscle of 12 hpi treated mice. Motor trigeminal nucleus showed minimal viral antigens positive cells in 12 hpi (K arrows) and 24 hpi (L arrows) treated mice. IHC with DAB chromogen and haematoxylin counterstain (A – P). Original magnification: 20x objective (M - P); 10x objective (E - L); 4x objective (A - D).

4.6.1.3 Viral titration analysis

Mean viral titres in the CNS and sera from mock-treated and treated mice are shown in Figure 4.32. Viral titres were below detection limit in all tissues of mice receiving pre-infection hyperimmune sera, at all times, except for the brainstem of a mouse (out of 4 mice) which showed a low titre of 0.25 log $CCID_{50}$. Moreover, CNS mean viral titres (brainstem, upper and lower spinal cord segments) in all treated mice were significantly lower than the mock-treated control group ($P< 0.05$). In general, mice treated at 12 hpi had lower mean viral titres compared to mice treated at 24 hpi although the difference was only significant for the upper spinal cord and the lower spinal cord ($P< 0.05$).

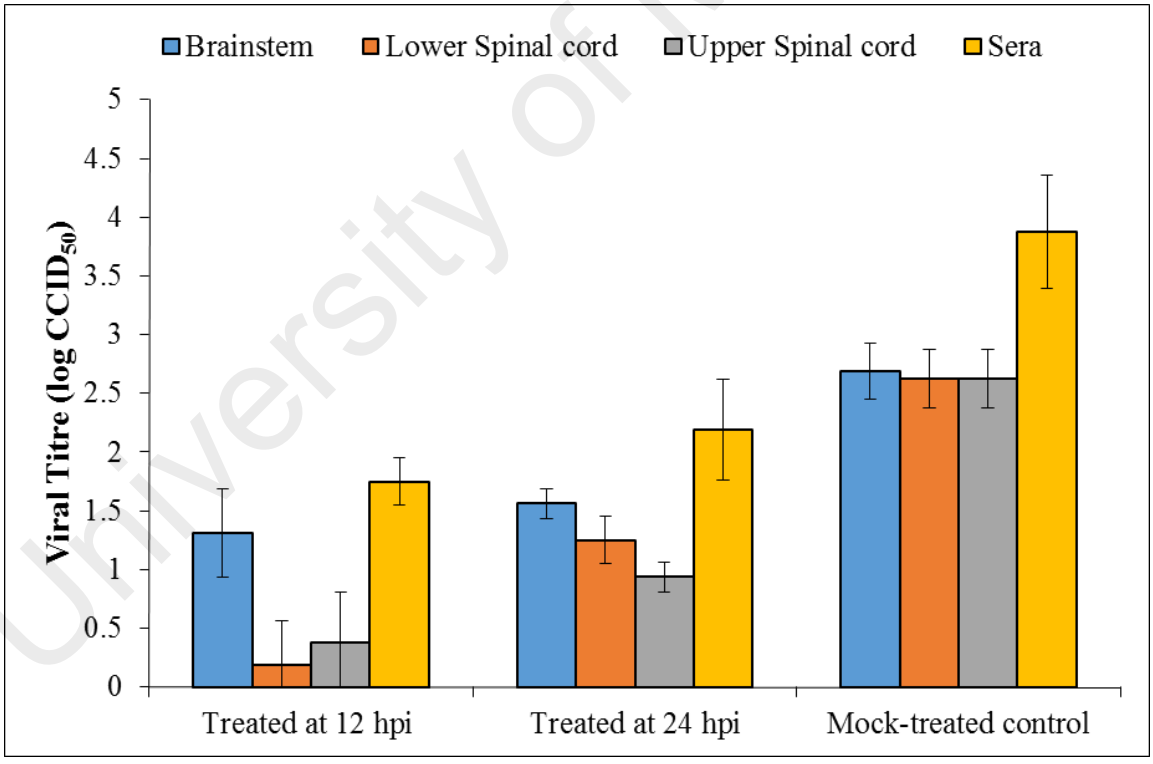

Figure 4.32: Viral titres in CNS tissues and sera following IM-inoculation and treated at 12 and 24 hpi, sacrificed at 72 hpi. Viral titres were all significantly ($P< 0.05$) lower in the groups treated at 12 hpi and 24 hpi against the controls for all the different CNS tissues and sera, respectively. Mean viral titres are expressed as log $CCID_{50}$ ± standard error of mean.

4.6.2 MAb in the treatment of MAVS-infected mice with CNS involvement

4.6.2.1 MAb production and characteristics

Anti-EV-A71 MAb was generated as a substitution for polyclonal antibodies in hyperimmune serum since production of polyclonal antibodies is often inconsistent. The MAb (designated as "3D1") was found to be an Ig-M isotype antibody with a concentration of 0.6 g/L. This MAb showed cross-neutralising activities against all the EV-A71 subgenotypes tested (Table 4.1). However, genotypes B3, B4, B5 and C5 showed lower neutralising titres at 1:16.

Table 4.1: Summary of the monoclonal antibody (3D1) neutralising titres against various EV-A71 subgenotypes

No.	Genbank Number	Name	Genotype	Titre
1.	AY207648	13903	B3	1:64
2.	-	MAVS*	B3	1:16
3.	AF376067	A10/4	B4	1:16
4.	-	18431	B5	1:16
5.	AY126012	8M/6/99	C2	1:128
6.	AY125966	001-KOR-00	C3	1:32
7.	AM490152	VN5559	C4	1:256
8.	AM490158	VN5784	C5	1:16

*MAVS was used for MAb generation.

4.6.2.2 Survival analysis

Mice IP-infected by MAVS were treated with various concentrations of MAb at different time points also via an IP route. All mock-treated mice (n= 4) challenged with MAVS started to show signs of disease such as hunching back and hindlimb weakness at 72 hpi and progressed to severe paralysis at 96 hpi. All mice were moribund/dead at 120 hpi (Figure 4.33 and 4.34).

Mouse groups (n= 4 each), treated daily with 120 µg of MAb at 24 and 48 hpi (D1 - 2), respectively, survived without any signs of infection after 21 dpi (Figure 4.33A and 4.34A). Whereas, mice (n= 4) treated with 60 µg of MAb started to show mild paralysis on both hindlimbs on 5 dpi, and started to recover on 8 - 9 dpi (Figure 4.34A). Weight loss was observed in 2 out of 4 mice at 6 dpi. Mice (n= 4) receiving 30 µg of MAb started to show paralysis at both hindlimbs at 4 dpi (Figure 4.34A). Half of the mice were moribund/dead on 8 - 9 dpi and another half recovered on 13 dpi (Figure 4.33A and 4.34A).

Treatment given daily at 72 and 96 hpi (D3 – 4), was still effective at higher MAb amounts. When given 120 µg of MAb, mice (n= 4) developed paralysis on both hindlimbs on 4 - 5 dpi, and partially recovered on 10 dpi with minor hindlimb weakness on 21 dpi; except for 1 mouse which was moribund/dead on 8 dpi (Figure 4.33B and 4.34B). For mice (n= 4) receiving 60 µg of MAb, paralysis was observed on 4 - 5 dpi, and 2 out of 4 mice were moribund/dead on 8 dpi (Figure 4.33B and 4.34B). The survivors showed minor hindlimb weakness on 21 dpi (Figure 4.34B). Whereas, mice (n= 4) receiving 30 µg of MAb developed paralysis on 4 - 5 dpi and were all moribund/dead on 5 - 6 dpi (Figure 4.33B and 4.34B).

In Experiment 3, mice (n= 4) treated daily with 120 µg of MAb at 24, 48 and 72 hpi (D1 – 3) remained healthy with no visible illness throughout the experiment (Figure

4.34C). Two out of 4 mice treated daily with 120 µg of MAb at 72, 96 and 120 hpi (D3 – 5) showed mild paralysis on 4 - 5 dpi and gradually recovered on 6 dpi (Figure 4.34C). All 4 mice survived but one of them showed minor hindlimb weakness on 21 dpi (Figure 4.33C and 4.34C). Thus MAb treatment seems to be helpful to ameliorate disease severity and to lower mortality (Figure 4.33 - 4.34).

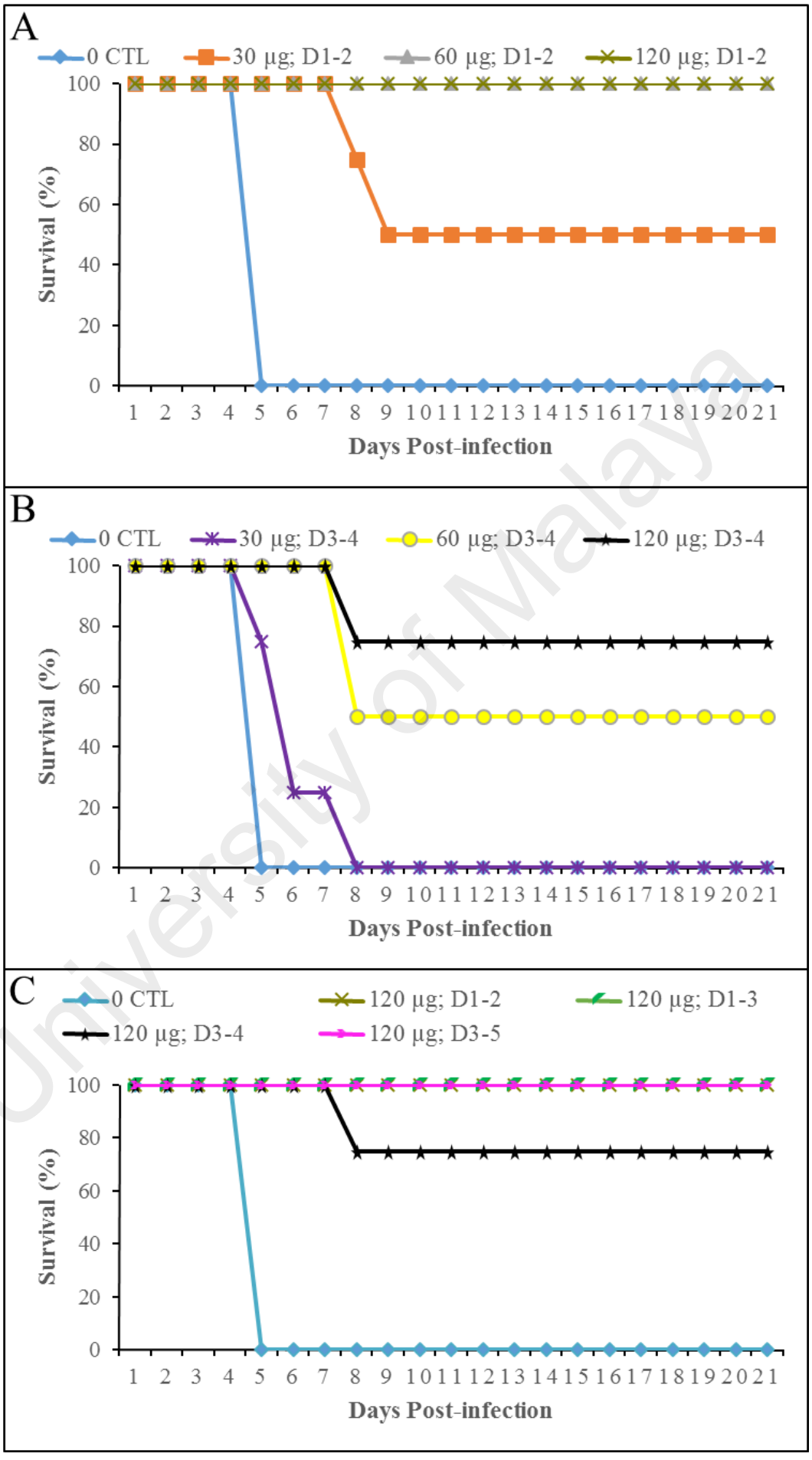

Figure 4.33: Survival graph of infected animals in mock-treated, and treated at 24 and 48 hpi (A); treated at 72 and 96 hpi (B); and treated daily for 3 consecutive days at 120 µg of MAb (C), for 21 days. Mice treated at 24 and 48 hpi (D1 – 2) (A) showed greatly improved survival. However, when mice were treated later at 72 and 96 hpi (D3 – 4), only mice receiving 60 µg and 120 µg of MAb showed improved survival rate (B). All mice treated daily for 3 consecutive days at 120 µg of MAb showed improved survival rate even though first treatment started at 72 hpi. All mock-treated animals died at 120 hpi. *CTL= mock-treated; D1-2= treated at 24 and 48 hpi; D3-4= treated at 72 and 96 hpi; D1-3= treated at 24, 48 and 72 hpi; D3-5= treated at 72, 96 and 120 hpi.

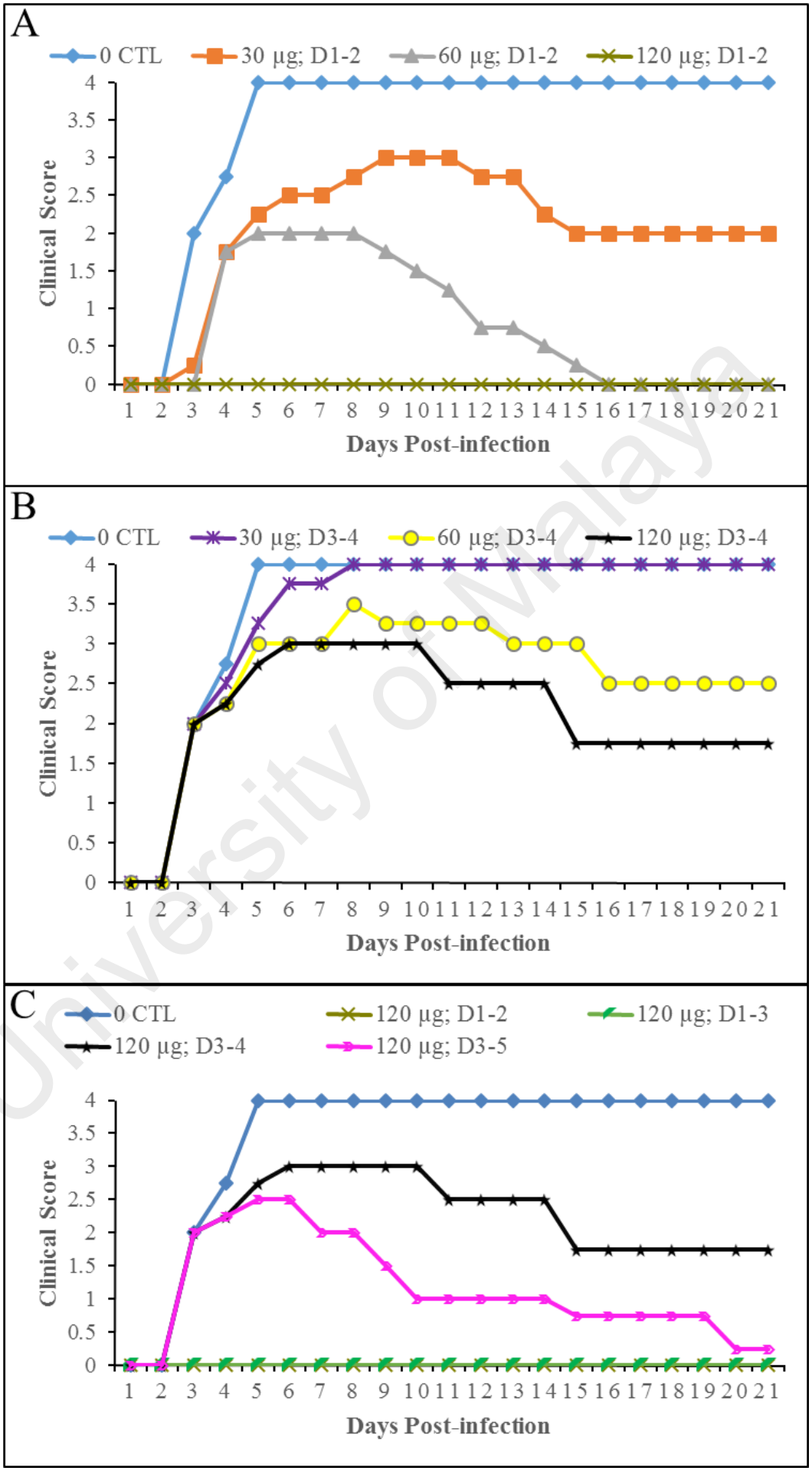

Figure 4.34: Clinical scores of infected animals in mock-treated, and treated at 24 and 48 hpi (A); treated at 72 and 96 hpi (B); and treated daily for 3 consecutive days at 120 µg of MAb (C), for 21 days. All mice treated at 120 µg of MAb showed improved clinical scores even though 1st treatment started at 72 hpi. Clinical scores were graded as follows: 0, healthy; 1, weight loss; 2, limb weakness; 3, hindlimb paralysis; and 4, moribund and death. Log-rank test analysis showed that all treated groups demonstrated statistically significant ($P < 0.05$) in survival from the control group. *CTL= mock-treated; D1-2= treated at 24 and 48 hpi; D3-4= treated at 72 and 96 hpi; D1-3= treated at 24, 48 and 72 hpi; D3-5= treated at 72, 96 and 120 hpi.

4.6.2.3 Pathological studies

Figure 4.35 shows the approximate topographic distribution of neuronal viral antigens/RNA or damaged neurons in CNS tissues in each mouse. In all 4 IP-infected, mock-treated mice sacrificed at 24 hpi (Figure 4.35, mouse C1 – C4), viral antigens could only be detected in the large skeletal muscles such as forelimb and hindlimb muscles and myositis was minimal. All other tissues including the CNS were negative and appeared normal under microscopic observation.

Viral antigens began to appear in CNS tissues in mice sacrificed at 72 hpi (Figure 4.35, mouse C5 – C8; Figure 4.36 I, M and Q), especially involving bilateral spinal cords (Figure 4.36 Q), where anterior horn cells were most severely infected (Figure 4.35, mouse C5 – C8). Furthermore, white matter axons immediately adjacent to infected anterior horn cells at or near the site where peripheral motor nerves usually exit, were positive for viral antigens too. Bilateral involvement of motor trigeminal nucleus, reticular formation and thalamus were observed. Severe myositis with dense viral antigens and inflammatory cells were observed in skeletal muscles (Figure 4.36 A and E). Brown adipose tissues showed some viral antigens with minimal inflammation.

Mice sacrificed at 96 hpi (Figure 4.35, mouse C9 – C12) showed similar infection to mice sacrificed at 72 hpi although the motor trigeminal nucleus and reticular formation were more severely involved. Similarly, skeletal muscles (Figure

4.36 B and F) and brown adipose tissues were also more severely infected. Infected neurons showed neuronal vacuolation and damage (Figure 4.36 J, N and R).

In mouse groups treated daily at 24, 48 and 72 hpi (Day 1 to day 3 (D1-3)) and sacrificed at 96 hpi (Figure 4.35, mouse A1 – A4; and Figure 4.38 K, O and S), there was no evidence of CNS infection. A few large skeletal muscles such as hindlimb muscles were positive for viral antigens (Figure 4.36 C and G). Viral antigens and inflammation were absent in all other tissues.

Overall, animals treated daily at 72, 96 and 120 hpi (D3-5) and sacrificed at 144 hpi (Figure 4.35, mouse A5 – A8), showed lower viral antigens density compared to mock-treated mice sacrificed at 72 and 96 hpi, respectively (Figure 4.35, mouse C5 – C12; and Figure 4.36). Viral antigens were observed mainly in the anterior horn cells of the spinal cords (Figure 4.36 T), motor trigeminal nucleus (Figure 4.36 L and P), reticular formation and hypothalamus of the brain. Infected neurons showed neuronal vacuolation and damage (Figure 4.36 L). A few fibres in systemic skeletal muscles (Figure 4.36 D and H) and brown adipose tissues were infected and inflamed.

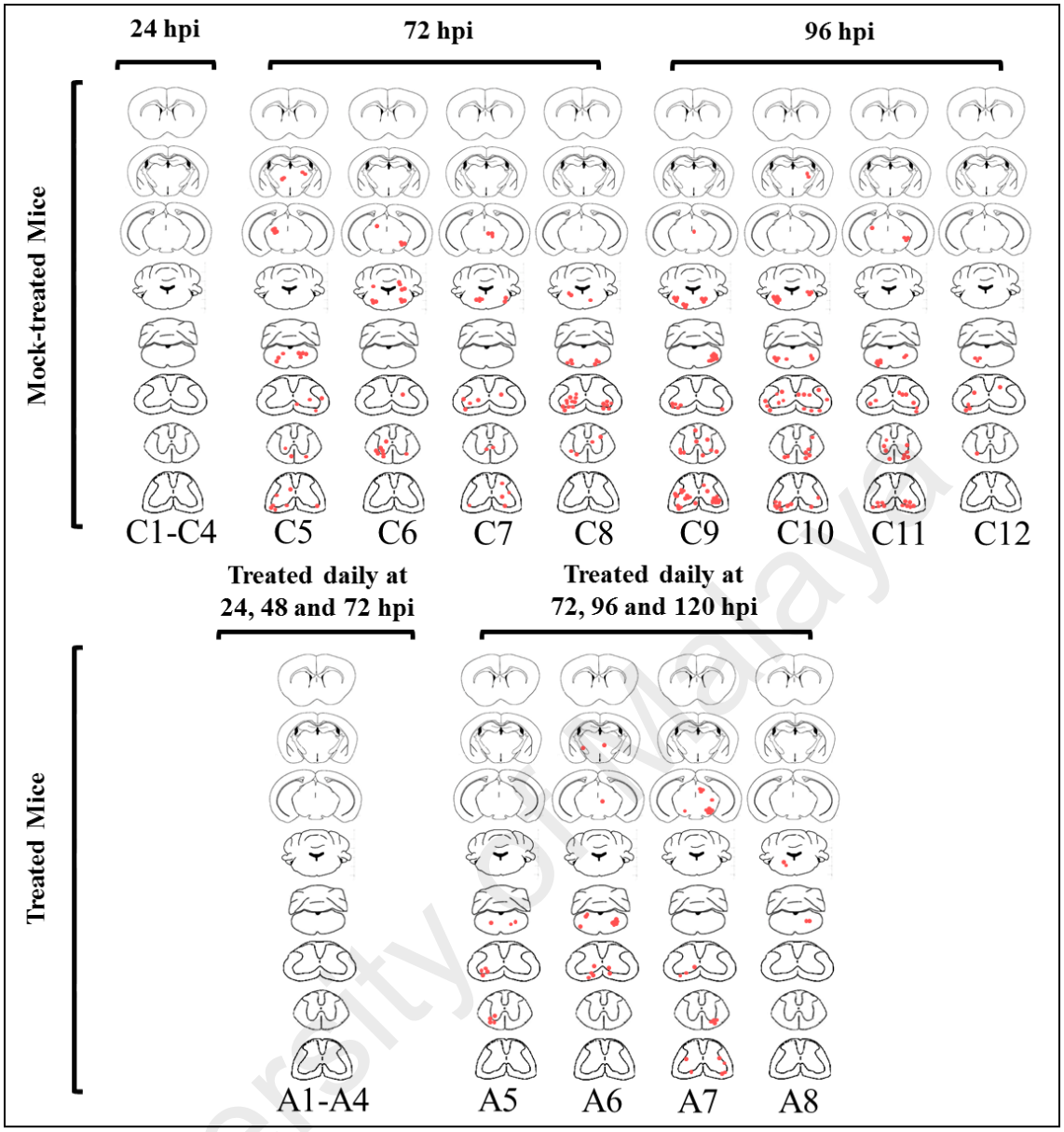

Figure 4.35: Approximation of the distribution of viral antigens in the CNS following IP-inoculation in mock-treated and treated animals. Viral antigens were not detectable in mice treated before CNS infection (A1-A4). In mice treated after CNS infection (A5-A8), viral antigens were far less than mock-treated mice (C9-C12). Each red dot represents the equivalent of a positive neuron/white matter axon. For each mouse, cross sections of cerebral cortex, diencephalon/cortex, midbrain/cortex, caudal pons/medulla/cerebellum, medulla/cerebellum, cervical, thoracic, and lumbar spinal cords are displayed.

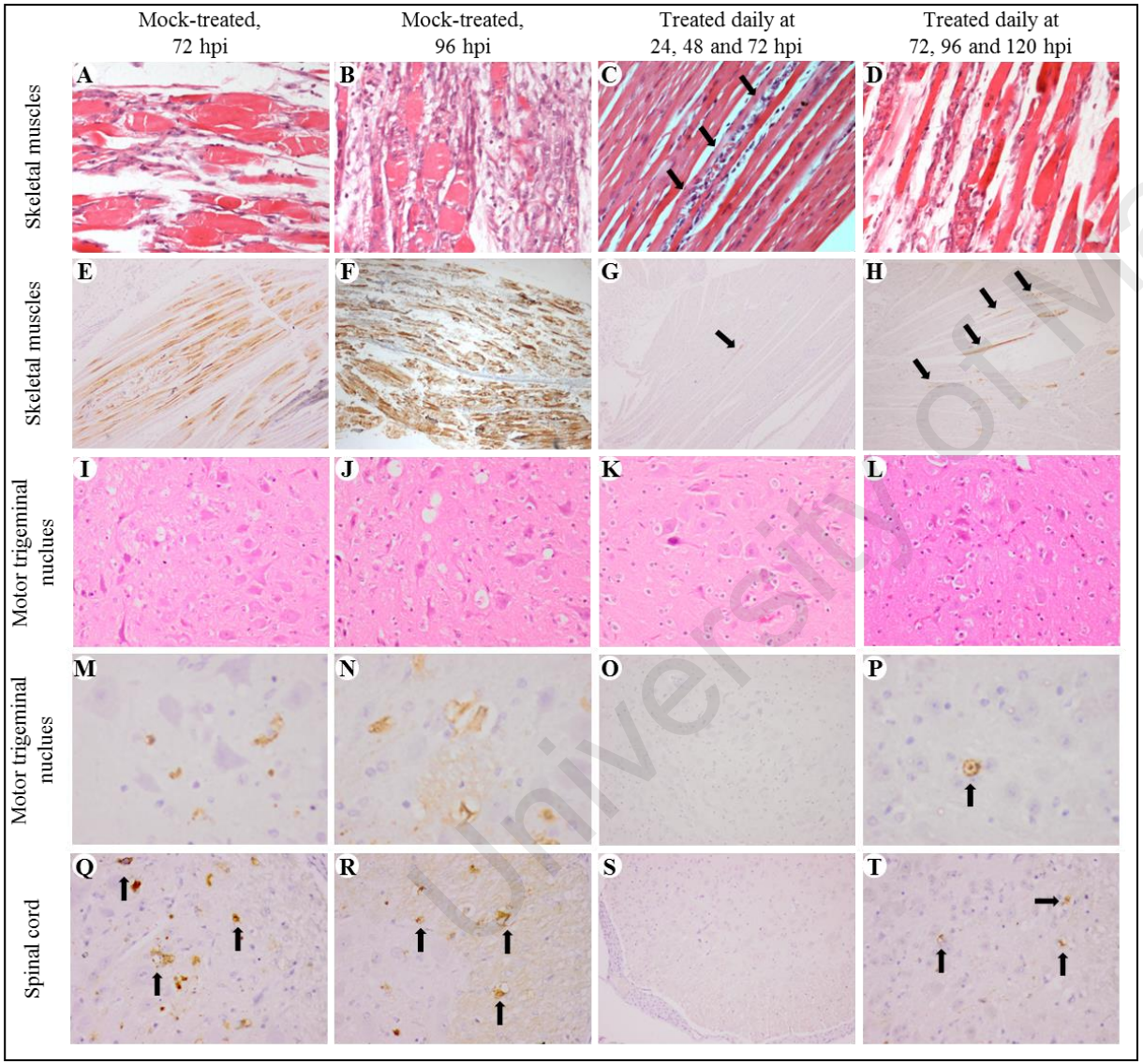

Figure 4.36: Pathological findings following IP-inoculation in mock-treated and treated animals at different hpi. Viral antigens were much less in all treated animals for all types of tissues. Viral antigens were not found in any CNS tissue in mice treated before CNS infection (K, O and S). H&E stain (A – D, I - L). IHC with DAB chromogen and haematoxylin counterstain (E – H, M - T). Original magnification: 40x objective (M, N and P); 20x objective (A – D, I – L, Q, R and T); 10x objective (O and S); 4x objective (E - H).

4.6.2.4 Viral titration analysis

In infected, mock-treated mice (n= 4, for each time point), virus was detectable in all muscles tissues examined as early as 24 hpi and titres increased over time (Figure 4.37). From 72 hpi onwards, virus was detectable in all the CNS tissues with highest titres in the lower spinal cord, upper spinal cord segment and brainstem with titres of 2.0, 1.8 and 1.3 log $CCID_{50}$, respectively (Figure 4.38).

CNS viral titres in mice (n= 4) treated daily at 24, 48 and 72 hpi were below detection limit (Figure 4.38). The left and right hindlimb muscles showed very low viral titres at 0.5 and 0.3 log $CCID_{50}$, respectively (Figure 4.37).

Although MAb treatment given daily at 72, 96 and 120 hpi was not as effective as mice treated at 24, 48 and 72 hpi, the mean viral titres in all tissues were still significantly lower ($P< 0.05$) compared to infected mock-treated mice at 96 hpi. Brainstem, upper and lower spinal cord viral titres that ranged from 1.2 - 1.4 log $CCID_{50}$ were significantly lower than the 3.4 to 4.1 log $CCID_{50}$ (Figure 4.38) range found in infected, mock-treated mice.

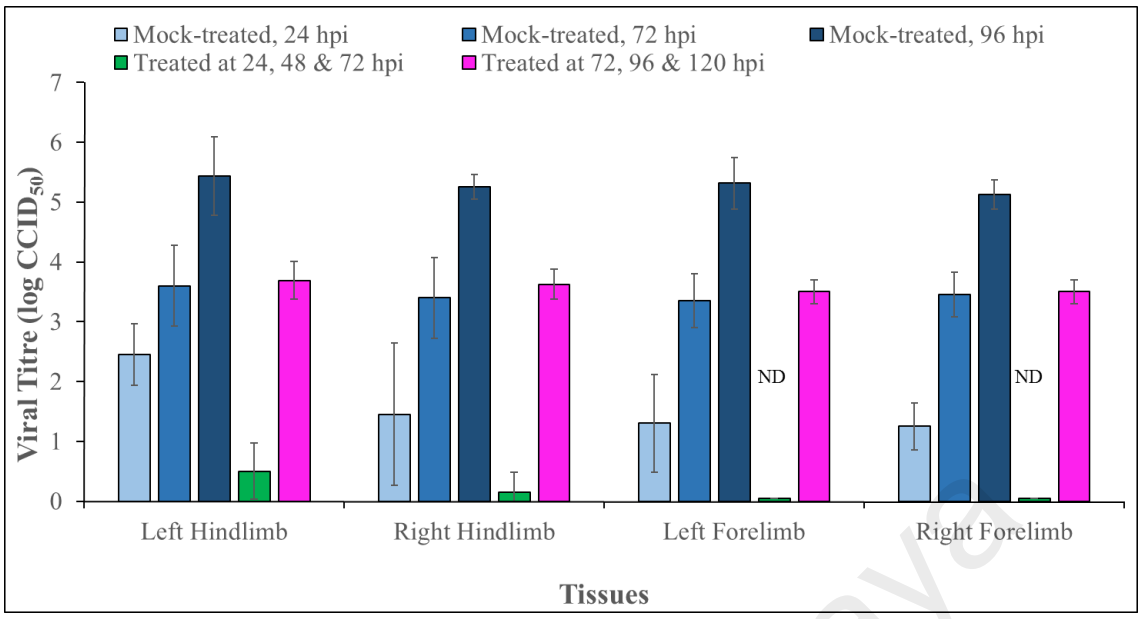

Figure 4.37: Viral titres in muscle tissues following IP-inoculation in mock-treated and treated animals. Mean viral titres of all treated animals were significantly lower ($P< 0.05$) against mock-treated groups. Mean viral titres are expressed as log $CCID_{50}$ ± standard error of mean. *ND= not detected.

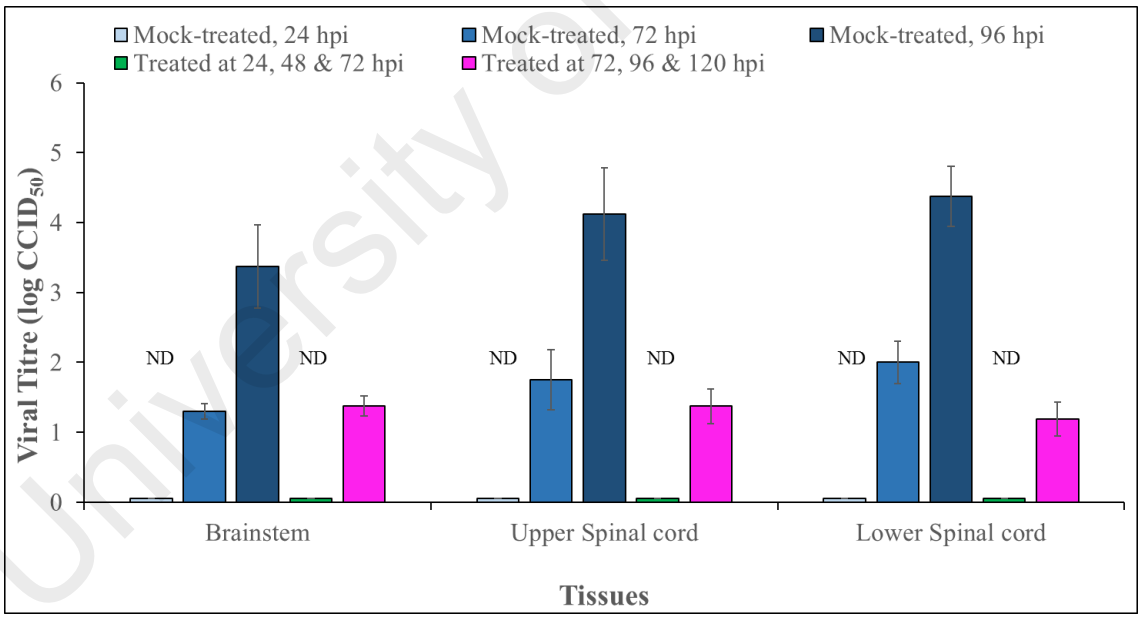

Figure 4.38: Viral titres in CNS following IP-inoculation in mock-treated and treated animals. Mean viral titres of all treated animals were significantly lower ($P< 0.05$) against mock-treated groups. Similar as mock-treated mice sacrificed at 24hpi, CNS viral titres from mice treated at 24, 48 and 72 hpi were all below detection limit. Mean viral titres are expressed as log $CCID_{50}$ ± standard error of mean. *ND= not detected.

4.6.2.5 Real-time PCR (qPCR) analysis

Overall, qPCR analysis (Figure 4.39 and Figure 4.40) shared a lot of similarity with viral titration assays. Viral copy numbers of all tissues from MAb treated mice (n= 4, for each group) were significantly lower (P< 0.05) than mock-treated mice. Whereas, viral copy numbers of all tissues from mice treated daily at 24, 48 and 72 hpi were all significantly lower (P< 0.05) compared to mice treated daily at 72, 96 and 120 hpi. In addition, no viral RNA was detected in the CNS tissues from mice treated before CNS infection (Figure 4.40).

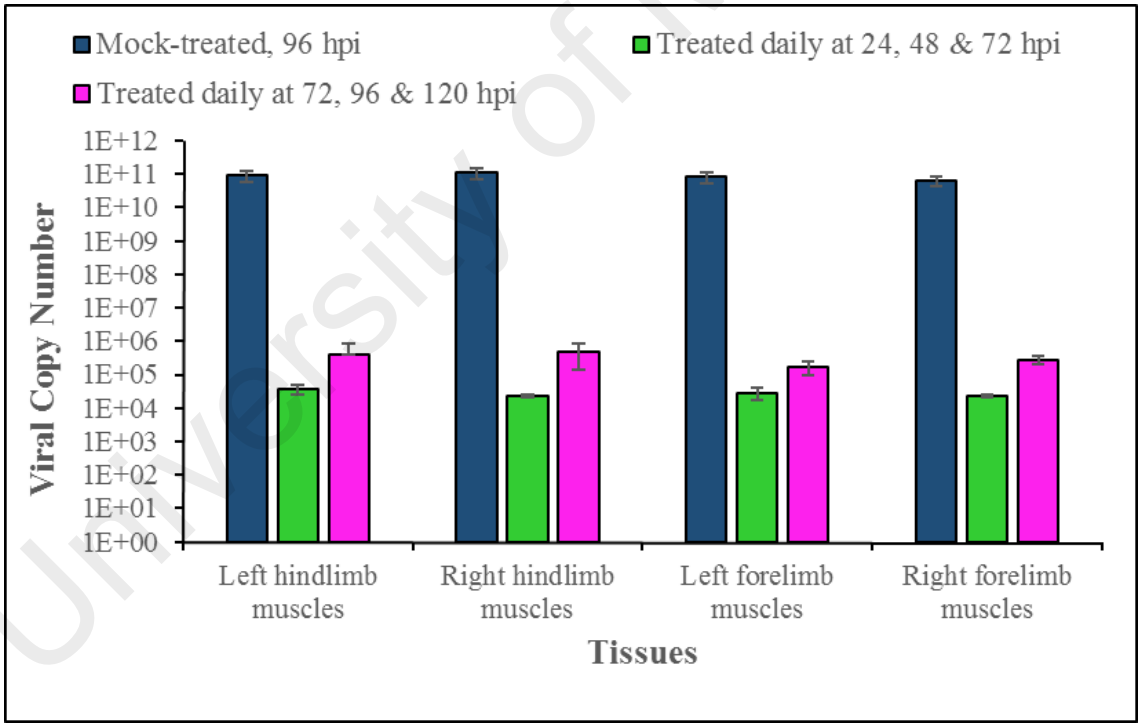

Figure 4.39: Viral copy number of muscle tissues following IP-inoculation in mock-treated and treated animals. Mean viral copy number of all type of tissues from all treated animals were significantly lower (P< 0.05) against mock-treated groups. Mean viral copy number of all tissues from mice treated at 24, 48 and 72 hpi were significantly lower (P< 0.05) compared to mice treated at 72, 96 and 120 hpi. Mean viral copy number are expressed as mean viral copy number ± standard error of mean. *ND= not detected.

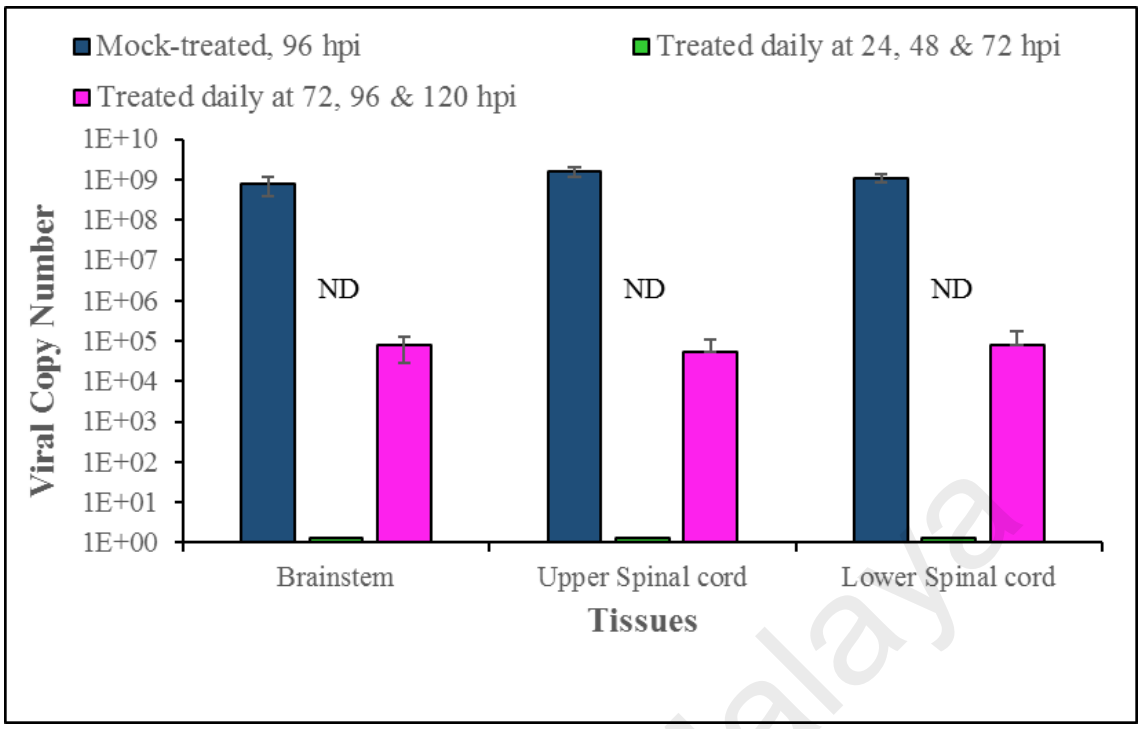

Figure 4.40: Viral copy number of CNS tissues following IP-inoculation in mock-treated and treated animals. Mean viral copy number of all type of tissues from all treated animals were significantly lower ($P < 0.05$) against mock-treated groups. Mean viral copy number of all tissues from mice treated at 24, 48 and 72 hpi were significantly lower ($P < 0.05$) compared to mice treated at 72, 96 and 120 hpi. Mean viral copy number are expressed as mean viral copy number ± standard error of mean. *ND= not detected.

5.0 Discussion

5.1 Enterovirus 71 Brainstem Infection via Cranial Nerves

EV-A71 infection can cause a diverse spectrum of diseases that are dermatotropic and/or neurotropic in nature (Solomon et al., 2010). Although CNS infection is rare, children with severe EV-A71 encephalomyelitis usually die from rapid cardio-respiratory collapse, often within a few hours of hospital admission (K. T. Wong et al., 2008). Recent findings from human autopsies or animal models of EV-A71 encephalomyelitis had suggested that retrograde axonal transport in motor nerves play an important role in EV-A71 neuroinvasion (Arita et al., 2007; C. S. Chen et al., 2007; Fujii et al., 2013; Lu et al., 2009; Ong et al., 2008; Tan et al., 2014; Wei et al., 2010; K. T. Wong et al., 2008; K. T. Wong et al., 2012; Yan, Wang, Liu, Yang, & Su, 2000; Yang et al., 2009). Hence, cranial nerves, in particular, motor components of these nerves, might be involved in rapid and direct EV-A71 invasion into the brainstem to cause sudden cardio-respiratory collapse.

After unilateral jaw/facial muscle injection, the results (Section 4.2, page 51) suggest that EV-A71 was indeed able to enter and directly infect the murine brainstem via cranial nerves, most likely by retrograde axonal transport rather than by the haematogenous route (via the blood-brain-barrier). Based on pathological findings (Section 4.2.1.1, page 51), viral antigens and RNA were first visualised within the cranial nerves and brainstem ipsilateral to the injected side as early as 24 hpi. This is the first time cranial nerve involvement has been demonstrated. The infected ipsilateral brainstem regions included motor trigeminal nucleus, reticular formation and facial nucleus, are mostly motor-related regions. We believe that inoculated MAVS after infecting skeletal muscles crossed the neuromuscular junctions into the distal motor nerve terminals. From there, virus travelled by retrograde axonal transport up motor nerves of the 5^{th} and 7^{th} cranial nerves to infect the motor trigeminal nucleus and facial

nucleus, respectively. In human EV-A71 acute flaccid paralysis, MRI examinations of the CNS have shown hyperintensities in ventral nerve roots and anterior horn areas of the spinal cord (F. Chen et al., 2013; Zeng et al., 2012). So far, brain MRI scans have not shown similar hyperintensities in cranial nerves. Previously, Ong et al. (2008) had also shown that the virus could enter the spinal cord via peripheral spinal motor nerves after unilateral thigh muscle infection in the same mouse model. Furthermore, the viral titration assays (section 4.2.1.2, page 59) demonstrated that brainstem viral titres were significantly higher ($P< 0.05$) than both upper and lower spinal cord segments up to 48 hpi, consistent with early infection of the brainstem. Taken together, we believe that EV-A71 was able to enter the CNS (brainstem and spinal cord) via retrograde axonal transport in peripheral motor nerves.

Following brainstem infection, the results showed greater involvement of the motor cortex compared to other cerebral areas (Figure 4.3, page 55) suggesting that within the CNS, the motor pathways (corticospinal/corticobulbar tracts) could spread virus beyond the brainstem and spinal cord. This is consistent with findings from other animal and human studies (Ong et al., 2008; K. T. Wong et al., 2008). The severely involved reticular formation is likely to facilitate viral spread within the CNS to the hypothalamus, other brainstem areas and beyond. Lateral cerebellar nucleus involvement could be via pathways that connect it to the red nucleus and the medulla. Similarly, the thalamus and other sensory neurons could become infected via the complex interlinks of other neural pathways in the CNS.

Viraemia was detected as early as 12 hpi, probably from the viral replication in the injected muscles and/or leakage of the site of inoculation. Viraemia was likely to have spread infection to contralateral and other skeletal muscles as early as 12 hpi (Figure 4.5, page 60). Viral titres in the blood were significantly ($P < 0.05$) higher than the titres in CNS tissues at all times. We speculate that following bilateral skeletal

muscle infection, MAVS continued to travel up respective motor nerves to involve other parts of the CNS (both ipsilateral and contralateral sides) as seen at later time points from 36 hpi onwards. There was bilateral marked increase of anterior horn cell infection in the spinal cords (Figure 4.3, page 55). Moreover, the role of viraemia to cause widespread CNS infection was clearly shown in section 4.2.3 (page 64), where infected mice in which viraemia was prevented/reduced by hyperimmune sera demonstrated only ipsilateral brainstem and muscle infection/inflammation; the contralateral CNS and other skeletal muscles were uninfected. If CNS infection occurred by the haematogenous route, one might expect early bilateral infection of the CNS at early time points and a similar degree of infection in the cerebral cortex, hippocampus, thalamus, hypothalamus and other brain regions due to simultaneous exposure to virus.

Following unilateral jaw/facial muscle injection, (Section 4.2, page 51) the motor trigeminal nucleus and reticular formation were the first sites of infection in the brainstem. Infection of the reticular formation was most likely via the rich and extensive neuronal inter-connections with the motor trigeminal and facial nuclei. Since the reticular formation extends to the whole brainstem, including the medulla, viral spread to medullary nuclei via the reticular formation is entirely possible (Conn & SpringerLink, 2008; Heimer, 1995; Wilson-Pauwels, Akesson, & Stewart, 2002). Although direct medullary infection via 9^{th} and 12^{th} cranial nerves was not done in these studies because of technical difficulties injecting muscle groups innervated by these nerves, viral transmission from motor trigeminal and facial nuclei to the medulla is likely to have occurred. In human infections, brain MRI examination revealed lesions mainly in dorsal pons and the whole medulla oblongata, findings that were confirmed by autopsy of patients with fatal encephalomyelitis (K. T. Wong et al., 2008; Zeng et al., 2012). Direct medullary infection, via 9^{th} and 12^{th} cranial nerves (motor components) could cause sudden death as a result of the involvement and inflammation of medullary

cardio-respiratory centres (Baker, 1957; Fu et al., 2004; Fu et al., 2006; Hoff, Nishimura, Garcia-Uria, & Miranda, 1981). The fact that patients with fatal encephalomyelitis almost always suffer a catastrophic terminal event, often within a few hours of hospital admission, is consistent with direct brainstem infection and destruction of the cardio-respiratory centres. Following medullary inflammation and damage, high levels of norepinephrine and epinephrine could be released to raise the pulmonary vascular pressure, leading to cardiac damage and arrhythmia, and neurogenic pulmonary oedema (Kao, Yang, Hsu, & Chen, 2004; Yang et al., 2009).

Another theory suggests that the terminal events in fatal encephalomyelitis is associated with a "cytokine storm". In many human studies, increased inflammatory cytokines including IL-1β, IL-6, IL-10, IL-13 and IFN-γ had been reported. These cytokines are believed to increase pulmonary vascular permeability leading to pulmonary oedema and death (T. Y. Lin, Chang, Huang, et al., 2002; S. M. Wang et al., 2003; S. M. Wang, Lei, & Liu, 2012). However, none of the animal models studied so far has demonstrated pulmonary oedema, including the current study (Y. F. Wang & Yu, 2014). The inflammatory cytokines could be associated with severe/terminal infection rather than the direct cause of death. Some authors believe direct brainstem infection to be more important than "cytokine storm"-induced pulmonary oedema/functional dysregulation as a cause of death (T. Y. Lin, Hsia, Huang, Wu, & Chang, 2003; S. M. Wang et al., 2003; S. M. Wang et al., 2012). Further investigations are needed to confirm this. Lastly, the possibility of myositis causing respiratory muscular paralysis and failure, and thereby contributing to death in mouse models cannot be ignored. However, myositis has not been reported in human EV-A71 encephalomyelitis.

5.2 Infectivity of EV-A71 in Neuronal Cells

The stereotyped distribution of inflammation and antigens/RNA in the human and murine CNS (Ong et al., 2008; K. T. Wong et al., 2008) could be due to at least two possibilities. Firstly, upon entering the spinal cord and brainstem via retrograde motor nerve transmission, viruses first infect the motor neuronal cell bodies in the spinal cord (anterior horn cells) and brainstem (e.g. cranial nerve nuclei) and spread from these neurons to other regions via established neural pathways. Secondly, assuming that haematogenous spread occurs, and there is an equitable distribution of virus, there may be different neuronal susceptibility in different CNS regions depending on the density/availability of SCARB2 receptors. The SCARB2 receptor is probably a primary determinant of viral entry into cells and hence, play an important role in tissue tropism (P. Chen et al., 2012; Yamayoshi et al., 2014; Yamayoshi et al., 2009). After virus has entered the CNS parenchyma either by peripheral nerves or haematogenous route, it is also possible that more distant neurons or groups of neurons with a higher density of viral receptors will more likely be infected in contrast to neurons with fewer SCARB2 receptors.

To investigate viral spread within the murine CNS, MAVS was inoculated into thalamus/hypothalamus and pons/medulla regions by an IC route (Section 4.3, page 68). The thalamus/hypothalamus and pons/medulla regions were chosen because according to the Allen Brain Atlas Data Portal, the C57BL/6J mouse at 56 days of age, expresses SCARB2 receptor in all parts of brain with the highest expressions in the pons, hypothalamus and medulla regions (Table 5.1) (Lein et al., 2007). We assume that this also applies to the ICR mice used in our experiments.

Table 5.1: Summary of SCARB2 expression in 12 major mouse brain structures/areas (Adapted from Lein et al., 2007).

No.	Brain Structure/Area	Expression Energy Value*	Log_2@
1.	Isocortex	10.75	3.43
2.	Olfactory area	7.67	2.94
3.	Hippocampal formation	9.00	3.17
4.	Cortical subplate	8.37	3.07
5.	Striatum	6.09	2.61
6.	Pallidum	8.98	3.17
7.	Thalamus	11.85	3.57
8.	Hypothalamus	12.40	3.63
9.	Midbrain	12.17	3.60
10.	Pons	12.71	3.67
11.	Medulla	12.32	3.62
12.	Cerebellum	6.35	2.67

* Expression energy was calculated and derived from SCARB2 RNA as detected by ISH in various brain areas.

@ Log_2 of the expression energy value defines the fold changes of SCARB2 expression.

The areas chosen for IC inoculation (thalamus/hypothalamus and pons/medulla) have among the highest SCARB2 expressions.

In both IC-infected mice (thalamus/hypothalamus and pons/medulla), MAVS was first detected around the injection site at 24 hpi. Infected cells were mainly close to the needle tract and comprised non-neuronal cells such as microglial cells or astrocytes with a minority of small neurons (Figure 4.12A (page 71) and Figure 4.16B (page 78)). In thalamus/hypothalamus inoculated mice, viral antigens/RNA were detected focally around the needle tract in the thalamus region, part of cerebral cortex (retrosplenial cortex and posterior parietal association cortex) (Figure 4.12A) and around the corpus callosum (Figure 4.12A). There was no evidence of viral infection in other CNS regions. Interestingly, although the needle tract passed through the pyramidal layer of the Ammon's horn and granular cell layer of dentate gyrus, both components of the

hippocampal formation, which demonstrate the strongest SCARB2 expression (Lein et al., 2007), there was very little infection of the neuronal cells. Only a few dentate gyrus neurons were positive for viral antigens/RNA in 2 mice (Figure 4.11, mouse A2 and A4, page 70).

In pons/medulla inoculated mice, viral antigens/RNA were only detectable focally around the needle tract in the brainstem reticular formation. Although the needle tract passed through the purkinje cell layer of the cerebellum which demonstrate the strongest SCARB2 expression (Lein et al., 2007), there was no infection of these neuronal cells.

At 48 and 72 hpi, around the needle tract, viral antigens/RNA were found to be reduced. These findings suggested that there was little, if any cell-to-cell viral spread (centrifugal spread) from the needle tract to surrounding neurons. It is assumed that following cytolysis of infected neurons, the released virus in the microenvironment/neurophil could infect the adjacent neurons, but this was not observed in our experiment. The reason for this surprising finding is unknown. It is possible that an innate immune response may inhibit the entry and replication to limit virus spread in adjacent neurons. Although strong neuronal mSCARB2 expression has been reported in the Allen Brain Atlas Data Portal (Lein et al., 2007), it is possible that the MAVS after adaptation, may not use mSCARB2 efficiently for viral entry. Using transfected L-929 (murine fibroblast cells), Yamayoshi et al. (2009) have reported that mSCARB2 may not be a functional receptor for EV-A71, due to its low efficiency for viral entry compared to hSCARB2. Furthermore, using IHC, Yu et al. (2014) found no correlation between the distribution of mSCARB2 and EV-A71 antigens in their mouse model. Hence, it is possible that our MAVS utilised an unknown receptor(s) for neuronal entry instead of mSCARB2. This unknown receptor(s) may not be present in sufficient quantities to support cell-to-cell virus spread in the thalamus/hypothalamus

and pons/medulla regions. Alternatively, an unknown viral co-receptor may be absent in these cells without which mSCARB2 alone is insufficient for viral entry as was shown in HIV infection (Fields et al., 2013). Further investigations are needed to confirm this.

At 48 hpi, viral antigens/RNA distribution away the needle tract was similar in both intra-thalamus/hypothalamus and intra-pons/medulla inoculated mice. The motor-related regions such as motor trigeminal nucleus and reticular formation, were positive for viral antigens/RNA bilaterally (Figure 4.11 (page 71) and Figure 4.15 (page 77)). We believe that retrograde transport from peripheral nerves is likely to have caused infection in these areas. This is because, these infected motor regions were further away from the thalamus/hypothalamus inoculated site compared to pons/medulla, but yet both showed similar bilateral neuronal involvement. As was shown in IM-inoculated mice (Section 4.2, page 51), the motor trigeminal nucleus and reticular formation were the first brainstem neurons to be infected at 24 hpi after retrograde axonal transmission. Bilateral infection of these regions was observed at 48 hpi, and the pattern of brainstem involvement was very similar to both intra-thalamus/hypothalamus and intra-pons/medulla inoculated mouse brains. Hence, the infection of these areas was similar to IM-inoculated mice, and probably originated from leaked MAVS into the blood causing viraemia. Disseminated viruses caused systemic skeletal muscle infection followed by retrograde viral transmission into the brainstem and spinal cord.

At 72 hpi, viral antigens/RNA distribution away the needle tract was again similar in both intra-thalamus/hypothalamus and intra-pons/medulla inoculated mice. Compared to 48 hpi, the same regions were also involved but other regions such as thalamus, hypothalamus, red nucleus, dentate nucleus and motor cortex were more severely infected. Compared to IM-inoculated mice at 72 hpi, viral antigens/RNA distribution was also similar.

Table 5.2 summarises the pathological changes in systemic skeletal muscles and motor trigeminal nucleus over various time points in IM, intra-thalamus/hypothalamus and intra-pons/medulla inoculated mice. The severity of the skeletal muscle and motor trigeminal nucleus infection over time were used as an indicator of systematic viral spread and retrograde viral transmission, respectively. As early as 24 hpi, systemic skeletal muscles showed evidence of viral antigens/RNA because of viraemia (serum viral titres always positive). In general, the density of viral antigens/RNA in skeletal muscles were always higher than in the CNS (brainstem/spinal cord) for all time points, especially at 48 and 72 hpi. However, intra-thalamus/hypothalamus and intra-pons/medulla inoculated mice demonstrated delayed skeletal muscle and corresponding CNS infection most likely due to lower serum viral titres. On the contrary, higher viraemia and earlier viral replication in skeletal muscles accelerated retrograde viral transport into the motor trigeminal nucleus to cause the earlier infection and higher brainstem viral titres in IM-inoculated mice (Table 5.2).

Serum viral titres in IM-inoculated mice were significantly higher than both intra-thalamus/hypothalamus and intra-pons/medulla inoculated mice at earlier and subsequent time points (Figure 4.5 (page 60), Figure 4.13 (page 73), Figure 4.17 (page 80)). This suggested that viraemia occurred earlier, either from increased viral leakage from injection site, early primary replication in injected muscles or other unknown factors. Presumably, the earlier and more severe involvement of the skeletal muscles and motor trigeminal nucleus could have caused earlier limb paralysis in IM-inoculated mice.

Table 5.2: Comparison of pathological findings in intra-muscular, intra-thalamus/hypothalamus and intra-pons/medulla inoculated mice.

Hours post-infection	Viral antigens in tissues			
		Route of infection		
		Intra-muscular (n= 4)	Intra-thalamus/ Hypothalamus (n = 5)	Intra-pons/medulla (n= 3)
24	Systemic Muscles	++	+	+
	Motor trigeminal nucleus	+	-	-
48	Systemic Muscles	+++	++	++
	Motor trigeminal nucleus	++	+	+
72	Systemic Muscles	+++	+++	+++
	Motor trigeminal nucleus	+++	++	++

In systemic muscle,

+ indicates viral antigens in only a few fibres of skeletal muscle with mild myositis

++ indicates less than half skeletal muscle fibres with viral antigens, and severe myositis

+++ indicates more than half skeletal muscle fibres with viral antigens, and severe myositis

In motor trigeminal nucleus,

+ indicates viral antigens in only a few neurons

++ indicates less than half neurons with viral antigens along with neuronal damage and degeneration

+++ indicates more than half neurons with viral antigens along with neuronal damage and degeneration

Figure 5.1 shows a comparison of brainstem viral titres from intra-muscular, intra-thalamus/hypothalamus and intra-pons/medulla inoculated mice sacrificed at 24, 48, and 72 hpi. At 24 hpi before significant retrograde transmission in cranial nerves occurred, brainstem viral titres in intra-pons/medulla inoculated mice were the highest. This is possibly due to the presence of the original inoculated virus, with probably little contribution from newly-synthesised virus, or virus from retrograde transmission. The higher brainstem titres in IM-inoculated mice compared to intra-thalamus/hypothalamus

inoculated mice was most likely due to virus reaching the brainstem earlier via cranial nerves.

At 48 hpi, both IC-inoculated mice showed similar ($P < 0.05$) viral titres confirming comparable early viral transmission rate into the brainstem from the peripheral nerves (Figure 5.1). Brainstem viral titres in intra-pons/medulla inoculated mice were lower than the titres obtained at 24 hpi, confirming that there is minimal *in situ* replication around the needle tract (inoculation site). Viral titres in IM-inoculated mice were significantly higher than both suggesting that the retrograde viral transmission from peripheral nerves, as previously described, contributed significantly to the viral titres. At 72 hpi, the same pattern of viral titre increase was observed.

As was discussed earlier, other unknown receptors may be present in our MAVS mouse system to facilitate viral entry into neurons, and this may also apply to viral transmission into the neuromuscular junction and nerve terminal from infected muscles, to lead to retrograde axonal transmission. We speculate that either an unknown receptor or co-receptor may be present within the neuromuscular junction in sufficient quantities to support viral entry. In poliovirus infection, human poliovirus receptor CD155-independent endocytosis and transport had been observed in mouse neuromuscular junction. Alternatively, CD155-independent endocytosis via an unknown receptor could also promote viral transmission through the neuromuscular junction (Ohka et al., 2009). Further investigations are needed to investigate how EV-A71 gains entry into the peripheral nerve terminal.

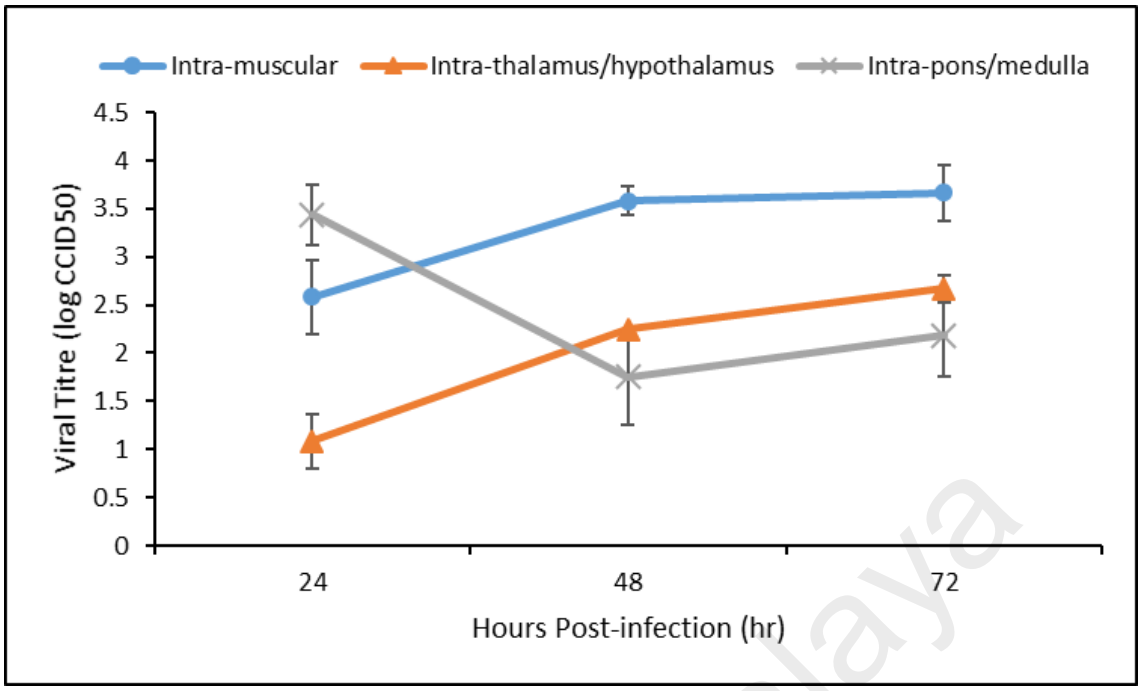

Figure 5.1: Comparison of brainstem viral titres from intra-muscular, intra-thalamus/hypothalamus and intra-pons/medulla inoculated mice sacrificed at 24, 48, and 72 hpi. Brainstem mean viral titres were increasing gradually over time for both intra-muscular and intra-thalamus/hypothalamus inoculated mice. Whereas, brainstem mean viral titres from intra-pons/medulla inoculated mice were highest at 24 hpi and dropped significantly ($P< 0.05$) at 48 hpi. Mean viral titres are expressed as the log $CCID_{50}$ ± standard error of mean.

As motor neurons appear to be a primary target of EV-A71 infection, primary motor neuron cells were used in *in vitro* experiments to investigate neuronal susceptibility and viral transport. Surprisingly, direct MAVS infection of ICR mouse derived primary motor neuron cells was minimal (< 1%) (Section 4.3.3, page 81). Since, previous studies suggested that EV-A71 could use hSCARB2 more efficiently than mSCARB2 receptor (Yamayoshi et al., 2009) to enter cells, we repeated the same experiment with primary motor neuron cells derived from hSCARB2 Tg mice. Although EV-A71 (non-MAVS) infection in primary motor neurons isolated from hSCARB2 Tg mice was higher (< 50%) than the ICR derived motor neuron cells, the infection was still not extensive (Figure 4.22 (page 85)) when compared to VERO or RD cells in which full infection (nearly 100%) was commonly achieved. Hence, it is

possible that our murine primary motor neuron cells derived from hSCARB2 Tg mice were more susceptible to EV-A71 infections, because the hSCARB2 was more efficient for viral entry compared to mSCARB2 (Yamayoshi et al., 2009). The relatively lower infection rate of hSCARB2 Tg mouse neurons compared to VERO and RD cells were similar to *in vitro* findings reported by H. I. Huang et al. (2014) and Yap et al. (2016). Using motor neurons derived from human neural stem cell or neural progenitor cells, they reported that differentiated neuronal cells were less susceptible to EV-A71 infection. They speculated that poor susceptibility of differentiated cells could be associated with deficiency of appropriate EV-A71 receptors, or reduced mitotic rate of these cells as was shown in Coxsackievirus infection. These may partially explain the pathological findings in both IC inoculated mice (thalamus/hypothalamus, section 4.3.1.1 (page 68), and pons/medulla, section 4.3.2.1 (page 74)), where non-neuronal cells around the needle tract such as glial cells or astrocytes were more infected than neuronal cells with apparently little or no cell-to-cell viral spread (centrifugal spread).

Using the microfluidic chamber culture system, axons of hSCARB2 motor neurons were directed to grow away from respective neuronal bodies into a fluidically isolated environment, designated as axon terminal chamber (contained only axon terminals). Whereas, the original motor neuron cells seeding chamber was designated as cell body chamber (contained mainly cell bodies). When virus was introduced into the axon terminal chamber, replicating virus was detected in the cell body chamber (Figure 4.23 page 86). In contrast, no replicating virus was detected in the axon terminal chamber after introduction of virus into the cell body chamber. In addition, cell body chamber viral titres did not show significant differences at all timepoints implying replication of EV-A71 in neuronal cells may be limited. Overall, this strongly suggests retrograde axonal transport of virus from axon terminal to cell body but not in the reverse direction. It is well known that microtubules are oriented with the (+) end at

axon terminal, and the (−) end toward the cell body. The kinesin family of motor proteins generally mediates (+) end-directed anterograde transport (from the cell body to the axon terminus), and dynein motor complexes generally mediate (−) end-directed retrograde transport (from axon terminus to cell body). If it is true that EV-A71 is transported in a retrograde fashion, after axonal terminal entry, virus particles must use the dynein motor complexes to move along microtubules toward the cell body (Kapitein & Hoogenraad, 2011). It has been found that another picornavirus, poliovirus, binds the dynein light chain Tctex-1 to engage the retrograde transport machinery (Ohka et al., 2004) via the poliovirus cellular receptor, CD155, which is endocytosed along with the virion. However, other neurotropic viruses such as the rabies virus could directly bind to the LC8 dynein light chain (part of the dynein motor complexes) for retrograde transport, without endocytic vesicles. As there is no information about EV-A71 retrograde transport to date, further investigations are needed. We also speculate that the virus may not utilise the kinesin motor complexes for anterograde transport as shown by our microfluidic chamber data.

Another possible explanation for no apparent anterograde transport of virus from the neuronal cell body to the axon terminal (Figure 4.23 (page 86)) may be that viral receptors, like SCARB2 and other receptor(s), are under or not expressed on the cell body. It has been reported that many viral endocytic cellular receptors are concentrated at nerve or axonal terminals including CD155 for poliovirus, and adenovirus receptor for coxsackievirus (Koyuncu, Hogue, & Enquist, 2013) thus favouring retrograde transport. Currently, we have no information on the distribution/expression of EV-A71 receptors on neuronal cell bodies and axon terminals in our Tg mouse.

In conclusion, at least in this mouse model, we believe the viral transmission into the CNS is mainly due to retrograde axonal transport from peripheral nerves. Virus spread into the CNS by a haematogenous/BBB route cannot be excluded completely,

since Volle et al. (2015) has found that human cerebral microvascular endothelial cells were infectable by EV-A71. If a haematogenous/BBB route into the CNS is involved, following viraemia, all CNS neurons should be theoretically more or less equally exposed to virus, and therefore have a similar chance to be infected. In all our mouse *in vivo* infection experiments, although there was high viraemia, widespread neuronal infection, for example, in the isocortex (cerebral hemisphere), was not observed at all time points. Instead, spinal cords and brainstem neurons were the most severely infected. As we have discussed earlier, we also believe that neuronal infection may not be related to the distribution/density of mSCARB2 (Yu et al., 2014). Moreover, our MAVS may use an unknown non-mSCARB2 receptor (s) (Fields et al., 2013) for viral entry.

5.3 Enterovirus 71 Provocation Acute Flaccid Paralysis

Provocation poliomyelitis had been linked to multiple IM-injections of various therapeutic agents or vaccines administered, predisposing patients who have concurrent poliovirus infection to AFP (Gromeier & Wimmer, 1998). It was thought that injured muscle tissues may increase poliovirus propagation and retrograde axonal transport up the peripheral nerves to cause this phenomenon. We speculated that muscle trauma could likewise predispose patients with EV-A71 infection to AFP similar to provocation poliomyelitis.

Using a mouse model developed for the study of EV-A71 provocation AFP (Section 4.5.1, page 87), the non-traumatised control mice only showed paralysis from 72 hpi onwards. In the repeatedly traumatised mouse group, the onset of paralysis was no different from the control group. The degree of myositis and density of viral antigens in skeletal muscles were the same between traumatised and non-traumatised groups. Similarly, viral antigens in the spinal cords were the same. Hence, the results showed that muscle injury did not seem to lead to increased viral replication in skeletal muscles and spinal cords, or increased retrograde transmission, suggesting that EV-A71 provocation AFP did not occur.

Using an IV-inoculated, CD155-Tg mouse model for poliovirus infection, it was found that poliovirus replicated efficiently in the traumatised muscles but not at all in non-traumatised muscles (Gromeier & Wimmer, 1998). This increase of virus growth in traumatised muscles was thought to increase retrograde axonal transport of poliovirus into the spinal cord to give rise to provocation poliomyelitis. The authors speculated that this may be due to increased poliovirus cellular binding in the muscles or increased viral load within inflamed muscle as a result of infiltrating inflammatory cells which were virus infected (Gromeier & Wimmer, 1998). Although EV-A71 possibly shares

the same retrograde axonal transmission pathway into the CNS, we are uncertain why our model did not show any evidence of provocation AFP. One possible reason may be the early and extensive infection in non-traumatised skeletal muscle seen in our model, may have obscured any further increase of viral replication as a result of trauma. As far as we are aware, EV-A71 provocation AFP has never been reported in humans but we believe it still remains a possibility. In human EV-A71 infection, there is apparently no evidence of myositis or skeletal muscle infection (Ong & Wong, 2015) but just like in the poliovirus Tg mouse model, IM-injections may increase viral replication in skeletal muscles leading to provocation paralysis.

5.4 Infectivity of EV-A71 (MAVS) in non-neuronal tissues

In our MAVS mouse model, skeletal muscle fibres showed remarkable degeneration, necrosis, varying degrees of inflammation and viral antigens/RNA. Although skeletal muscle infection has not been found in humans so far, EV-A71 had been reported to exhibit strong myotropism in mouse, hamster, monkey and gerbil models infected with clinical isolates of EV-A71 and/or adapted virus strains (Phyu et al., 2016; Y. F. Wang & Yu, 2014). Tg and immuno-deficient mouse models also showed myotropism (Y. F. Wang & Yu, 2014). Interestingly, skeletal muscle infection was reported in younger mice only (Y. F. Wang & Yu, 2014). In addition, human rhabdomyosarcoma cell lines (neoplastic cells with skeletal muscle differentiation) are readily susceptible to EV-A71, and have been used extensively by other investigators and us for virus isolation and detection (Leong & Chow, 2006).

We produced a light-sensitive virus which could infect and replicate in cells as usual, but newly-synthesised viruses will not be light-sensitive. Therefore, light-protected virus titres would include both original and newly-synthesised virus, whereas light-treated virus titres were all newly-synthesised viruses. The results in section 4.5.2 (page 92) demonstrated a high replication rate of virus in skeletal muscles, and light-treated virus titres were not significantly ($P < 0.05$) different from light-protected titres at all time points. Thus, most of the isolated viruses were newly-synthesised (> 90%). Furthermore, virus isolated from the lower spinal cords were mostly newly-synthesised viruses (Figure 4.27, page 91). These results suggested that the inoculated virus replicated very efficiently in the injected muscles to produce a large amount of virus progeny which then underwent retrograde transport to the lower spinal cord. These observations confirmed the IHC and ISH findings that skeletal muscles are highly susceptible to infection. The exact pathogenic mechanisms involved in the skeletal

muscle infection and injury by EV-A71, and its role in retrograde axonal transport into the CNS is currently unknown (section 5.1, page 114).

Similar to the skeletal muscle infection, EV-A71 could replicate extensively in murine brown adipose tissues, which was also seen in coxsackieviruses, cytomegalovirus and rabies (Aronson & Shwartzman, 1956; Botvinkin, Nikiforova, & Sidorov, 1985; Bruggeman, Bruning, Grauls, van den Bogaard, & Bosman, 1987; Roberts & Boyd, 1987). In the mouse model, both skeletal muscle and brown adipose tissue infection are probably important primary replication sites contributing to persistent high viraemia. Again, there is no information on viral replication in human adipose tissues so far. If human brown adipose tissues could be readily infected by EV-A71, it is conceivable that the young children who have higher amounts of brown adipose tissues, could be predisposed to higher viraemia, and presumably more severe infection.

In our mouse model, skin lesions were absent with no evidence of squamous epithelial cell infection. A few researchers had made observations of skin lesions in their animal models. However, to date, only 2 groups had found viral antigens/RNA in skin epidermis in a hamster model (Phyu et al., 2016) and a Tg mouse model (Fujii et al., 2013). Currently, there is no data on human epidermal squamous cell infection but virus has been cultured in fluid from skin vesicles suggesting that human epidermis is also susceptible to infection. Hence, the epidermis could be an important secondary viral replication site contributing significantly to viraemia.

In our mouse model, other major organs, including oral mucosa, gastrointestinal tissues, pancreas, liver, heart, lung, kidney, thymus, lymph nodes, Peyer's patches and spleen were all negative for viral antigens/RNA. These observations had been reported in many different mouse models (Y. F. Wang & Yu, 2014). Interestingly, using the

same MAVS on a hamster model, Phyu et al. (2016), found widespread viral antigens/RNA in the squamous epithelium of the oral cavity and tongue but not in any large extent in gastrointestinal mucosa. Similarly, Fujii et al. (2013) also reported viral antigens in oral mucosa of a Tg mouse model. These recent findings are consistent with oropharyngeal lesions in HFMD and herpangina, and the fact that viruses could be readily isolated from throat swabs. In fact, higher oral viral yields than rectal swabs were often obtained (M. H. Ooi, Solomon, et al., 2007). Hence, it is probable that the virus first infects and undergoes primary replication in the oral cavity, although viral antigens within human oral mucosa has not been demonstrated before. Recently, Y. He et al. (2014) had shown the presence of viral antigens/RNA in human tonsillar crypt squamous epithelia, and suggested this as another important source of primary replication and oral viral shedding. In addition, salivary and lacrimal gland acinar cells in the hamster model can be infected suggesting that salivary and tear secretions could contribute to virus shedding, respectively.

In our mouse and other animal models, myocarditis and/or viral antigens/RNA were generally absent, or if present, usually very mild and focal, similar to human findings. Lymphoid cells found in lymph nodes, spleen, and Peyer's patches (small intestine) may showed focal viral antigens/RNA and positive virus isolation in some of the animal models (Khong et al., 2012; Y. F. Wang & Yu, 2014; Zhang et al., 2011), including the Tg mouse model (Fujii et al., 2013) but so far there is no convincing evidence for antigens/RNA localisation in human lymphoid tissues. Further studies are needed to confirm if lymphoid tissues are significant replication sites as was assumed to be the case in poliovirus infection.

In conclusion, despite the relatively restricted tissue tropism compared to the hamster model and Tg mouse model, we believe our mouse model is useful to study

neuroinvasion and neuropathogenesis because the CNS findings were very similar to the pathology of human EV-A71 encephalomyelitis.

5.5 Prevention and treatment of EV-A71 CNS infection

Fatal EV-A71 encephalomyelitis and AFP often occur suddenly and within a few days of infection. Clinical observations suggested that some patients who are more likely to develop severe or fatal complications can be identified (C. C. Huang et al., 1999). In these patients, early preventive antiviral treatment could potentially reduce mortality and serious sequelae (M. H. Ooi, Wong, Lewthwaite, Cardosa, & Solomon, 2010). Since no licensed vaccines or effective antivirals are available, neutralising antibodies and other treatment modalities may be useful for this purpose.

Several recent studies have demonstrated that treatment with specific polyclonal antibodies and MAbs were able to confer partial or complete protection to experimentally-infected mice, when given shortly after or before EV-A71 challenge (Table 5.3) (Bek et al., 2011; G. H. Chang et al., 2010; H. W. Chang et al., 2013; Foo et al., 2007; Y. X. Li et al., 2014; Z. Li et al., 2014; Liou et al., 2010; Ng et al., 2015; Tian et al., 2012; Xu et al., 2014). However, none of these studies have evaluated the effectiveness of treatment after encephalomyelitis has been established by CNS viral culture and/or demonstration of viral antigens/RNA. Instead, previous studies evaluated the effectiveness of treatment based solely on survival/health scores of murine models. This may not be sufficient since myositis as well as CNS infection is often severe in these models, and observed limb weakness/paralysis could be due to myositis and/or CNS infection. Incidentally, human EV71-associated myositis has not been reported so far, and encephalomyelitis is believed to be one of the major causes of death in EV71 infection (K. T. Wong et al., 2008).

Our results showed that polyclonal antibodies could improve the survival rate of IM-infected mice with proven encephalomyelitis, by significantly reducing CNS viral titres and viral antigens/RNA (Figure 4.31, page 98; Figure 4.32, page 99). Furthermore, the distribution of viral antigens/RNA were more restricted compared to mock-treated controls. In addition, when polyclonal antibodies were given before MAVS infection, CNS infection was prevented (4 hr before infection). This was also shown in other studies (Deng et al., 2015; Dong et al., 2011; Kiener et al., 2014; Ong et al., 2010; Tian et al., 2012; Zhao et al., 2013). Polyclonal antibodies seem to be able to control and ameliorate CNS infection in a dose- and time- dependent manner.

Polyclonal antibodies are subject to limited quantities, and poor reproducibility due to batch-to-batch variability in neutralising properties. In addition, inappropriate use of polyclonal antibodies could lead to allergic reactions, kidney failure and other serious complications (Orbach, Katz, Sherer, & Shoenfeld, 2005). Hence, we produced a MAb against EV-A71 to test on our IP-infected, 2-week-old mouse model, which consistently developed CNS infection (as confirmed by viral titres and pathological analysis) as early as 72 hpi and rapidly died at 120 hpi (Section 4.6.2, page 100).

All mice IP-treated at maximum doses of 120 µg of MAb before CNS infection (treated at 24, 48 and 72 hpi) remained healthy throughout the experiment. Skeletal muscle and brown adipose tissue infection were minimal, and CNS infection was prevented (Figure 4.36, page 109). The absence of CNS viral titres and viral antigens/RNA suggested that there was no significant CNS infection or retrograde axonal viral transmission up peripheral motor nerves. Inhibition of viraemia and viral replication by MAb were most probably responsible for this. Other previous studies in which pre-infection antibody treatments were given also prevented limb paralysis with no reported mortality (Deng et al., 2015; Dong et al., 2011; Kiener et al., 2014; Ng et al., 2015; Ong et al., 2010; Tian et al., 2012; Zhao et al., 2013).

Table 5.3: Summary of studies on post-infection passive immunisation and treatment modalities in EV-A71 infected mice

No.	Treatment modality[++]	Mouse type	Age at infection (days) /route*	Untreated group		Treated group		CNS infection demonstrated[@]	Reference
				Duration of survival (days)	Survival rate (%)	Treatment started (hpi)	Survival rate (%)		
1	Polyclonal	Balb/c	1 / IP	1 - 7	0	1	70	ND[¤]	(Tian et al., 2012)
2	Polyclonal	Balb/c	Neonatal / IC	5 - 9	0	4	100	ND	(Y. X. Li et al., 2014)
3	Polyclonal	Balb/c	1 / IP	3 - 10	0	24	100	ND	(Bek et al., 2011)
4	Polyclonal	Balb/c	1 / IP	3 - 10	0	24	80	ND	(Foo et al., 2007)
5	MAb	Balb/c	1 / IP	5 - 12	9	24	100	ND	(Xu et al., 2014)
6	MAb	Balb/c	2 / IP	3 - 8	0	24	69	ND	(G. H. Chang et al., 2010)
7	MAb	Balb/c	1 / IP	5 - 9	0	24	100	ND	(Z. Li et al., 2014)
						72	100		
						96	20		
						96, 120, 144	50		
						120, 144, 168	20		
8	MAb	hSCARB2 Tg	7 / SC	6 - 7	0	3	100	ND	(H. W. Chang et al., 2013)
						24	90		
						48	0		
9	IgY	ICR	1 / IP	nil	0 - 20	24, 48, 72	100	ND	(Liou et al., 2010)
						48, 72, 96	79		
						72, 96, 120	20		
10	Polyclonal	ICR	14 / IM	4	0	12	50	Yes	Current study (Section 4.6.1, page 94)
						24	25		
11	MAb	ICR	14 / IP	5	0	24, 48	100	No	Current study (Section 4.6.2, page 100)
						24, 48, 72	100		
						72, 96	75	Yes	
						72, 96, 120	100		

[++] polyclonal= polyclonal antibodies; MAb= monoclonal antibodies; IgY= functionality similar to mammalian IgG, is the major antibody in bird.
* IP= intra-peritoneal; IC= intra-cerebral; SC= subcutaneous; IM= intra-muscular
[@] CNS infection demonstrated via histopathology analysis (IHC and ISH), virus titres and/or viral copy numbers (real-time PCR).
¤ ND = Not done

We found that optimal MAb treatment was still useful to ameliorate disease even after CNS infection was established at 72 hpi. Mice given the 3-dose regime (at 72, 96 and 120 hpi) (Table 5.3) showed lower clinical scores compared to mock-treated control mice (all mice were moribund and sacrificed at 96 hpi) (Figure 4.34, page 105). Even at 144 hpi (a day after the treatment was completed), viral titres/RNA and antigens from sacrificed animals were significantly lower in all tissues examined compared to mock-treated animals sacrificed at 96 hpi (Figure 4.37 (page 111), 4.38, (page 111), 4.39, (page 112)). Moreover, viral antigens/RNA were restricted to smaller areas of the brainstem and hypothalamus (Figure 4.35, page 108). In the 4 animals from the same experiment which were not sacrificed at 144 hpi but followed up for 21 dpi, only a single mouse showed minor weakness on both hindlimbs, while the others recovered completely from limb paralysis. As expected, mice treated earlier at 24, 48 and 72 hpi, presented better clinical scores and no evidence of CNS infection (Table 5.3).

Although not directly comparable to our studies, most other studies showed a similar dose- and time-dependent response to treatment (Table 5.3). Z. Li et al. (2014) tested a 3-dose treatment protocol on infected mice, in a study whose design is similar to ours although their untreated mice survived infection longer, from 5 to 9 dpi. An increase in treatment dose and frequency, had increased the survival rate from 20% to 50%. Surviving mice were either healthy throughout the experiment or showed only minor paralysis/reduced body weight, followed by complete recovery at 21 dpi. Unfortunately, no information on CNS infection was available.

Although the mechanism of virus elimination from the CNS is uncertain, theoretically, the antibodies could i) reduce neuronal infection, by reducing retrograde axonal transport into the CNS; ii) by eliminating viruses in infected neurons; and iii) by preventing viral spread from infected to uninfected neurons. Whether these antibodies were involved in virus elimination from infected neurons or prevention of virus spread

in the CNS parenchyma is uncertain, as it is generally assumed that IgM is too large to cross the healthy BBB into the CNS. However, alteration of BBB permeability as a result of pro-inflammatory cytokines such as TNF, IL-1β and IL-6, could allow antibodies to enter the CNS parenchyma (de Vries, Kuiper, de Boer, Van Berkel, & Breimer, 1997). Alternatively, as shown in, previous studies the rat BBB is not fully developed until four weeks postnatal (Schulze & Firth, 1992). The immature BBB in 2-week-old mice may facilitate movement of antibodies into the parenchyma (Saunders, Liddelow, & Dziegielewska, 2012). Whether some or all these factors could impact on future successful development of antibody therapy using the same approach in patients needs to be further investigated.

In conclusion, our results highlight the potential use of MAbs as an effective treatment for EV-A71 before and after CNS infection in our mouse model. Further investigations are needed to determine the usefulness of a humanised monoclonal IgG as a prophylactic and/or therapeutic agent against EV-A71 encephalomyelitis.

6.0 Conclusion

EV-A71 could cause rapid and direct brainstem infection, most likely via retrograde axonal transport in the motor components of cranial nerves in our EV-A71 encephalomyelitis mouse model. Surprisingly, direct inoculation of virus into the CNS parenchyma, including the brainstem, did not result in efficient neuron-to-neuron centrifugal spread from the needle tract. Moreover, there appears to be no clear correlation between mSCARB2 and EV-A71 antigen distribution suggesting possible involvement of other unknown viral entry receptors and/or co-receptors. EV-A71 provocation AFP, if any, could not be demonstrated in our mouse model as there was no significant increased viral infection of the spinal cord following muscle traumatic injury. CNS infection by EV-A71 can be prevented and established CNS infection ameliorated by neutralising MAb. All treated mice with CNS infection survived with better clinical scores and less pathological changes and evidence of virus infection.

7.0 Limitation and future studies

1. Experimentally infected mice may not be able to model human infection completely. Since pulmonary oedema and skin lesions were not observed in our mouse model. However neuronotropism in the CNS shared many features with human encephalomyelitis. Hence, our mouse model remains valid and useful for gaining further insights into EV-A71 neuropathogenesis. Nonetheless, our findings should be confirmed in more recently described transgenic mouse model (Fujii et al., 2013) or orally-infected hamster model (Phyu et al., 2016).

2. The mechanisms of retrograde axonal transport in EV-A71 CNS infection,viral transport across neuromuscular junction and transsynaptic transmission need to be investigated.

3. The relatively low infectivity of motor neuron cell bodies should be further investigated.

4. EV-A71 provocation AFP was not shown in our mouse model could be due to early and extensive infection in non-traumatised muscle. The experiment could be repeated with transgenic mouse model which demonstrated lesser muscle infection (Fujii et al., 2013).

5. Mouse MAb was not fully characterised and its mechanism of action is not clear. Further investigations are needed to determine the usefulness of a humanised MAb as a therapeutic agent against human EV-A71 encephalomyelitis.

References

Adams, M. J., King, A. M., & Carstens, E. B. (2013). Ratification vote on taxonomic proposals to the International Committee on Taxonomy of Viruses (2013). *Arch Virol, 158*(9), 2023-2030.

Arita, M., Ami, Y., Wakita, T., & Shimizu, H. (2008). Cooperative effect of the attenuation determinants derived from poliovirus sabin 1 strain is essential for attenuation of enterovirus 71 in the NOD/SCID mouse infection model. *J Virol, 82*(4), 1787-1797.

Arita, M., Nagata, N., Iwata, N., Ami, Y., Suzaki, Y., Mizuta, K., . . . Shimizu, H. (2007). An attenuated strain of enterovirus 71 belonging to genotype a showed a broad spectrum of antigenicity with attenuated neurovirulence in cynomolgus monkeys. *J Virol, 81*(17), 9386-9395.

Arita, M., Shimizu, H., Nagata, N., Ami, Y., Suzaki, Y., Sata, T., . . . Miyamura, T. (2005). Temperature-sensitive mutants of enterovirus 71 show attenuation in cynomolgus monkeys. *J Gen Virol, 86*(5), 1391-1401.

Aronson, S. M., & Shwartzman, G. (1956). The histopathology of brown fat in experimental poliomyelitis. *Am J Pathol, 32*(2), 315-333.

Baker, A. B. (1957). Poliomyelitis. 16. A study of pulmonary edema. *Neurology, 7*(11), 743-751.

Bedard, K. M., & Semler, B. L. (2004). Regulation of picornavirus gene expression. *Microbes Infect, 6*(7), 702-713.

Bek, E. J., Hussain, K. M., Phuektes, P., Kok, C. C., Gao, Q., Cai, F., . . . McMinn, P. C. (2011). Formalin-inactivated vaccine provokes cross-protective immunity in a mouse model of human enterovirus 71 infection. *Vaccine, 29*(29-30), 4829-4838.

Botvinkin, A. D., Nikiforova, T. A., & Sidorov, G. N. (1985). Experimental rabies in hibernator rodents. *Acta Virol, 29*(1), 44-50.

Brown, B. A., Oberste, M. S., Alexander, J. P., Jr., Kennett, M. L., & Pallansch, M. A. (1999). Molecular epidemiology and evolution of enterovirus 71 strains isolated from 1970 to 1998. *J Virol, 73*(12), 9969-9975.

Bruggeman, C. A., Bruning, J. H., Grauls, G., van den Bogaard, A. E., & Bosman, F. (1987). Presence of cytomegalovirus in brown fat. Study in a rat model. *Intervirology, 27*(1), 32-37.

Caine, E. A., Partidos, C. D., Santangelo, J. D., & Osorio, J. E. (2013). Adaptation of enterovirus 71 to adult interferon deficient mice. *PLoS One, 8*(3), e59501.

Cao, R., Han, J., Deng, Y., Yu, M., Qin, E., & Qin, C. (2010). Presence of high-titer neutralizing antibodies against enterovirus 71 in intravenous immunoglobulin manufactured from Chinese donors. *Clin Infect Dis, 50*(1), 125-126.

Cao, R., Han, J., Qin, E., & Qin, C. (2011). [Mechanism of intravenous immunoglobulin therapy for severe hand-foot-mouth disease: a review]. *Sheng Wu Gong Cheng Xue Bao, 27*(5), 712-716.

Cao, R. Y., Dong, D. Y., Liu, R. J., Han, J. F., Wang, G. C., Zhao, H., . . . Qin, C. F. (2013). Human IgG subclasses against enterovirus Type 71: neutralization versus antibody dependent enhancement of infection. *PLoS One, 8*(5), e64024.

Cardosa, M. J., Perera, D., Brown, B. A., Cheon, D., Chan, H. M., Chan, K. P., . . . McMinn, P. (2003). Molecular epidemiology of human enterovirus 71 strains and recent outbreaks in the Asia-Pacific region: comparative analysis of the VP1 and VP4 genes. *Emerg Infect Dis, 9*(4), 461-468.

Chang, G. H., Luo, Y. J., Wu, X. Y., Si, B. Y., Lin, L., & Zhu, Q. Y. (2010). Monoclonal antibody induced with inactived EV71-Hn2 virus protects mice against lethal EV71-Hn2 virus infection. *Virol J, 7*, 106.

Chang, H. W., Lin, Y. W., Ho, H. M., Lin, M. H., Liu, C. C., Shao, H. Y., . . . Chow, Y. H. (2013). Protective efficacy of VP1-specific neutralizing antibody associated with a reduction of viral load and pro-inflammatory cytokines in human SCARB2-transgenic mice. *PLoS One, 8*(7), e69858.

Chang, S. C., Lin, J. Y., Lo, L. Y., Li, M. L., & Shih, S. R. (2004). Diverse apoptotic pathways in enterovirus 71-infected cells. *J Neurovirol, 10*(6), 338-349.

Chen, C. S., Yao, Y. C., Lin, S. C., Lee, Y. P., Wang, Y. F., Wang, J. R., . . . Yu, C. K. (2007). Retrograde axonal transport: a major transmission route of enterovirus 71 in mice. *J Virol, 81*(17), 8996-9003.

Chen, F., Li, J. J., Liu, T., Wen, G. Q., & Xiang, W. (2013). Clinical and neuroimaging features of enterovirus71 related acute flaccid paralysis in patients with hand-foot-mouth disease. *Asian Pac J Trop Med, 6*(1), 68-72.

Chen, H., Zhang, Y., Yang, E., Liu, L., Che, Y., Wang, J., . . . Li, Q. (2012). The effect of enterovirus 71 immunization on neuropathogenesis and protein expression profiles in the thalamus of infected rhesus neonates. *Virology, 432*(2), 417-426.

Chen, N., & Reis, C. S. (2002). Distinct roles of eicosanoids in the immune response to viral encephalitis: or why you should take NSAIDS. *Viral Immunol, 15*(1), 133-146.

Chen, P., Song, Z., Qi, Y., Feng, X., Xu, N., Sun, Y., . . . Li, W. (2012). Molecular determinants of enterovirus 71 viral entry: cleft around GLN-172 on VP1 protein interacts with variable region on scavenge receptor B 2. *J Biol Chem, 287*(9), 6406-6420.

Chen, Y. C., Yu, C. K., Wang, Y. F., Liu, C. C., Su, I. J., & Lei, H. Y. (2004). A murine oral enterovirus 71 infection model with central nervous system involvement. *J Gen Virol, 85*(1), 69-77.

Chu, W. M., Ostertag, D., Li, Z. W., Chang, L., Chen, Y., Hu, Y., . . . Karin, M. (1999). JNK2 and IKKbeta are required for activating the innate response to viral infection. *Immunity, 11*(6), 721-731.

Chua, B. H., Phuektes, P., Sanders, S. A., Nicholls, P. K., & McMinn, P. C. (2008). The molecular basis of mouse adaptation by human enterovirus 71. *J Gen Virol, 89*(7), 1622-1632.

Chua, K. B., Chua, B. H., Lee, C. S., Chem, Y. K., Ismail, N., Kiyu, A., & Kumarasamy, V. (2007). Genetic diversity of enterovirus 71 isolated from cases of hand, foot and mouth disease in the 1997, 2000 and 2005 outbreaks, Peninsular Malaysia. *Malays J Pathol, 29*(2), 69-78.

Chung, C. Y., Chen, C. Y., Lin, S. Y., Chung, Y. C., Chiu, H. Y., Chi, W. K., . . . Hu, Y. C. (2010). Enterovirus 71 virus-like particle vaccine: improved production conditions for enhanced yield. *Vaccine, 28*(43), 6951-6957.

Collins, F. M. (1974). Vaccines and cell-mediated immunity. *Bacteriol Rev, 38*(4), 371-402.

Conn, P. Michael, & SpringerLink. (2008). *Neuroscience in medicine* (3rd ed.). Totowa, NJ: Humana Press.

de Vries, H. E., Kuiper, J., de Boer, A. G., Van Berkel, T. J., & Breimer, D. D. (1997). The blood-brain barrier in neuroinflammatory diseases. *Pharmacol Rev, 49*(2), 143-155.

Deng, Y. Q., Ma, J., Xu, L. J., Li, Y. X., Zhao, H., Han, J. F., . . . Qin, C. F. (2015). Generation and characterization of a protective mouse monoclonal antibody against human enterovirus 71. *Appl Microbiol Biotechnol, 99*(18), 7663-7671.

Dong, C., Liu, L., Zhao, H., Wang, J., Liao, Y., Zhang, X., . . . Li, Q. (2011). Immunoprotection elicited by an enterovirus type 71 experimental inactivated vaccine in mice and rhesus monkeys. *Vaccine, 29*(37), 6269-6275.

Dotzauer, A., & Kraemer, L. (2012). Innate and adaptive immune responses against picornaviruses and their counteractions: An overview. *World J Virol, 1*(3), 91-107.

Elgert, K.D. (2009). *Immunology: Understanding The Immune System*. New York: Wiley.

Fan, P., Li, X., Sun, S., Su, W., An, D., Gao, F., . . . Jiang, C. (2015). Identification of a common epitope between enterovirus 71 and human MED25 proteins which may explain virus-associated neurological disease. *Viruses, 7*(4), 1558-1577.

Fields, B.N., Knipe, D.M., & Howley, P.M. (2013). *Fields Virology* (6th ed.): United kingdon: Wolters Kluwer Health.

Foo, D. G., Alonso, S., Chow, V. T., & Poh, C. L. (2007). Passive protection against lethal enterovirus 71 infection in newborn mice by neutralizing antibodies elicited by a synthetic peptide. *Microbes Infect, 9*(11), 1299-1306.

Fu, Y. C., Chi, C. S., Chiu, Y. T., Hsu, S. L., Hwang, B., Jan, S. L., . . . Chang, Y. (2004). Cardiac complications of enterovirus rhombencephalitis. *Arch Dis Child, 89*(4), 368-373.

Fu, Y. C., Chi, C. S., Lin, N. N., Cheng, C. C., Jan, S. L., Hwang, B., . . . Chiu, Y. T. (2006). Comparison of heart failure in children with enterovirus 71 rhombencephalitis and cats with norepinephrine cardiotoxicity. *Pediatr Cardiol, 27*(5), 577-584.

Fujii, K., Nagata, N., Sato, Y., Ong, K. C., Wong, K. T., Yamayoshi, S., . . . Koike, S. (2013). Transgenic mouse model for the study of enterovirus 71 neuropathogenesis. *Proc Natl Acad Sci U S A, 110*(36), 14753-14758.

Gitlin, L., Barchet, W., Gilfillan, S., Cella, M., Beutler, B., Flavell, R. A., . . . Colonna, M. (2006). Essential role of mda-5 in type I IFN responses to polyriboinosinic:polyribocytidylic acid and encephalomyocarditis picornavirus. *Proc Natl Acad Sci U S A, 103*(22), 8459-8464.

Gong, X., Zhou, J., Zhu, W., Liu, N., Li, J., Li, L., . . . Duan, Z. (2012). Excessive proinflammatory cytokine and chemokine responses of human monocyte-derived macrophages to enterovirus 71 infection. *BMC Infect Dis, 12*, 224.

Gorson, K. C., & Ropper, A. H. (2001). Nonpoliovirus poliomyelitis simulating Guillain-Barre syndrome. *Arch Neurol, 58*(9), 1460-1464.

Gromeier, M., & Wimmer, E. (1998). Mechanism of injury-provoked poliomyelitis. *J Virol, 72*(6), 5056-5060.

Han, J. F., Cao, R. Y., Deng, Y. Q., Tian, X., Jiang, T., Qin, E. D., & Qin, C. F. (2011). Antibody dependent enhancement infection of enterovirus 71 in vitro and in vivo. *Virol J, 8*, 106.

He, D. L., Xia, N. S., Xu, F. H., Cheng, T., Weng, Z. X., Ge, S. X., . . . Chen, Z. M. . (2012). Enterovirus 71 neutralized epitope polypeptide and application thereof: Google Patents.

He, Y., Ong, K. C., Gao, Z., Zhao, X., Anderson, V. M., McNutt, M. A., . . . Lu, M. (2014). Tonsillar crypt epithelium is an important extra-central nervous system site for viral replication in EV71 encephalomyelitis. *Am J Pathol, 184*(3), 714-720.

Heimer, Lennart. (1995). *The human brain and spinal cord : functional neuroanatomy and dissection guide* (2nd ed.). New York ; London: Springer.

Hemming, V. G. (2001). Use of intravenous immunoglobulins for prophylaxis or treatment of infectious diseases. *Clin Diagn Lab Immunol, 8*(5), 859-863.

Hinson, V. K., & Tyor, W. R. (2001). Update on viral encephalitis. *Curr Opin Neurol, 14*(3), 369-374.

Ho, M. (2000). Enterovirus 71: the virus, its infections and outbreaks. *J Microbiol Immunol Infect, 33*(4), 205-216.

Hoff, J. T., Nishimura, M., Garcia-Uria, J., & Miranda, S. (1981). Experimental neurogenic pulmonary edema. Part 1: The role of systemic hypertension. *J Neurosurg, 54*(5), 627-631.

Huang, C. C. (2001). Neurologic complications of enterovirus 71 infection in children: lessons from this Taiwan epidemic. *Acta Paediatr Taiwan, 42*(1), 5-7.

Huang, C. C., Liu, C. C., Chang, Y. C., Chen, C. Y., Wang, S. T., & Yeh, T. F. (1999). Neurologic complications in children with enterovirus 71 infection. *N Engl J Med, 341*(13), 936-942.

Huang, H. I., Lin, J. Y., Chen, H. H., Yeh, S. B., Kuo, R. L., Weng, K. F., & Shih, S. R. (2014). Enterovirus 71 infects brain-derived neural progenitor cells. *Virology, 468-470*, 592-600.

Jackson, Alan C. (2013). *Viral infections of the human nervous system Birkhäuser advances in infectious diseases* (pp. 1 online resource). Retrieved from http://eproxy.lib.hku.hk/login?url=http://link.springer.com/openurl?genre=book&isbn=978-3-0348-0424-0

Jarvis, D. L. (2009). Baculovirus-insect cell expression systems. *Methods Enzymol, 463*, 191-222.

Jiao, X. Y., Guo, L., Huang, D. Y., Chang, X. L., & Qiu, Q. C. (2014). Distribution of EV71 receptors SCARB2 and PSGL-1 in human tissues. *Virus Res, 190*, 40-52.

John, T. J., & Vashishtha, V. M. (2013). Eradicating poliomyelitis: India's journey from hyperendemic to polio-free status. *Indian J Med Res, 137*(5), 881-894.

Jolles, S., Sewell, W. A., & Misbah, S. A. (2005). Clinical uses of intravenous immunoglobulin. *Clin Exp Immunol, 142*(1), 1-11.

Kao, S. J., Yang, F. L., Hsu, Y. H., & Chen, H. I. (2004). Mechanism of fulminant pulmonary edema caused by enterovirus 71. *Clin Infect Dis, 38*(12), 1784-1788.

Kapitein, L. C., & Hoogenraad, C. C. (2011). Which way to go? Cytoskeletal organization and polarized transport in neurons. *Mol Cell Neurosci, 46*(1), 9-20.

Kato, H., Takeuchi, O., Sato, S., Yoneyama, M., Yamamoto, M., Matsui, K., . . . Akira, S. (2006). Differential roles of MDA5 and RIG-I helicases in the recognition of RNA viruses. *Nature, 441*(7089), 101-105.

Kemball, C. C., Alirezaei, M., & Whitton, J. L. (2010). Type B coxsackieviruses and their interactions with the innate and adaptive immune systems. *Future Microbiol, 5*(9), 1329-1347.

Khong, W. X., Yan, B., Yeo, H., Tan, E. L., Lee, J. J., Ng, J. K., . . . Alonso, S. (2012). A non-mouse-adapted enterovirus 71 (EV71) strain exhibits neurotropism, causing neurological manifestations in a novel mouse model of EV71 infection. *J Virol, 86*(4), 2121-2131.

Kiener, T. K., Jia, Q., Meng, T., Chow, V. T., & Kwang, J. (2014). A novel universal neutralizing monoclonal antibody against enterovirus 71 that targets the highly conserved "knob" region of VP3 protein. *PLoS Negl Trop Dis, 8*(5), e2895.

Kim, Y. I., Song, J. H., Kwon, B. E., Kim, H. N., Seo, M. D., Park, K., . . . Chang, S. Y. (2015). Pros and cons of VP1-specific maternal IgG for the protection of Enterovirus 71 infection. *Vaccine, 33*(48), 6604-6610.

Koyuncu, O. O., Hogue, I. B., & Enquist, L. W. (2013). Virus infections in the nervous system. *Cell Host Microbe, 13*(4), 379-393.

Ku, Z., Ye, X., Huang, X., Cai, Y., Liu, Q., Li, Y., . . . Huang, Z. (2013). Neutralizing antibodies induced by recombinant virus-like particles of enterovirus 71 genotype C4 inhibit infection at pre- and post-attachment steps. *PLoS One, 8*(2), e57601.

Lancaster, K. Z., & Pfeiffer, J. K. (2010). Limited trafficking of a neurotropic virus through inefficient retrograde axonal transport and the type I interferon response. *PLoS Pathog, 6*(3), e1000791.

Lee, H., Cifuente, J. O., Ashley, R. E., Conway, J. F., Makhov, A. M., Tano, Y., . . . Hafenstein, S. (2013). A strain-specific epitope of enterovirus 71 identified by cryo-electron microscopy of the complex with fab from neutralizing antibody. *J Virol, 87*(21), 11363-11370.

Lein, E. S., Hawrylycz, M. J., Ao, N., Ayres, M., Bensinger, A., Bernard, A., . . . Jones, A. R. (2007). Genome-wide atlas of gene expression in the adult mouse brain. Allen Mouse Brain Atlas. Retrieved from http://mouse.brain-map.org/experiment/show/72081482

Leong, W. F., & Chow, V. T. (2006). Transcriptomic and proteomic analyses of rhabdomyosarcoma cells reveal differential cellular gene expression in response to enterovirus 71 infection. *Cell Microbiol, 8*(4), 565-580.

Levinson, W., & Jawetz, E. (1992). *Medical Microbiology & Immunology: Examination and Board Review.* Boston: Appleton & Lange.

Li, M. L., Hsu, T. A., Chen, T. C., Chang, S. C., Lee, J. C., Chen, C. C., . . . Shih, S. R. (2002). The 3C protease activity of enterovirus 71 induces human neural cell apoptosis. *Virology, 293*(2), 386-395.

Li, Y. X., Zhao, H., Cao, R. Y., Deng, Y. Q., Han, J. F., Zhu, S. Y., . . . Qin, C. F. (2014). Recombinant tandem multi-linear neutralizing epitopes of human enterovirus 71 elicited protective immunity in mice. *Virol J, 11*, 79.

Li, Z., Xu, L., He, D., Yang, L., Liu, C., Chen, Y., . . . Xia, N. (2014). In Vivo Time-Related Evaluation of a Therapeutic Neutralization Monoclonal Antibody against Lethal Enterovirus 71 Infection in a Mouse Model. *PLoS One, 9*(10), e109391.

Liang, C. C., Sun, M. J., Lei, H. Y., Chen, S. H., Yu, C. K., Liu, C. C., . . . Yeh, T. M. (2004). Human endothelial cell activation and apoptosis induced by enterovirus 71 infection. *J Med Virol, 74*(4), 597-603.

Liang, Z., & Wang, J. (2014). EV71 vaccine, an invaluable gift for children. *Clin Transl Immunology, 3*(10), e28.

Lim, X. F., Jia, Q., Khong, W. X., Yan, B., Premanand, B., Alonso, S., . . . Kwang, J. (2012). Characterization of an isotype-dependent monoclonal antibody against linear neutralizing epitope effective for prophylaxis of enterovirus 71 infection. *PLoS One, 7*(1), e29751.

Lin, S. Y., Yeh, C. T., Li, W. H., Yu, C. P., Lin, W. C., Yang, J. Y., . . . Hu, Y. C. (2015). Enhanced enterovirus 71 virus-like particle yield from a new baculovirus design. *Biotechnol Bioeng, 112*(10), 2005-2015.

Lin, T. Y., Chang, L. Y., Hsia, S. H., Huang, Y. C., Chiu, C. H., Hsueh, C., . . . Wu, M. H. (2002). The 1998 enterovirus 71 outbreak in Taiwan: pathogenesis and management. *Clin Infect Dis, 34 Suppl 2*, S52-57.

Lin, T. Y., Chang, L. Y., Huang, Y. C., Hsu, K. H., Chiu, C. H., & Yang, K. D. (2002). Different proinflammatory reactions in fatal and non-fatal enterovirus 71 infections: implications for early recognition and therapy. *Acta Paediatr, 91*(6), 632-635.

Lin, T. Y., Hsia, S. H., Huang, Y. C., Wu, C. T., & Chang, L. Y. (2003). Proinflammatory cytokine reactions in enterovirus 71 infections of the central nervous system. *Clin Infect Dis, 36*(3), 269-274.

Lin, Y. W., Wang, S. W., Tung, Y. Y., & Chen, S. H. (2009). Enterovirus 71 infection of human dendritic cells. *Exp Biol Med (Maywood), 234*(10), 1166-1173.

Lin, Y. W., Yu, S. L., Shao, H. Y., Lin, H. Y., Liu, C. C., Hsiao, K. N., . . . Chow, Y. H. (2013). Human SCARB2 transgenic mice as an infectious animal model for enterovirus 71. *PLoS One, 8*(2), e57591.

Liou, J. F., Chang, C. W., Tailiu, J. J., Yu, C. K., Lei, H. Y., Chen, L. R., & Tai, C. (2010). Passive protection effect of chicken egg yolk immunoglobulins on enterovirus 71 infected mice. *Vaccine, 28*(51), 8189-8196.

Liu, C. C., Chou, A. H., Lien, S. P., Lin, H. Y., Liu, S. J., Chang, J. Y., . . . Chong, P. (2011). Identification and characterization of a cross-neutralization epitope of Enterovirus 71. *Vaccine, 29*(26), 4362-4372.

Liu, J., Dong, W., Quan, X., Ma, C., Qin, C., & Zhang, L. (2012). Transgenic expression of human P-selectin glycoprotein ligand-1 is not sufficient for enterovirus 71 infection in mice. *Arch Virol, 157*(3), 539-543.

Liu, L., Mo, Z., Liang, Z., Zhang, Y., Li, R., Ong, K. C., . . . Li, Q. (2015). Immunity and clinical efficacy of an inactivated enterovirus 71 vaccine in healthy Chinese children: a report of further observations. *BMC Med, 13*(1), 226.

Lu, M., Meng, G., He, Y. X., Zheng, J., Liao, S. L., Zhong, Y. F., . . . Gao, Z. F. (2009). [Pathology of enterovirus 71 infection: an autopsy study of 5 cases]. *Zhonghua Bing Li Xue Za Zhi, 38*(2), 81-85.

Lum, L. C., Wong, K. T., Lam, S. K., Chua, K. B., & Goh, A. Y. (1998). Neurogenic pulmonary oedema and enterovirus 71 encephalomyelitis. *Lancet, 352*(9137), 1391.

Luo, S. T., Chiang, P. S., Chao, A. S., Liou, G. Y., Lin, R., Lin, T. Y., & Lee, M. S. (2009). Enterovirus 71 maternal antibodies in infants, Taiwan. *Emerg Infect Dis, 15*(4), 581-584.

Mao, Q. Y., Wang, Y., Bian, L., Xu, M., & Liang, Z. (2016). EV71 vaccine, a new tool to control outbreaks of hand, foot and mouth disease (HFMD). *Expert Rev Vaccines, 15*(5), 599-606.

Mawdsley, S. E. (2014). Polio provocation: solving a mystery with the help of history. *Lancet, 384*(9940), 300-301.

McMinn, P. C. (2002). An overview of the evolution of enterovirus 71 and its clinical and public health significance. *FEMS Microbiol Rev, 26*(1), 91-107.

McMinn, P., Stratov, I., Nagarajan, L., & Davis, S. (2001). Neurological manifestations of enterovirus 71 infection in children during an outbreak of hand, foot, and mouth disease in Western Australia. *Clin Infect Dis, 32*(2), 236-242.

Meng, T., Kolpe, A. B., Kiener, T. K., Chow, V. T., & Kwang, J. (2011). Display of VP1 on the surface of baculovirus and its immunogenicity against heterologous human enterovirus 71 strains in mice. *PLoS One, 6*(7), e21757.

Nathanson, N., & Langmuir, A. D. (1995). The Cutter incident. Poliomyelitis following formaldehyde-inactivated poliovirus vaccination in the United States during the Spring of 1955. II. Relationship of poliomyelitis to Cutter vaccine. 1963. *Am J Epidemiol, 142*(2), 109-140.

Ng, Q., He, F., & Kwang, J. (2015). Recent Progress towards Novel EV71 Anti-Therapeutics and Vaccines. *Viruses, 7*(12), 6441-6457.

Offit, P. A. (2005). The Cutter incident, 50 years later. *N Engl J Med, 352*(14), 1411-1412.

Ohka, S., Matsuda, N., Tohyama, K., Oda, T., Morikawa, M., Kuge, S., & Nomoto, A. (2004). Receptor (CD155)-dependent endocytosis of poliovirus and retrograde axonal transport of the endosome. *J Virol, 78*(13), 7186-7198.

Ohka, S., Sakai, M., Bohnert, S., Igarashi, H., Deinhardt, K., Schiavo, G., & Nomoto, A. (2009). Receptor-dependent and -independent axonal retrograde transport of poliovirus in motor neurons. *J Virol, 83*(10), 4995-5004.

Ohka, S., Yang, W. X., Terada, E., Iwasaki, K., & Nomoto, A. (1998). Retrograde transport of intact poliovirus through the axon via the fast transport system. *Virology, 250*(1), 67-75.

Ong, K. C., Badmanathan, M., Devi, S., Leong, K. L., Cardosa, M. J., & Wong, K. T. (2008). Pathologic characterization of a murine model of human enterovirus 71 encephalomyelitis. *J Neuropathol Exp Neurol, 67*(6), 532-542.

Ong, K. C., Devi, S., Cardosa, M. J., & Wong, K. T. (2010). Formaldehyde-inactivated whole-virus vaccine protects a murine model of enterovirus 71 encephalomyelitis against disease. *J Virol, 84*(1), 661-665.

Ong, K. C., & Wong, K. T. (2015). Understanding Enterovirus 71 neuropathogenesis and its impact on other neurotropic Enteroviruses. *Brain Pathol, 25*(5), 614-624.

Ooi, E. E., Phoon, M. C., Ishak, B., & Chan, S. H. (2002). Seroepidemiology of human enterovirus 71, Singapore. *Emerg Infect Dis, 8*(9), 995-997.

Ooi, M. H., Solomon, T., Podin, Y., Mohan, A., Akin, W., Yusuf, M. A., . . . Cardosa, J. (2007). Evaluation of different clinical sample types in diagnosis of human enterovirus 71-associated hand-foot-and-mouth disease. *J Clin Microbiol, 45*(6), 1858-1866.

Ooi, M. H., Wong, S. C., Lewthwaite, P., Cardosa, M. J., & Solomon, T. (2010). Clinical features, diagnosis, and management of enterovirus 71. *Lancet Neurol, 9*(11), 1097-1105.

Ooi, M. H., Wong, S. C., Mohan, A., Podin, Y., Perera, D., Clear, D., . . . Solomon, T. (2009). Identification and validation of clinical predictors for the risk of neurological involvement in children with hand, foot, and mouth disease in Sarawak. *BMC Infect Dis, 9*, 3.

Ooi, M. H., Wong, S. C., Podin, Y., Akin, W., del Sel, S., Mohan, A., . . . Solomon, T. (2007). Human enterovirus 71 disease in Sarawak, Malaysia: a prospective clinical, virological, and molecular epidemiological study. *Clin Infect Dis, 44*(5), 646-656.

Orbach, H., Katz, U., Sherer, Y., & Shoenfeld, Y. (2005). Intravenous immunoglobulin: adverse effects and safe administration. *Clin Rev Allergy Immunol, 29*(3), 173-184.

Oshiumi, H., Okamoto, M., Fujii, K., Kawanishi, T., Matsumoto, M., Koike, S., & Seya, T. (2011). The TLR3/TICAM-1 pathway is mandatory for innate immune responses to poliovirus infection. *J Immunol, 187*(10), 5320-5327.

Pathinayake, P. S., Hsu, A. C., & Wark, P. A. (2015). Innate immunity and immune evasion by Enterovirus 71. *Viruses, 7*(12), 6613-6630.

Paust, S., Senman, B., & von Andrian, U. H. (2010). Adaptive immune responses mediated by natural killer cells. *Immunol Rev, 235*(1), 286-296.

Phyu, W. K., Ong, K. C., & Wong, K. T. (2016). A Consistent Orally-infected hamster model for Enterovirus A71 encephalomyelitis demonstrates squamous lesions in the paws, skin and oral cavity reminiscent of hand-foot-and-mouth disease. *PLoS One, 11*(1), e0147463.

Plevka, P., Perera, R., Cardosa, J., Kuhn, R. J., & Rossmann, M. G. (2012). Crystal structure of human enterovirus 71. *Science, 336*(6086), 1274.

Premanand, B., Kiener, T. K., Meng, T., Tan, Y. R., Jia, Q., Chow, V. T., & Kwang, J. (2012). Induction of protective immune responses against EV71 in mice by baculovirus encoding a novel expression cassette for capsid protein VP1. *Antiviral Res, 95*(3), 311-315.

Roberts, G. B., & Boyd, J. F. (1987). The histopathology of enterovirus infections of new-born mice. *J Infect, 15*(1), 45-56.

Saunders, N. R., Liddelow, S. A., & Dziegielewska, K. M. (2012). Barrier mechanisms in the developing brain. *Front Pharmacol, 3*, 46.

Schmidt, N. J., Lennette, E. H., & Ho, H. H. (1974). An apparently new enterovirus isolated from patients with disease of the central nervous system. *J Infect Dis, 129*(3), 304-309.

Schulze, C., & Firth, J. A. (1992). Interendothelial junctions during blood-brain barrier development in the rat: morphological changes at the level of individual tight junctional contacts. *Brain Res Dev Brain Res, 69*(1), 85-95.

Seder, R. A., & Hill, A. V. (2000). Vaccines against intracellular infections requiring cellular immunity. *Nature, 406*(6797), 793-798.

Solomon, T., Lewthwaite, P., Perera, D., Cardosa, M. J., McMinn, P., & Ooi, M. H. (2010). Virology, epidemiology, pathogenesis, and control of enterovirus 71. *Lancet Infect Dis, 10*(11), 778-790.

Strebel, P. M., Ion-Nedelcu, N., Baughman, A. L., Sutter, R. W., & Cochi, S. L. (1995). Intramuscular injections within 30 days of immunization with oral poliovirus vaccine--a risk factor for vaccine-associated paralytic poliomyelitis. *N Engl J Med, 332*(8), 500-506.

Takeuchi, O., & Akira, S. (2008). MDA5/RIG-I and virus recognition. *Curr Opin Immunol, 20*(1), 17-22.

Tan, S. H., Ong, K. C., & Wong, K. T. (2014). Enterovirus 71 can directly infect the brainstem via cranial nerves and infection can be ameliorated by passive immunization. *J Neuropathol Exp Neurol, 73*(11), 999-1008.

Tian, X., Su, X., Li, X., Li, H., Li, T., Zhou, Z., . . . Zhou, R. (2012). Protection against enterovirus 71 with neutralizing epitope incorporation within adenovirus type 3 hexon. *PLoS One, 7*(7), e41381.

Tirado, S. M., & Yoon, K. J. (2003). Antibody-dependent enhancement of virus infection and disease. *Viral Immunol, 16*(1), 69-86.

Tung, W. H., Sun, C. C., Hsieh, H. L., Wang, S. W., Horng, J. T., & Yang, C. M. (2007). EV71 induces VCAM-1 expression via PDGF receptor, PI3-K/Akt, p38 MAPK, JNK and NF-kappaB in vascular smooth muscle cells. *Cell Signal, 19*(10), 2127-2137.

Tyler, K. L. (2009). Emerging viral infections of the central nervous system: Part 1. *Archives of Neurology, 66*(8), 939-948.

Volle, R., Archimbaud, C., Couraud, P. O., Romero, I. A., Weksler, B., Mirand, A., . . . Bailly, J. L. (2015). Differential permissivity of human cerebrovascular endothelial cells to enterovirus infection and specificities of serotype EV-A71 in crossing an in vitro model of the human blood-brain barrier. *J Gen Virol, 96*(7), 1682-1695.

Wang, S. M., Chen, I. C., Su, L. Y., Huang, K. J., Lei, H. Y., & Liu, C. C. (2010). Enterovirus 71 infection of monocytes with antibody-dependent enhancement. *Clin Vaccine Immunol, 17*(10), 1517-1523.

Wang, S. M., Lei, H. Y., Huang, K. J., Wu, J. M., Wang, J. R., Yu, C. K., . . . Liu, C. C. (2003). Pathogenesis of enterovirus 71 brainstem encephalitis in pediatric patients: roles of cytokines and cellular immune activation in patients with pulmonary edema. *J Infect Dis, 188*(4), 564-570.

Wang, S. M., Lei, H. Y., Huang, M. C., Su, L. Y., Lin, H. C., Yu, C. K., . . . Liu, C. C. (2006). Modulation of cytokine production by intravenous immunoglobulin in patients with enterovirus 71-associated brainstem encephalitis. *J Clin Virol, 37*(1), 47-52.

Wang, S. M., Lei, H. Y., & Liu, C. C. (2012). Cytokine immunopathogenesis of enterovirus 71 brain stem encephalitis. *Clin Dev Immunol, 2012*, 876241.

Wang, S. M., Liu, C. C., Tseng, H. W., Wang, J. R., Huang, C. C., Chen, Y. J., . . . Yeh, T. F. (1999). Clinical spectrum of enterovirus 71 infection in children in southern Taiwan, with an emphasis on neurological complications. *Clin Infect Dis, 29*(1), 184-190.

Wang, W., Duo, J., Liu, J., Ma, C., Zhang, L., Wei, Q., & Qin, C. (2011). A mouse muscle-adapted enterovirus 71 strain with increased virulence in mice. *Microbes Infect, 13*(10), 862-870.

Wang, Y. F., Chou, C. T., Lei, H. Y., Liu, C. C., Wang, S. M., Yan, J. J., . . . Yu, C. K. (2004). A mouse-adapted enterovirus 71 strain causes neurological disease in mice after oral infection. *J Virol, 78*(15), 7916-7924.

Wang, Y. F., & Yu, C. K. (2014). Animal models of enterovirus 71 infection: applications and limitations. *J Biomed Sci, 21*(1), 31.

Warren, H. S., & Smyth, M. J. (1999). NK cells and apoptosis. *Immunol Cell Biol, 77*(1), 64-75.

Wei, D., Li, K. X., & Chen, E. (2010). [Autopsy report of two cases with enterovirus type 71 infection brainstem encephalitis and literature review]. *Zhonghua Er Ke Za Zhi, 48*(3), 220-223.

Weng, K. F., Chen, L. L., Huang, P. N., & Shih, S. R. (2010). Neural pathogenesis of enterovirus 71 infection. *Microbes Infect, 12*(7), 505-510.

Weng, K. F., Li, M. L., Hung, C. T., & Shih, S. R. (2009). Enterovirus 71 3C protease cleaves a novel target CstF-64 and inhibits cellular polyadenylation. *PLoS Pathog, 5*(9), e1000593.

Wilson-Pauwels, L., Akesson, E.J., & Stewart, P.A. (2002). *Cranial nerves : in health and disease* (2nd ed.). Hamilton, Ont. London: BC Decker.

Wilton, T., Dunn, G., Eastwood, D., Minor, P. D., & Martin, J. (2014). Effect of formaldehyde inactivation on poliovirus. *J Virol, 88*(20), 11955-11964.

Wong, K. T., Munisamy, B., Ong, K. C., Kojima, H., Noriyo, N., Chua, K. B., . . . Nagashima, K. (2008). The distribution of inflammation and virus in human enterovirus 71 encephalomyelitis suggests possible viral spread by neural pathways. *J Neuropathol Exp Neurol, 67*(2), 162-169.

Wong, K. T., Ng, K. Y., Ong, K. C., Ng, W. F., Shankar, S. K., Mahadevan, A., . . . Takasaki, T. (2012). Enterovirus 71 encephalomyelitis and Japanese encephalitis can be distinguished by topographic distribution of inflammation and specific intraneuronal detection of viral antigen and RNA. *Neuropathol Appl Neurobiol, 38*(5), 443-453.

Wong, S. S., Yip, C. C., Lau, S. K., & Yuen, K. Y. (2010). Human enterovirus 71 and hand, foot and mouth disease. *Epidemiol Infect, 138*(8), 1071-1089.

World Health Organization. (2011). A guide to clinical management and public health response for hand, foot and mouth disease (HFMD). Retrieved from http://www.wpro.who.int/emerging_diseases/documents/HFMDGuidance/en/

Xu, L., He, D., Li, Z., Zheng, J., Yang, L., Yu, M., . . . Xia, N. (2014). Protection against lethal enterovirus 71 challenge in mice by a recombinant vaccine candidate containing a broadly cross-neutralizing epitope within the VP2 EF loop. *Theranostics, 4*(5), 498-513.

Yamamoto, K. R., Alberts, B. M., Benzinger, R., Lawhorne, L., & Treiber, G. (1970). Rapid bacteriophage sedimentation in the presence of polyethylene glycol and its application to large-scale virus purification. *Virology, 40*(3), 734-744.

Yamayoshi, S., Fujii, K., & Koike, S. (2014). Receptors for enterovirus 71. *Emerg Microbes Infect, 3*(7), e53.

Yamayoshi, S., Yamashita, Y., Li, J., Hanagata, N., Minowa, T., Takemura, T., & Koike, S. (2009). Scavenger receptor B2 is a cellular receptor for enterovirus 71. *Nat Med, 15*(7), 798-801.

Yan, J. J., Wang, J. R., Liu, C. C., Yang, H. B., & Su, I. J. (2000). An outbreak of enterovirus 71 infection in Taiwan 1998: a comprehensive pathological, virological, and molecular study on a case of fulminant encephalitis. *J Clin Virol, 17*(1), 13-22.

Yang, Y., Wang, H., Gong, E., Du, J., Zhao, X., McNutt, M. A., . . . Zheng, J. (2009). Neuropathology in 2 cases of fatal enterovirus type 71 infection from a recent epidemic in the People's Republic of China: a histopathologic, immunohistochemical, and reverse transcription polymerase chain reaction study. *Hum Pathol, 40*(9), 1288-1295.

Yao, P. P., Qian, L., Xia, Y., Xu, F., Yang, Z. N., Xie, R. H., . . . Zhu, H. P. (2012). Enterovirus 71-induced neurological disorders in young gerbils, Meriones unguiculatus: development and application of a neurological disease model. *PLoS One, 7*(12), e51996.

Yap, M. S., Tang, Y. Q., Yeo, Y., Lim, W. L., Lim, L. W., Tan, K. O., . . . Heng, B. C. (2016). Pluripotent human embryonic stem cell derived neural lineages for in vitro modelling of enterovirus 71 infection and therapy. *Virol J, 13*(1), 5.

Yu, P., Gao, Z., Zong, Y., Bao, L., Xu, L., Deng, W., . . . Qin, C. (2014). Histopathological features and distribution of EV71 antigens and SCARB2 in human fatal cases and a mouse model of enterovirus 71 infection. *Virus Res, 189*, 121-132.

Zeng, H., Wen, F., Gan, Y., & Huang, W. (2012). MRI and associated clinical characteristics of EV71-induced brainstem encephalitis in children with hand-foot-mouth disease. *Neuroradiology, 54*(6), 623-630.

Zhang, Y., Cui, W., Liu, L., Wang, J., Zhao, H., Liao, Y., . . . Li, Q. (2011). Pathogenesis study of enterovirus 71 infection in rhesus monkeys. *Lab Invest, 91*(9), 1337-1350.

Zhao, M., Bai, Y., Liu, W., Xiao, X., Huang, Y., Cen, S., . . . Zeng, Y. (2013). Immunization of N terminus of enterovirus 71 VP4 elicits cross-protective antibody responses. *BMC Microbiol, 13*, 287.

Zhu, F. C., Meng, F. Y., Li, J. X., Li, X. L., Mao, Q. Y., Tao, H., . . . Shen, X. L. (2013). Efficacy, safety, and immunology of an inactivated alum-adjuvant enterovirus 71 vaccine in children in China: a multicentre, randomised, double-blind, placebo-controlled, phase 3 trial. *Lancet, 381*(9882), 2024-2032.

Zhu, Fengcai, Xu, Wenbo, Xia, Jielai, Liang, Zhenglun, Liu, Yan, Zhang, Xuefeng, . . . Wang, Nan. (2014). Efficacy, Safety, and Immunogenicity of an Enterovirus 71 Vaccine in China. *N Engl J Med, 370*(9), 818-828.

List of publications and papers presented

1. Tan, S. H., Ong, K. C., & Wong, K. T. (2014). Enterovirus 71 Can Directly Infect the Brainstem via Cranial Nerves and Infection Can Be Ameliorated by Passive Immunization. *J Neuropathol Exp Neurol, 73*(11), 999-1008.

2. Liu, L., Mo, Z., Liang, Z., Zhang, Y., Li, R., Ong, K. C., . . . Li, Q. (2015). Immunity and clinical efficacy of an inactivated enterovirus 71 vaccine in healthy Chinese children: a report of further observations. *BMC Med, 13*(1), 226.

3. Tan, S. H., Ong, K. C., David, P., & Wong, K. T. (2016). A monoclonal antibody to ameliorate central nervous system infection and improve survival in a murine model of human Enterovirus-A71 encephalomyelitis. *Antivir Res. In press.*